ARIZONA DEPARTMENT OF TRANSPORTATION

REPORT NUMBER: FHWA/AZ 85/237

FIELD TESTING OF MONOTUBE SPAN-TYPE SIGN STRUCTURES

Prepared by:
Kipp A. Martin
Mohammad R. Ehsani
Reidar Bjorhoude

MARCH 1986

Prepared for:
Arizona Department of Transportation
206 S. 17th Avenue
Phoenix, Arizona 85007
in cooperation with
U.S. Department of Transportation
Federal Highway Administration

"The contents of this report reflect the views of the authors who are responsible for the facts and the accuracy of the data peresented herein. The contents do not necessarily reflect the official views or policies of the Arizona Department of Transportation or the Federal Highway Administration. This report does not constitute a standard, specification, or regulation. Trade or manufacturers' names which may appear herein are cited only because they are considered essential to the objectives of the report. The U. S. Government and The State of Arizona do not endorse products or manufacturers."

CHNICAL REPORT STANDARD TITLE PAG

1. Report No.	2. Government Accession No.	3. Recipient's Catalog No.
FHWA/AZ-86/237		

4. Title and Subtitle	5. Report Date
FIELD TESTING OF MONOTUBE SIGN SUPPORT STRUCTURES	September, 1985
	6. Performing Organization Code

7. Author(s)	8. Performing Organization Report No.
K. A. Martin, M. R. Ehsani and Reidar Bjorhovde	ATTI-85-5

9. Performing Organization Name and Address	10. Work Unit No.
Arizona Transportation and Traffic Institute College of Engineering and Mines UNIVERSITY OF ARIZONA Tucson, Arizona 85721	11. Contract or Grant No. HPR-1-25(237)
	13. Type of Report and Period Covered FINAL July 1984-September 1985
12. Sponsoring Agency Name and Address Arizona Transportation Research Center Arizona Department of Transportation ARIZONA STATE UNIVERSITY Tempe, Arizona 85281	14. Sponsoring Agency Code

15. Supplementary Notes Prepared in cooperation with the U. S. Department of Transportation, Federal Highway Administration, from a study of monotube sign support structures. The opinions and conclusions are those of the authors, and not necessarily of the Federal Highway Administration.

16. Abstract

The report presents the results of full-scale tests of actual monotube sign support structures in the field, along with detailed theoretical analyses of the structures and comparisons of the analytical and experimental results. Two structures were tested under actual service conditions: A 100-foot span structure in Phoenix, Arizona, and a 60-foot span structure in Tucson, Arizona, were instrumented with strain gages and an anemometer, to determine in-service strains due to winds of various speeds. Since the structures had been erected earlier, no measurements could be made of dead load strains. The same two structures were also analyzed by two- and three-dimensional finite element modeling, using static as well as dynamic (due to vortex shedding) loads. It was found that the correlation between computed and measured strains was good, especially considering the complexity of the analyses. Maximum in-plane stresses occurred at the midspan of the beam for both structures, and the maximum out-of-plane stresses occurred at the column base. The maximum wind load stress was approximately 11 ksi (100 foot structure). This level did not vary a great deal with the wind speed. Resonance was not observed at any wind speed, due to the combined effects of structural damping and short duration of wind loads. This is in agreement with the results of an earlier study. It is also shown that the $d^2/400$ dead load deflection requirement of AASHTO cannot be met. Recommendations for design criteria and further studies are made.

17. Key Words	18. Distribution Statement
Monotube; sign support structures; single span; full-scale testing; theoretical evaluation; static; dynamic; stresses; design criteria	No restrictions. This document is available to the public through the National Technical Information Service, Springfield, VA 22161

19. Security Classif. (of this report)	20. Security Classif. (of this page)	21. No. of Pages	22. Price
UNCLASSIFIED	UNCLASSIFIED	160	

Form DOT F 1700.7 (8-69)

ACKNOWLEDGEMENTS

The investigation described in this report was funded by the Arizona Department of Transportation in cooperation with the Federal Highway Administration under Project No. HPR-1-25 (237).

The authors are sincerely appreciative of the continuous support and helpful suggestions of the staff of the Arizona Transportation Research Center. In particular, the untiring efforts of Mike Sarsam and Frank R. McCullagh were crucial to the success of this work. Much assistance was provided by Richard D. Wingfield of the Arizona Department of Transportation and Charles Mele of the City of Tucson Department of Transportation during the field testing in Phoenix and Tucson. The help of the Arizona DOT and the City of Tucson DOT was invaluable in securing access to the sign structures and the mounting of the gages.

Dr. R. A. Jimenez, Director of the Arizona Transportation and Traffic Institute, provided assistance in the administration of the research project.

Tom Demma, electronics technician of the Department of Civil Engineering at the University of Arizona, solved a great many problems associated with the testing, installation and use of the multitude of electronic components. Computation assistance for the GIFTS program was given by Thomas R. Cram of the Computer-Aided Engineering Center of the University of Arizona.

Sincere thanks are due Carole Goodman who did an excellent job in typing the report.

METRIC CONVERSION TABLE

This report utilizes U.S. customary units of measurement. The following may be used to convert to SI units.

1 inch	=	25.4 mm
1 foot	=	0.305 m
1 mile	=	1.61 Km
1 sq. in.	=	645 mm^2
1 lb mass	=	0.454 kg
1 lb force	=	4.45 N
1 psi	=	6.89 kPa

TABLE OF CONTENTS

LIST OF FIGURES

LIST OF FIGURES (Continued)

LIST OF FIGURES (Continued)

LIST OF TABLES

LIST OF TABLES (Continued)

Chapter 1

INTRODUCTION

For almost as long as there have been roads, there has been a need for road signs to display information to travelers. As the width of the roads grew, so did the size of the structures, until today spans in excess of 100 feet are not uncommon.

To support signs over these large spans, truss type structures have traditionally been used. These typically consist of two columns supporting a truss or tri-cord element. The traffic signs are arranged in the desired locations and bolted in place. Figure 1 shows a typical truss type structure.

The design of sign support structures is based on the American Association of State Highway and Transportation Officials' (AASHTO) 1975 "Standard Specifications for Structural Supports for Highway Signs, Luminaries and Traffic Signals" (1), which was revised in 1978 and 1979, and one of its predecessors, the AASHTO 1968 "Specifications for the Design and Construction of Structural Supports for Highway Signs". In the remainder of this report these will be referred to as the Specifications.

The Specifications set minimum performance guidelines. Among these are criteria governing deflections. Essentially, the maximum static dead load deflection, in units of feet, is limited to the empirical value of $d^2/400$, where d is the depth of the sign in feet. If the deflection of a sign-support structure is found to be excessive, the designer can satisfy the Specifications simply by specifying a deeper sign (i.e., larger d). The rationale and consequences of this approach will be discussed in some

detail in later chapters. An extensive evaluation of the deflection requirement has been given by Ehsani and Bjorhovde (2).

Over the years, the performance of the truss structures has generally been satisfactory. However, there are some drawbacks to their use. They are expensive to fabricate and in many cases the application of the deflection requirement produces a structure which is not as economical as some of the pre-engineered structures that are available. One of the latter types that has seen increased use is the monotube sign support structure. In addition to being more economical, the monotube structure also has the advantage of being more attractive than most truss structures.

As shown in Fig. 2, monotube structures are constructed of linearly tapering tubular elements that have a constant wall thickness. They consist of two columns supporting a beam in a fashion similar to the truss type structures. The columns are one piece tapered members, with the largest diameter at the base. The beam normally consists of two tapered pieces that are joined with the largest diameter at midspan. Beams of longer spans may consist of 3 pieces, with the middle one having a constant diameter. Figure 3 shows one of these longer 3-piece spans. For both types, the beam is connected to the column by simple supports, as shown in Fig. 4.

Currently, the Specifications do not provide sufficiently detailed guidelines for the design of monotube structures. As a result, the manufacturers of these structures utilize individual design criteria that make direct comparisons between different products very difficult. In

Figure 1. Typical Truss Sign Support Structure

Figure 2. Typical Monotube Sign Support Structure

Figure 3. Long Span Monotube Sign Support Structure

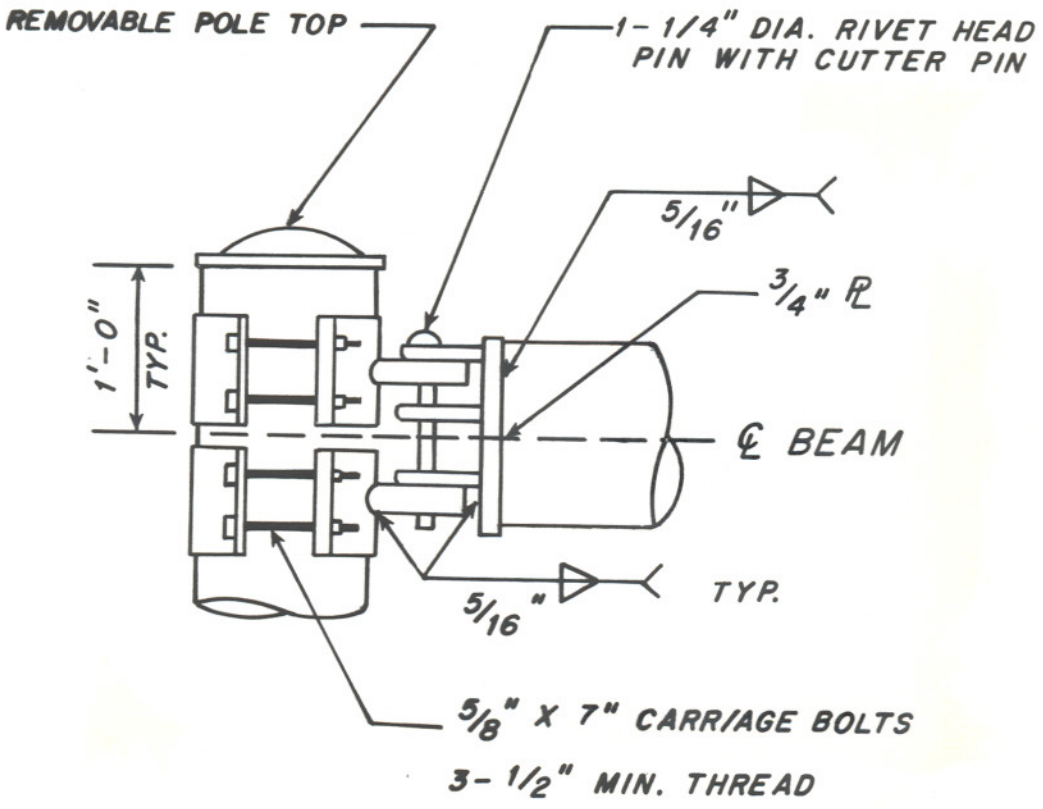

Figure 4. Typical Monotube Structure Beam-to-Column Connection

addition, the structures tend to vary widely in material as well as cross-sectional properties. This has placed the transportation authorities in the position of having to accept or reject different designs with no rational guidelines to follow.

The absence of adequate design guidelines can partly be attributed to the sparsity of research and engineering data on the strength and behavior of monotube structures. The first major work in this area was a project conducted by Ehsani and Bjorhovde (3) in 1984 at the University of Arizona. This study modeled a monotube structure using the finite element method to determine its response to various static and dynamic loads. It was found that the $d^2/400$ deflection criterion was inappropriate for monotube structures. Dead load deflections in excess of the $d^2/400$ limit were calculated, although the stresses associated with these deflections were well below the magnitudes of the allowable levels.

The first monotube study was purely analytical and the accuracy of the results obtained is a function of the assumptions that were made to model the structure. It is important to compare such theoretical results with actual performance data for a real structure, to verify the modeling as well as the responses that have been found. The latter should be obtained from testing, preferably using a full-scale structure being subjected to a variety of service conditions. With such test data and correlations in hand, improved design guidelines can be developed.

Chapter 2

SCOPE

Before the validity of any analytical study can be fully accepted, its results should be compared to the actual behavior of the subject in question. While the study by Ehsani and Bjorhovde (3) provided detailed data on the behavior of monotube structures, it lacked comparison with the performance of an actual structure.

The study presented here was conducted in three parts. In the first, two actual structures were modeled for computer analysis. These were analyzed for various static and dynamic loads to determine their response to different wind speeds. The data that were collected include dynamic histograms, deflections and stresses for a variety of wind speeds.

Part two involved field testing of the same two structures. By testing the structures under service conditions, the true response was obtained. Strains at critical points on the structure were recorded, along with the wind speed corresponding to these strains.

The final part of the study was aimed at comparing and evaluating the results obtained in the first two parts. Through this comparison, it would be possible to judge the validity of the computer model, as well as to reveal any problem conditions such as resonance.

This study has been limited to monotube structures as described in Chapter 1. Cantilever structures were not considered, and fatigue related problems have also been ignored due to time limitations.

Chapter 3

STRUCTURAL RESPONSE UNDER WIND LOADS

For most sign structures, the only loads acting on the structure are gravity and wind. The forces due to gravity are simply the self weight of the structure; their magnitude and effect on the structure are relatively easy to determine.

In contrast to the gravity loads, which are static, wind loads are dynamic. There are a number of reasons for this dynamic nature. First, the magnitude of the wind is not constant. The wind tends to gust. The direction of the wind also changes. Finally, the cross-sectional shape of the structural elements may cause dynamic behavior.

An object placed in an air stream will cause a disturbance in that air stream. This disturbance will create pressure on the object, the size and shape of which will determine the intensity and distribution of the pressure. As an illustration, it is this phenomenon that creates the lift on an airplane wing. The wing is shaped such that as air flows around it, the pressure on the wing surface is larger on the bottom than on the top, as shown in Fig. 5. Thus, the airplane rises.

In addition to lift, another force that is exerted on the object is drag. This has been experienced by anyone trying to pedal a bicycle into the wind. As long as the velocity of the airstream is constant, the drag force remains constant. Drag is therefore considered a static force.

The magnitude of the drag force, shown in Fig. 6, can be computed as:

$$F = \rho C_D A V_o^2 \quad (1)$$

where F is the drag force, A is the projected area of the object perpendicular to the flow, ρ is the density of the air, V_o is the velocity of the airstream, and C_D is the coefficient of drag for the object (4). Table 1 gives the coefficient of drag for some common shapes.

If the object in the air stream has an irregular shape, the pressure distribution will also be irregular. Thus, for a certain range of wind speeds, the object may develop vibrations or oscillations normal to the direction of flow (5). A common example of the phenomenon is the oscillation observed in telephone cables in a strong wind. Sometimes, these oscillations can result in excessive deformations or even collapse of a structure. This happens when the vibrations induced by the airflow have a frequency that is equal or close to one of the natural frequencies of the structure, and reflects the condition of structural resonance.

The occurrence of resonance means that the structure will continue to oscillate with no additional energy or load applied to the structure. Probably the most famous structural failure where resonance at least played a part was the collapse of the Tacoma Narrows Bridge in the State of Washington. This bridge failed at a wind speed of 42 mph, although it had been designed to withstand winds up to 100 mph if no oscillations had occurred (6). However, the wind-induced vibrations were close to one of the natural frequencies of the bridge and this contributed to the collapse.

The wind-induced vibrations are caused by a phenomenon known as vortex shedding. Fluid flowing around an object will develop vortices in

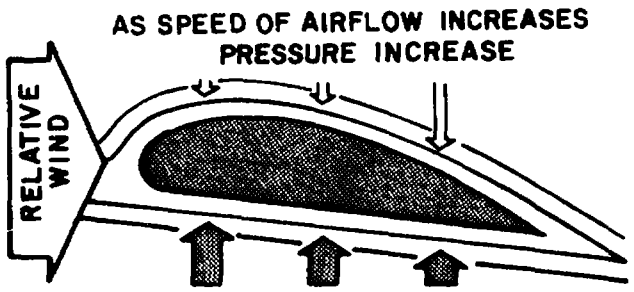

Figure 5. Airfoil Illustrating Principle of Lift

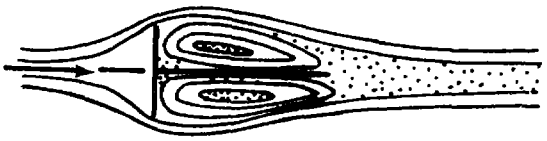

Figure 6. Drag on Plate in Air Stream

TABLE 1. Drag Coefficient for Various Shapes

Form of Body	L/D	R	C_D
Circular Disk			
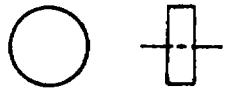		$>10^3$	1.12
Rectangular Plate			
(L = length, D = width)	1	$>10^3$	1.16
	5		1.20
	20		1.50
	∞		1.90
Tandem Disks			
(L = Spacing)	0	$>10^3$	1.12
	1		0.93
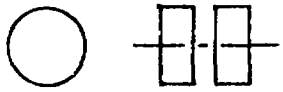	2		1.04
	3		1.54
Cylinder			
(axis parallel to flow)	0	$>10^3$	1.12
	1		0.91
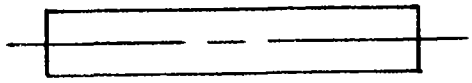	2		0.85
	4		0.87
	7		0.99
Cylinder			
(axis perpendicular to flow)	1	10^5	0.63
	5		0.74
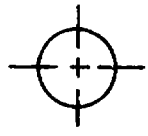	20		0.90
	∞		1.20
	5	$>5 \times 10^5$	0.35
Streamlined Foil			
	∞	$>4 \times 10^4$	0.07

the wake. These will alternate from one side of the object to the other, as illustrated in Fig. 7 for flow around a cylinder.

The study of these vortices was originated by von Karman (6), using a double row of vortices in two-dimensional flow. He found that the only stable equilibrium configuration for the double row resulted when the vortices of one row were exactly opposite to points half-way between the vortices in the other row. Von Karman also found that for the rows to be stable, they would have to be spaced at 0.281 times the distance between two adjacent vortices of one row. Such an arrangement is known as a Karman vortex sheet and is illustrated in Fig. 8.

Von Karman based this treatment of vortex shedding on the assumption of a perfect fluid. By definition, the only property possessed by a perfect fluid is density. Therefore, this treatment does not reflect the influence of fluid viscosity. Flow of a viscous fluid is accompanied by a pressure gradient that is proportional to the dynamic viscosity of the fluid. Since the density and viscosity for air are both relatively small, the viscosity can have as much effect on fluid flow as the density and must be taken into account. The Reynolds number, R, characterizes the relative importance of viscous action, with a higher number indicating a lesser importance (4). Therefore, an infinite value of R corresponds to a flow in which viscous resistance plays no part.

For flow past a cylinder, a number of changes occur as the Reynolds number increases. For instance, for small values of R, the flow is smooth and unseparated. For higher values of R, two symmetrical standing vortices form behind the cylinder, as shown in Fig. 9. As R increases,

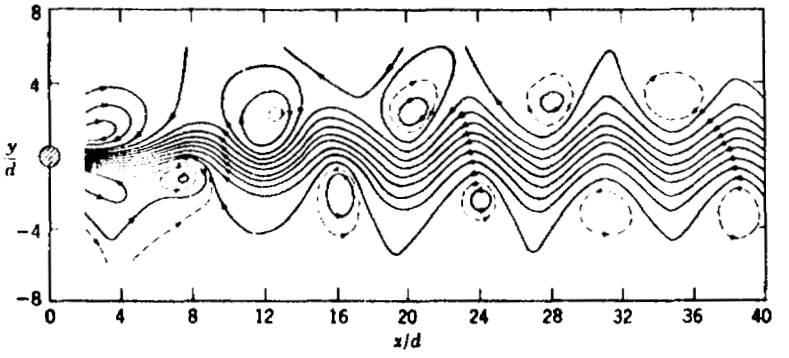

Figure 7. Vortices for Flow around Cylinder

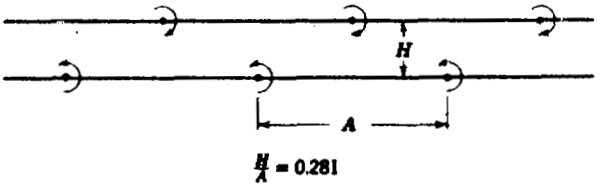

Figure 8. Karman Vortex Sheet

these vortices stretch downstream. When R is approximately 40, the vortices alternate in detaching from the two sides of the cylinder and move downstream. This is the start of vortex shedding.

For R values between 40 and 300, the shedding is very regular in both amplitude and frequency and can be approximated by a Karman sheet. As R increases past 300, the flow becomes irregular. The vortices are still shedding with a predominant frequency, but their amplitude is not easily determined, since it is more or less random. This irregular flow continues until R equals 3×10^5. At this point, the flow is so turbulent that the vortex sheet is no longer recognizable.

For the range of Reynolds numbers where vortex shedding does occur, the frequency with which the vortices are shed can be expressed non-dimensionally by the Strouhal number, S. Since the vortex shedding frequency varies with R, S also varies with R, as shown in Fig. 10.

For monotube structures, the fluid is air and the structure can be considered a long cylinder. The Reynolds number is then defined as (6):

$$R = 780.5 \cdot V \cdot D \qquad (2)$$

where V is the airspeed in miles per hour and D is the cylinder diameter in inches. It can be seen that except when dealing with very small cylinders and low wind speeds, R will be greater than 300. For values of R between 300 and 3×10^5, the shedding frequency is sinsoidual but with a random amplitude. For R larger than 3×10^5, both the frequency and the amplitude are random.

For the range of $300 < R < 3 \times 10^5$, the vortex shedding forces must be determined from the pressure distribution.

Figure 9. Standing Vortices for Flow around Cylinder

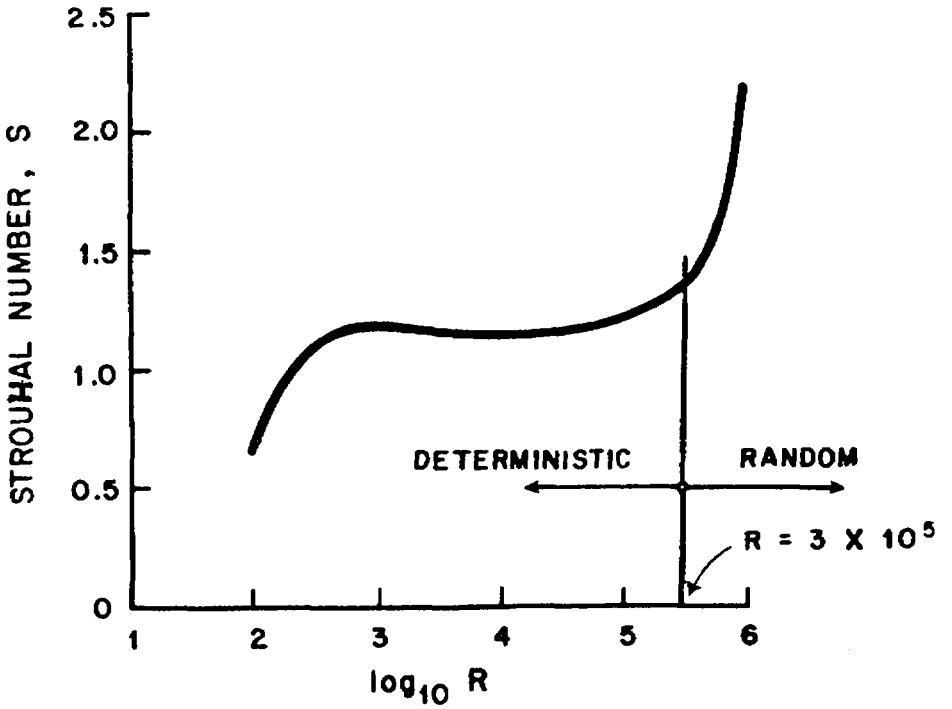

Figure 10. Relationship between the Reynolds Number and the Strouhal Number

The generally accepted expression for this force is (7):

$$F(t) = 1/2\,\gamma V^2 A_p C_L \sin \Omega t \qquad (3)$$

where F(t) is the time dependent vortex shedding force, γ is the density of air, V is the wind velocity, A_p is the projected area of the cylinder, C_L is the coefficient of lift, Ω is the shedding frequency, and t is the time. To account for the random force amplitude, Weaver (8) experimentally determined the root-mean-square (rms) values of C_L, denoted as $\bar{C}_L$, and using these, the expression for the vortex shedding forces becomes (4):

$$F(t) = 1/2\,\gamma A_p \bar{C}_L \sin \Omega t \qquad (4)$$

The determination of Ω is critical in the use of this equation. The vortex shedding frequency is determined from the equation (2)

$$\Omega = \frac{SV}{D} \qquad (5)$$

where S is the Strouhal number, V is the air speed, and D is the cylinder diameter.

As an example, the forcing function for a wind speed of 15 mph and a cylinder 14 in. in diameter will be determined. From Eq. (2), $\log_{10} R = \log_{10} (780.5 \cdot 15 \cdot 14) = 5.21$. From Fig. 11, the corresponding Strouhal number is S = 1.48.

From Eq. (5), using S = 1.48, V = 15 mph = 264 in/sec. and D = 14 in., the value of is found to be

$$\Omega = \frac{1.48(264)}{14} = 27.91 \text{ rad/sec.}$$

F(t) is now determined from Eq. (4), using $\bar{C}_L = 1.0$, as

$$F(t) = 1/2\ (0.002378)\ (22.0)^2\ A_p(1.0)\ \sin\ (27.91t)$$

$$= 0.575\ A_p\ \sin\ (27.91t)$$

where the wind speed is 22.0 ft/sec. From this expression, the forces on the structure can be determined, given the corresponding values of A_p.

For the monotube structure, the vibrations caused by the vortex shedding are more pronounced in the beam, as it is a simply supported element. These vibrations are also more pronounced in longer spans. In the range of wind speeds where $300 < R < 3x10^5$, the vibrations are usually of small amplitude, unless their frequency is close to the resonant frequency of the structure. In this case, the deflections may be excessive.

As stated in Chapter 1, the quantity $d^2/400$ is an empirically derived value. This criterion was originally developed primarily for use with truss type structures, where vortex shedding has a much smaller effect. This provision is very restrictive. Even structures with large signs (≈ 7 feet deep) can deflect no more than 0.125 inches. Other codes (9,10) are not as restrictive in their deflection criterion. A deflection criterion should therefore be developed for the monotube structures, independent of that used for trusses.

Chapter 4

ANALYSIS OF MONOTUBE STRUCTURES

To help in developing the design guidelines, as well as to provide data for a detailed comparison with the results of full-scale testing, extensive structural analyses were performed. This evaluation was done by modeling the two tested structures using the finite element method. The response of the models under static and dynamic loading was found, including the determination of the first ten natural frequencies for two- and three-dimensional behavior. Detailed stress and deflection computations were also made.

4.1 Modeled Structures

For this study, the Arizona Department of Transportation provided shop drawings and site plans for two sign structures. Both of these structures had been designed in accordance with the AASHTO specifications (1). The first structure has a span of 60 feet, and is located across the north-bound lanes of Miracle Mile, just north of Glenn Avenue in Tucson, Arizona. This structure is shown in Fig. 11a. The second structure has a span of 100 feet, and is located across University Drive west of the intersection of University Drive and Hohokam Expressway in Phoenix, Arizona. This structure is shown in Fig. 11b.

The dimensions of the Tucson structure are given in Fig. 12. The columns are linearly tapering single tubes, with the largest diameter at the base. Due to the site topography, the west column is 21" shorter than the east column, in order for the beam to be level. The beam is also

Figure 11a. Tucson Monotube Structure

Figure 11b. Phoenix Monotube Structure

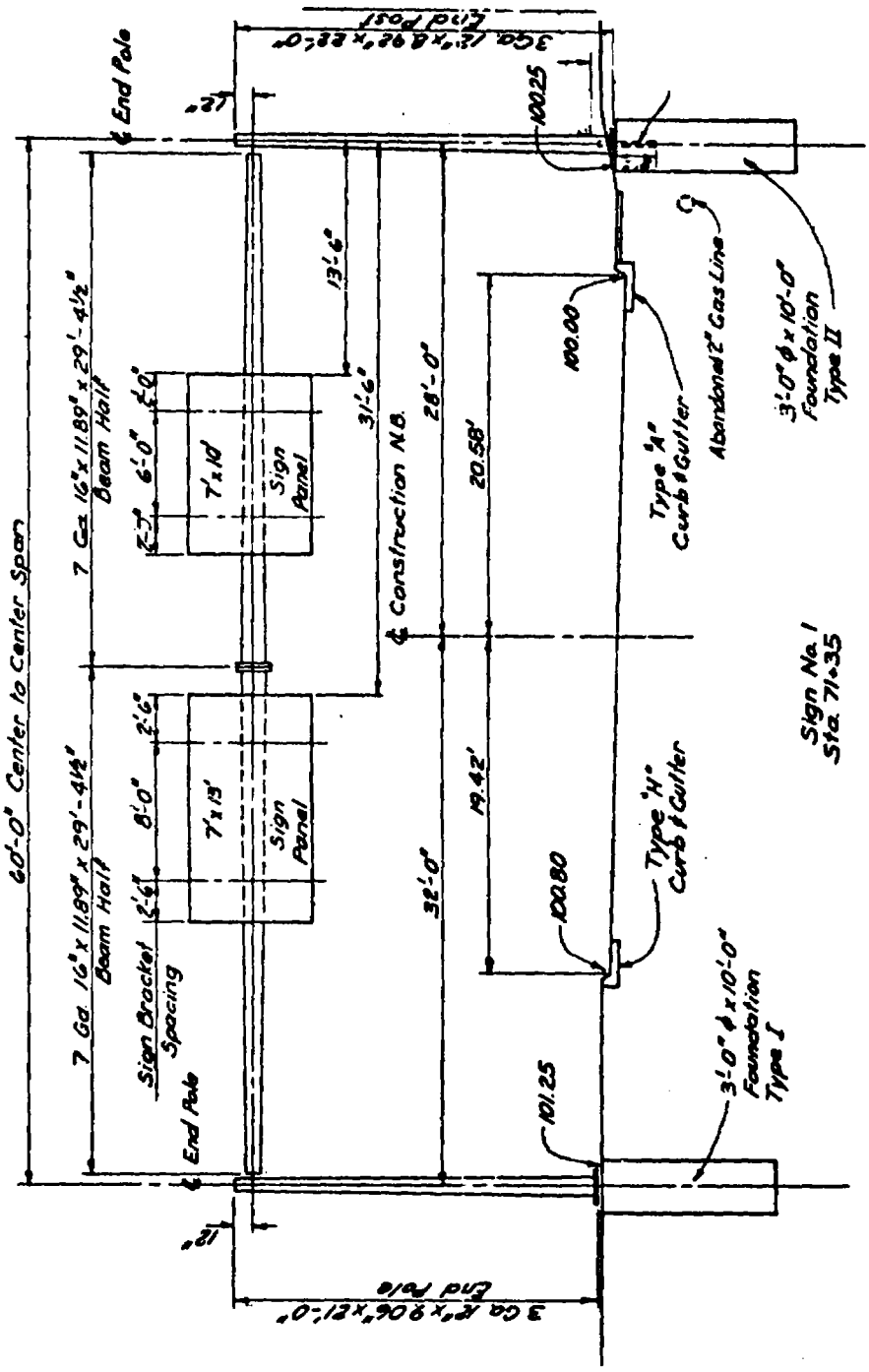

Figure 12. Dimensions of Tucson Monotube Structure

constructed of linearly tapering elements. It is spliced with the largest diameter at midspan.

The beam-to-column connection is shown in Fig. 13. It provides some moment resistance to vertical loads and essentially free rotation under horizontal loads. This connection also offsets the center line of the beam 18" from the centerline of the column, thus producing a true three-dimensional structure.

The details of the column base and foundation are shown in Fig. 14. The column base can be reasonably assumed to be fully fixed in all directions. The location of the traffic signs can be seen in Fig. 12.

The dimensions of the Phoenix structure are given in Fig. 15. The columns are of similar construction to the Tucson structure. The beam, however, is made of three segments instead of two, with the splices between segments at approximately the third points. The two outer segments have their largest diameter at the splices and taper linearly to the ends. The interior segment is of constant diameter. The beam is also cambered, so that the centroidal axis at midspan is 17" above the centroidal axis at the ends of the beam.

The beam-to-column connection for the Phoenix structure is not the same as the Tucson structure. While the moment resistances are comparable, the connection is such that the axes of the columns and the beam all lie in the same plane. This connection is shown in Fig. 16. The column base is similar to that shown in Fig. 14 and can also be assumed to be fully fixed. The locations of the signs for this structure are shown in Fig. 15.

Figure 13. Beam-to-Column Connection for Tucson Monotube Structure

Figure 14. Column Foundation for Tucson Monotube Structure

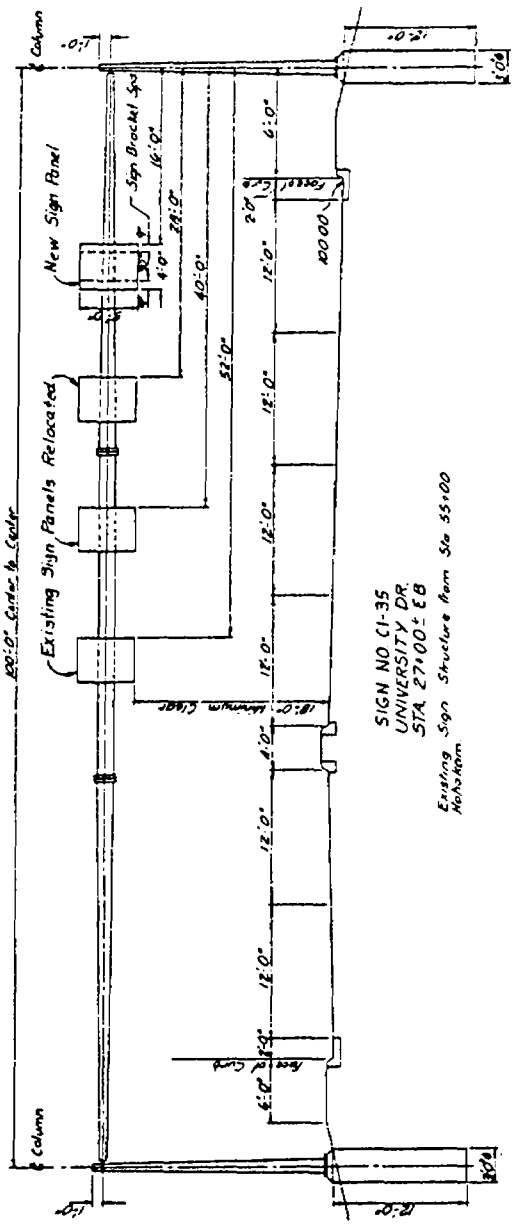

Figure 15. Dimensions of Phoenix Monotube Structure

Figure 16. Beam-to-Column Connection for Phoenix Monotube Structure

4.2 Computer Programs

The structural analysis of the monotube structures was accomplished using a set of computer programs collectively known as GIFTS (Graphics-oriented Interactive Finite element analysis Time-sharing System) (8). These programs constitute a finite element pre- and post-processing and analysis package, which can be loaded and run on a variety of minicomputers and time-sharing systems. It can be used with a standard alphanumeric terminal or with a graphics terminal. For this study, the GIFTS package was run on a Data General Eclipse computer of the Department of Aerospace and Mechanical Engineering at the University of Arizona.

Each of the GIFTS programs (modules) is fully compatible with all of the other modules. A module may perform a specific function, such as computing the natural frequencies of a structure, or a class of functions such as mesh definition and element generation. Many of the modules can be operated in either batch mode or interactively. In batch mode, the modules obtain commands and data from a pre-existing steering file. In interactive mode, the user must input the commands and data through the keyboard.

GIFTS can handle many different loads and load cases, and the stresses and deflections can be computed for each load case. Plots of the deflected structure or the stress distribution on any cross-section can also be provided.

4.3 Finite Element Model Development

Using the guidelines of the GIFTS package (11), a finite element model for each structure was developed. These models are shown in Figs. 17a and 17b for the Tucson and Phoenix structures, respectively.

The elements in both structures were modeled as beam elements with one node at each end. In order to be as realistic as possible, each node was allowed to have three translational degrees of freedom (i.e., displacements in the x-, y-, and z-directions), as well as three rotational degrees of freedom (rotations about the x-, y-, and z-axes). The x-, y-, and z-axes for each model are shown in Figs. 17a and 17b. These axes were considered to be the global axes for each model. The scale for this figure is shown on the lower left corner. For example, the length of the axes if Fig. 17a equals 60 inches.

In GIFTS, a variety of cross-sectional shapes can be used for the beam elements, including the standard I-section and a hollow, circular section. Thus, the hollow circular sections were used for the beam and column elements while the I-shape was used for the elements connecting the beam and the columns. GIFTS, however, cannot accept non-prismatic (e.g., tapered) elements. To circumvent this limitation, each element was assumed to have a constant cross-section, with dimensions equal to the average of the two end cross-sections of the element in the actual structure. In addition, a larger number of elements than would normally be required were used in each model. The wall thickness of the circular elements was taken as the minimum specified on the shop drawings. A list of element diameters and thicknesses is given in Tables 2a and 2b.

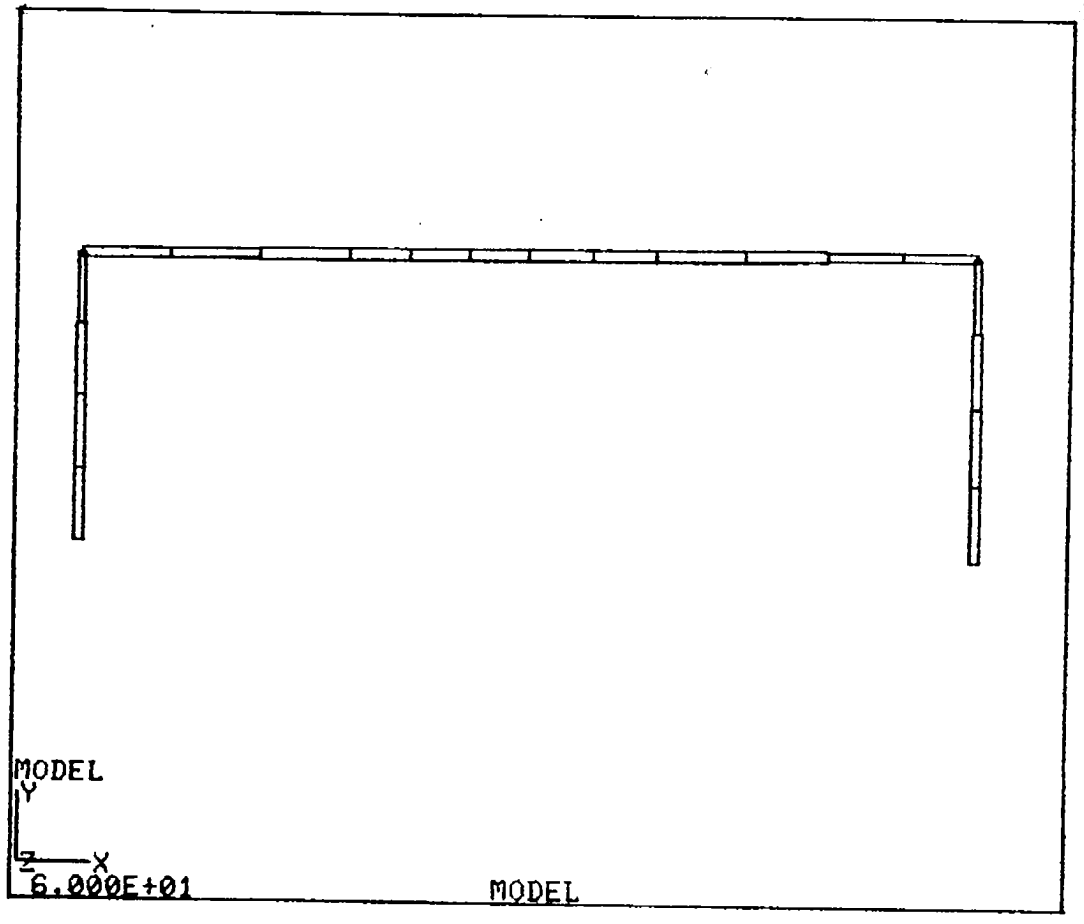

Figure 17a. Finite Element Model of Tucson Monotube Structure (Elevation)

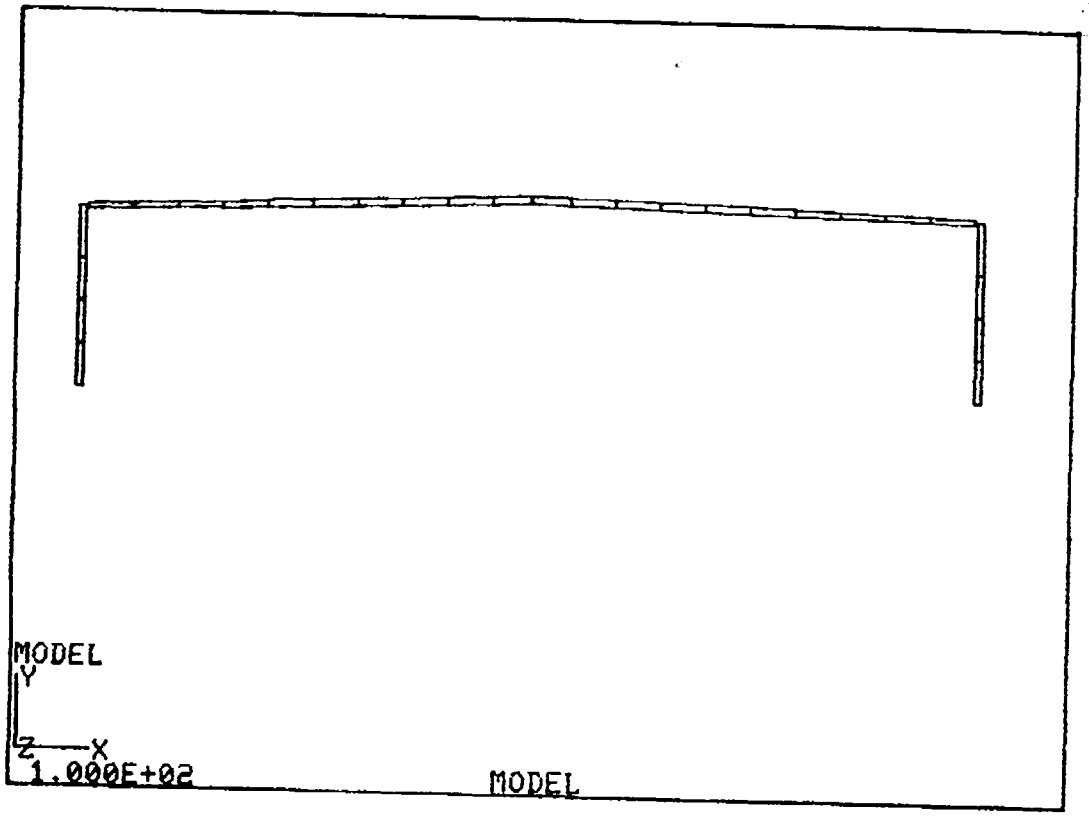

Figure 17b. Finite Element Model of Phoenix Monotube Structure (Elevation)

Table 2a. Element Diameters and Thicknesses for Tucson Structure.

Element No.	I-Node	J-Node	Dia. (in)	Thicknesses (in.)
3	1	2	12.78	0.239
4	32	33	12.92	"
5	2	3	11.92	"
6	31	32	12.04	"
7	3	4	11.08	"
8	30	31	11.14	"
9	4	5	10.22	"
10	29	30	10.24	"
11	11	12	12.96	0.179
12	12	13	13.72	"
13	13	14	14.48	"
14	14	15	15.12	"
15	15	16	15.18	"
16	16	17	15.68	"
17	17	18	16.12	"
18	18	19	15.58	"
19	19	20	14.92	"
20	20	21	14.20	"
21	21	22	13.42	"
22	22	23	12.90	"

Table 2b. Element Diameters and Thicknesses for Phoenix Structure.

Element No.	I-Node	J-Node	Dia. (in)	Thicknesses (in.)
3	1	2	14.40	0.239
4	30	31	14.40	"
5	2	3	14.18	"
6	29	30	14.18	"
7	3	4	13.50	"
8	28	29	13.50	"
9	4	5	12.80	"
10	27	28	12.80	"
11	6	7	11.60	0.179
12	7	8	12.54	"
13	8	9	13.48	"
14	9	10	14.40	"
15	10	11	15.32	"
16	11	12	16.26	"
17	12	13	17.20	"
18	13	14	17.66	"
19	14	15	17.66	"
20	15	16	17.66	"
21	16	17	17.66	"
22	17	18	17.66	"
23	18	19	17.66	"
24	19	20	17.20	"
25	20	21	16.26	"
26	21	22	15.32	"
27	22	23	14.40	"
28	23	24	13.48	"
29	24	25	12.54	"
30	25	26	11.60	"

The most difficult element to model was that representing the beam-to-column connection. The shear capacity of a connection is based on its cross-sectional area, while the flexural capacity depends on the moment of inertia. To ensure a realistic behavior for shear, the connection was modeled as a short I-section beam with the same area as the actual connection. The weak axis of the I-beam was oriented to give the least bending resistance in the horizontal direction, reflecting the simple support condition for the beam under the action of horizontal (perpendicular to the plane of the monotube structure) loads. The element was proportioned to give a moment capacity in the vertical direction approximating that of the real connection. The I- section was actually similar to a flat plate, as the flanges were only slightly wider than the web and of negligible thickness ($1x10^{-20}$ in.). The connection element for the Tucson structure was 10" x 0.825" in section and 18" long. The connection element for the Phoenix structure was 7.1" x 1.25" and 7.8" long.

In selecting the nodal mesh for each structure, a node was placed at the actual attachment points of each traffic sign for signs wider than 4 feet, and at the center of the sign for signs 4 feet wide or less. In this manner, the mass of the signs would be applied at a node. A node was also placed at the midspan of the beam, to be able to determine deflections and stresses at this important point.

The element lengths were maintained between 4 and 6 feet, and wherever it was possible, the elements were given the same length. This was difficult to accomplish for the Tucson structure, primarily due to the

sign locations. The Phoenix structure, however, was more easily modeled with elements of constant length.

4.4 Static Loads on Structure

As explained in Chapter 3, air flowing past an object will create a drag force. However, for wind speeds less than about 23 mph the drag will be negligible, although the drag on the signs may be significant. The 23 mph wind speed is the upper limit for which the vortex shedding is deterministic. Using Eq. (1) and the tables for the coefficient of drag, C_D, published by Rouse (4), the drag force on the signs was computed for the wind speeds considered. These forces are shown in Tables 3a and 3b for the Tucson and Phoenix structures, respectively. A static analysis was then performed for the various wind speeds, using the drag on the signs and the self weight of the structure. The results of this analysis will be discussed in detail later in this chapter.

The static analysis was performed by applying the drag force as a horizontal load, perpendicular to the axes of the beam and the columns. The loads were applied at the nodes corresponding to the attachment points of the signs. In addition, the weight of the signs was included as a lumped mass applied at these nodes. GIFTS can automatically calculate the mass of each element, and applies these masses in lumped form at the nodes.

Table 3a. Drag Forces on Signs of Tucson Structure (lbs.).

	7' x 13' Sign		7' x 10' Sign	
Wind Speed (MPH)	Node 14	Node 16	Node 19	Node 20
2.5	0.785	0.785	0.605	0.605
5.0	3.145	3.145	2.410	2.410
7.5	7.075	7.075	5.425	5.425
10.0	12.580	12.580	9.640	9.640
12.5	19.655	19.655	15.650	15.650
15.0	28.305	28.305	21.690	21.690
17.5	38.525	38.525	29.525	29.525
20.0	50.32	50.32	38.560	38.560
22.5	63.685	63.685	48.805	48.805
23.2*	67.710	67.710	51.885	51.885

*This is the maximum wind speed that was recorded for this structure.

Table 3b. Drag Forces on Signs of Phoenix Structure (lbs.).

Wind Speed (MPH)	All Signs are 4' x 5' Node 15	Node 18	Node 20	Node 22
2.5	0.353	0.353	0.353	0.353
5.0	1.411	1.411	1.411	1.411
7.5	3.175	3.175	3.175	3.175
10.0	5.644	5.644	5.644	5.644
12.5	8.819	8.819	8.819	8.819
15.0	12.699	12.699	12.699	12.699
17.5	17.285	17.285	17.285	17.285
20.0	22.576	22.576	22.576	22.576
22.1*	27.566	27.566	27.566	27.566

*This is the maximum wind speed that was recorded for this structure.

4.5 Dynamic Loads on Structure

The equation for the vortex shedding frequency, Eq. (5), is heavily dependent on the diameter of the cylinder. This means that for the tapered cylinders of the monotube structure, the shedding frequency will vary along the length of the member. This condition is difficult, if not impossible to model. Therefore, each structure was divided into three subassemblies, where the columns and the beam each was considered as one. An average diameter was determined for each subassembly, using the diameters of the elements in the subassembly. This average diameter was then used to compute the vortex shedding frequency and the corresponding forces for each node. The average diameters of each substructure are given in Table 4. The simplification will not result in any significant differences between the wind loads on the actual and the modeled structures.

To perform a dynamic analysis of a structure using GIFTS, the loads on the structure at specific points in time must be entered into the GIFTS modules. GIFTS assumes a linear load variation over any individual time interval. For this study, the loads were determined at 0.5 second intervals for a total time of 32 seconds. This gives a sum of 64 load increments. The time of 32 seconds was chosen on the basis of the earlier monotube study (3), which found that this would be a sufficient period to detect any form of excessive deformation (i.e., resonance). However, it should be noted that apart from a wind tunnel, the probability of a structure experiencing a constant wind speed for as long a period as 32

Table 4. Average Diameters of Finite Element Subassemblies (in).

	Tucson	Phoenix
Column 1	11.50	13.81
Column 2	11.59	13.81
Beam	14.40	15.20

seconds will be extremely small. The wind generally blows in gusts, and while the variation in velocity may not be great, it is sufficient to keep the structure from vibrating at one frequency for any extended period of time. The probability of actual resonance occurring is therefore negligible (2,3).

The loads were given as nodal loads. The magnitudes of these loads were determined using Eq. (4), the average diameter of the subassemblies, and the tributary projected area of each node. The loads were determined as acting normal to the axis of the subassembly and perpendicular to the direction of the wind.

Dynamic analyses were performed for each structure for wind speeds ranging from 2.5 mph to 20 mph in steps of 2.5 mph. For the Tucson structure, additional analyses were performed for wind speeds of 22.5 and 23.2 mph. For the Phoenix structure, an additional analysis was performed for a wind speed of 22.1 mph. Above these maximum wind speeds, the vortex shedding forces are of random magnitude, and thus considered beyond the scope of this study. The 2.5 mph interval was chosen as a compromise between accuracy, data entry time, and computer cost.

GIFTS allows the user to choose one of four approaches for dynamic analysis. These are Houbolt's Scheme, Newmark's Beta Method, Wilson's Theta Method, and the Trapezoidal Rule (8). Houbolt's Scheme was chosen for this study, since it is generally more accurate than the Trapezoidal Rule and does not need to use the arbitrary constants of Newmark's and Wilson's Methods. While recommended values for these constants exist, it is not known if they are applicable for monotube structures.

4.6 Natural Frequencies of Vibration

The natural frequencies of a structure are representative of the dynamic response of the structure in the absence of any external loads. They are the frequencies at which the structure will vibrate when no energy is being provided to the structural system and can be determined by an iterative technique such as subspace iteration.

The natural vibration characteristics of a structure are important when the structure is subjected to dynamic forces. The frequencies of the loads and those of the structure may combine in such a manner as to give a response that is a magnification of a natural frequency. In the worst case, the loading frequency equals a natural frequency. This causes the structure to develop ever-increasing deflections and thus constitutes resonances; the consequences of which were discussed in Chapter. 3.

The structure can be modeled as a distributed or lumped mass system. The distributed mass system results in a structure with an infinite number of degrees of freedom. The lumped mass system results in a structure with the number of degrees of freedom given by:

$$NDF = (NP \cdot NFP) - (NFP)_S \qquad (6)$$

where NP = the number of nodal points in structure, NFP = the number of degrees of freedom at each node, and $(NFP)_S$ is the total number of suppressed degrees of freedom. The value of NDF therefore takes into account whether the structure has been modeled as a two- (2D) or three-dimensional (3D) system.

GIFTS uses the subspace iteration technique, which is based on the lumped mass approach. In the computation of the natural frequencies, the

models that were used for the static and dynamic analyses also were utilized. The structural damping has been conservatively assumed to be zero.

Tables 5a and 5b give the natural frequencies for the first 10 modes for both structures. These include 2D as well as 3D data. The 2D data represents displacements in the x- and y-directions, since the displacements in the out-of-plane direction (z-direction) have been suppressed.

From Table 5a, it can be seen for the Tucson (60 foot) structure, the following 2D and 3D modes have the same frequencies:

$$f_1 \text{ (2D)} = f_2 \text{ (3D)} = 2.834 \text{ cps}$$

$$f_2 \text{ (2D)} = f_3 \text{ (3D)} = 3.265 \text{ cps}$$

$$f_3 \text{ (2D)} = f_6 \text{ (3D)} = 12.290 \text{ cps}$$

$$f_4 \text{ (2D)} = f_8 \text{ (3D)} = 27.301 \text{ cps}$$

$$f_5 \text{ (2D)} \approx f_{10} \text{ (3D)} = 31.760 \text{ cps}$$

Similarly, for the Phoenix (100 foot) structure, Table 5b gives

$$f_1 \text{ (2D)} = f_1 \text{ (3D)} = 1.467 \text{ cps}$$

$$\text{(2D)} = f_3 \text{ (3D)} = 3.055 \text{ cps}$$

$$f_3 \text{ (2D)} = f_5 \text{ (3D)} = 5.001 \text{ cps}$$

$$f_4 \text{ (2D)} = f_8 \text{ (3D)} = 10.872 \text{ cps}$$

$$f_5 \text{ (2D)} = f_{10} \text{ (3D)} = 19.263 \text{ cps}$$

Since the 2D modes are all in-plane, this indicates that the above mentioned 3D modes are dominated by in-plane behavior.

Figures 18 and 19 show the first two 3D mode shapes for the Tucson structure. Figures 20 and 21 show the first two 3D mode shapes for the

Table 5a. Natural Frequencies of Tucson Structure (CPS).

Mode	2-D	3-D
1	2.834	2.295
2	3.265	2.834
3	12.290	3.265
4	27.301	4.293
5	31.760	7.925
6	34.714	12.290
7	47.312	16.646
8	74.169	27.301
9	92.693	29.307
10	102.730	31.934

Table 5b. Natural Frequencies of Phoenix Structure (CPS).

Mode	2-D	3-D
1	1.467	1.467
2	3.055	1.479
3	5.001	3.055
4	10.872	3.868
5	19.263	5.001
6	29.481	6.193
7	36.518	9.118
8	37.522	10.872
9	42.252	13.874
10	56.589	19.263

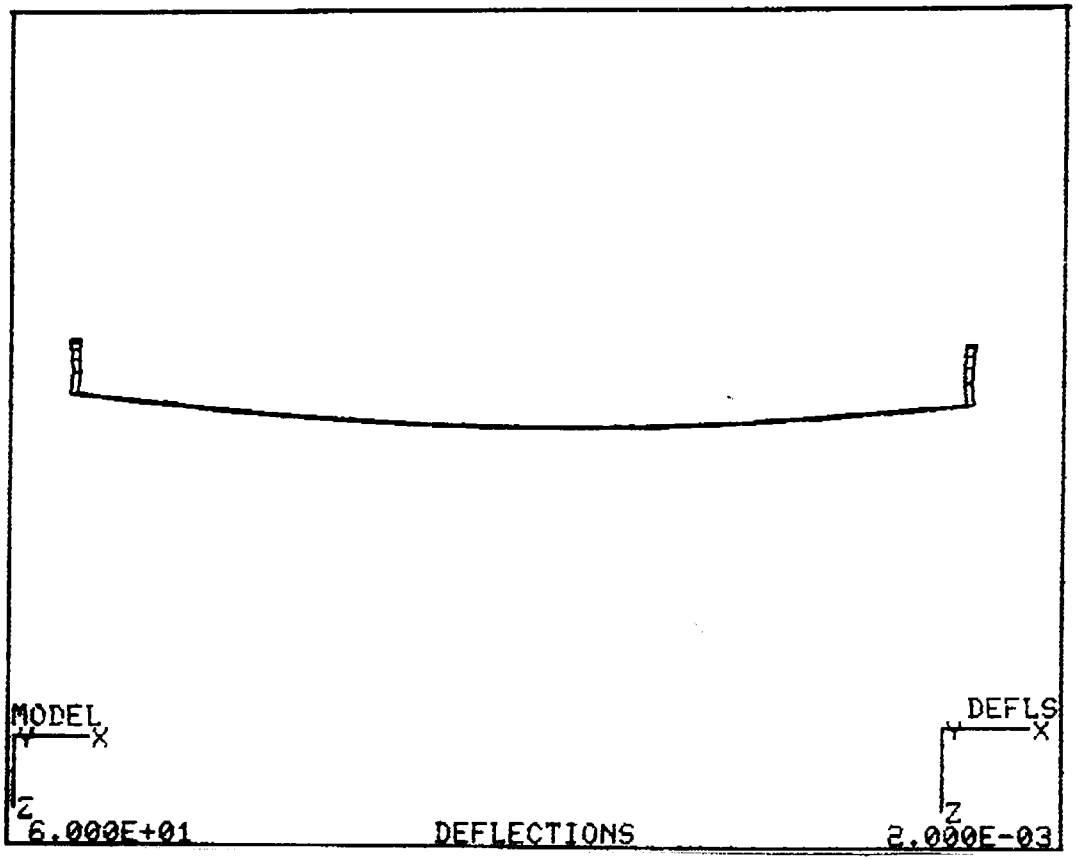

Figure 18. First Natural 3D Mode Shape for Tucson Monotube Structure (Plan View of Deflected Structure)

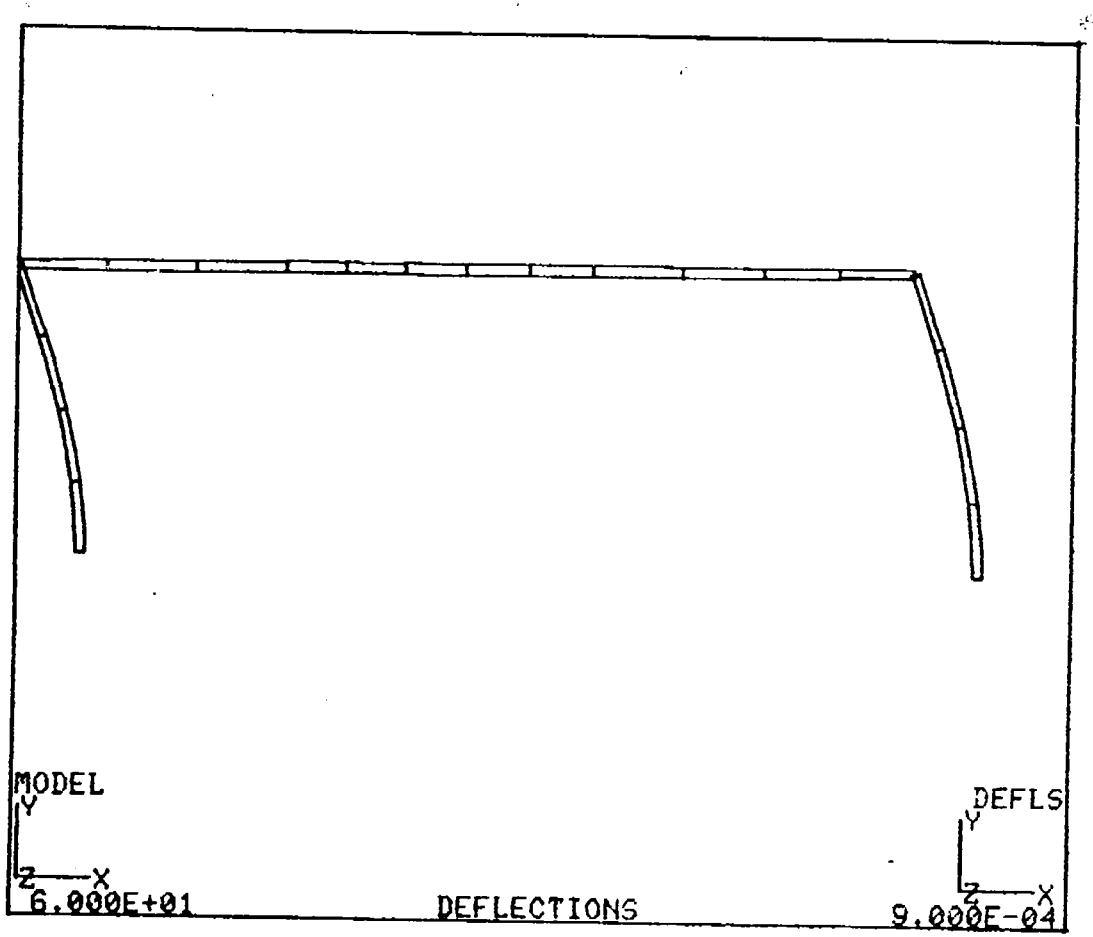

Figure 19. Second Natural 3D Mode Shape for Tucson Monotube Structure (Elevation of Deflected Structure)

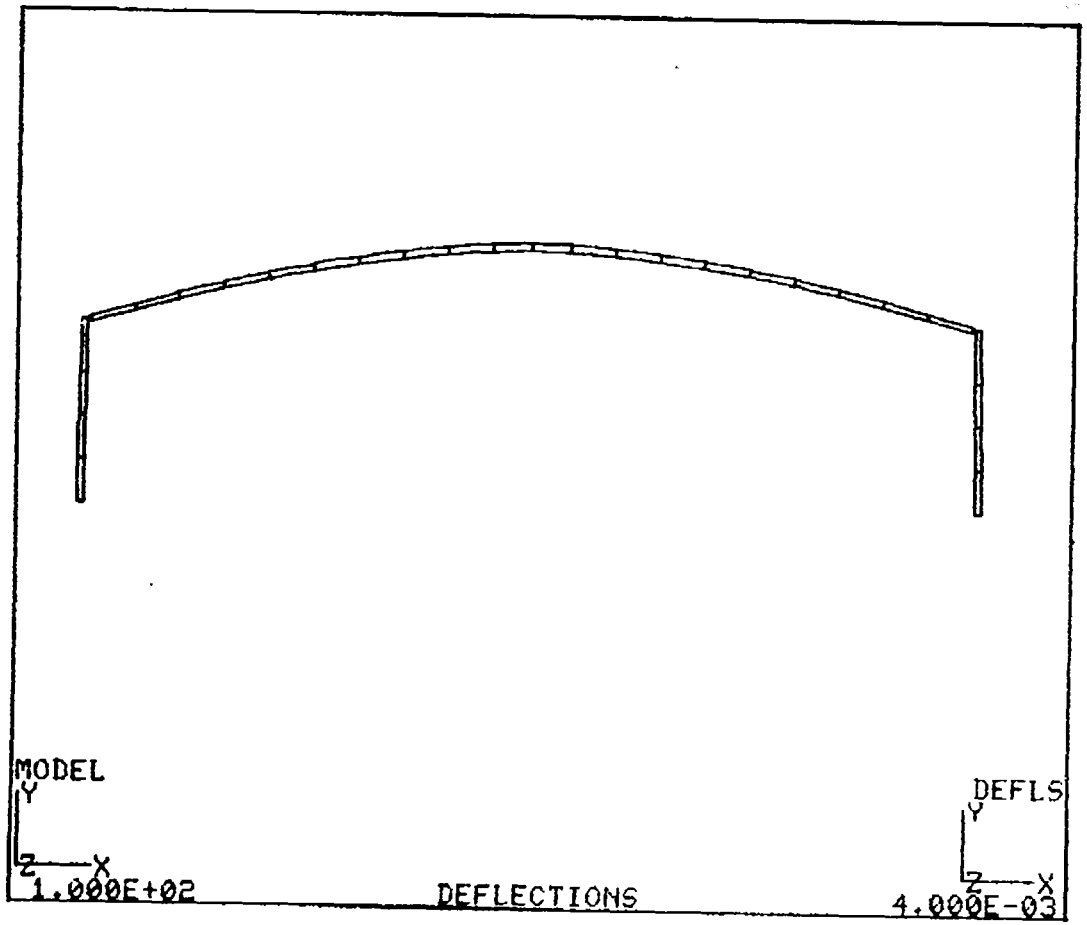

Figure 20. First Natural 3D Mode Shape for Phoenix Monotube Structure (Elevation of Deflected Structure)

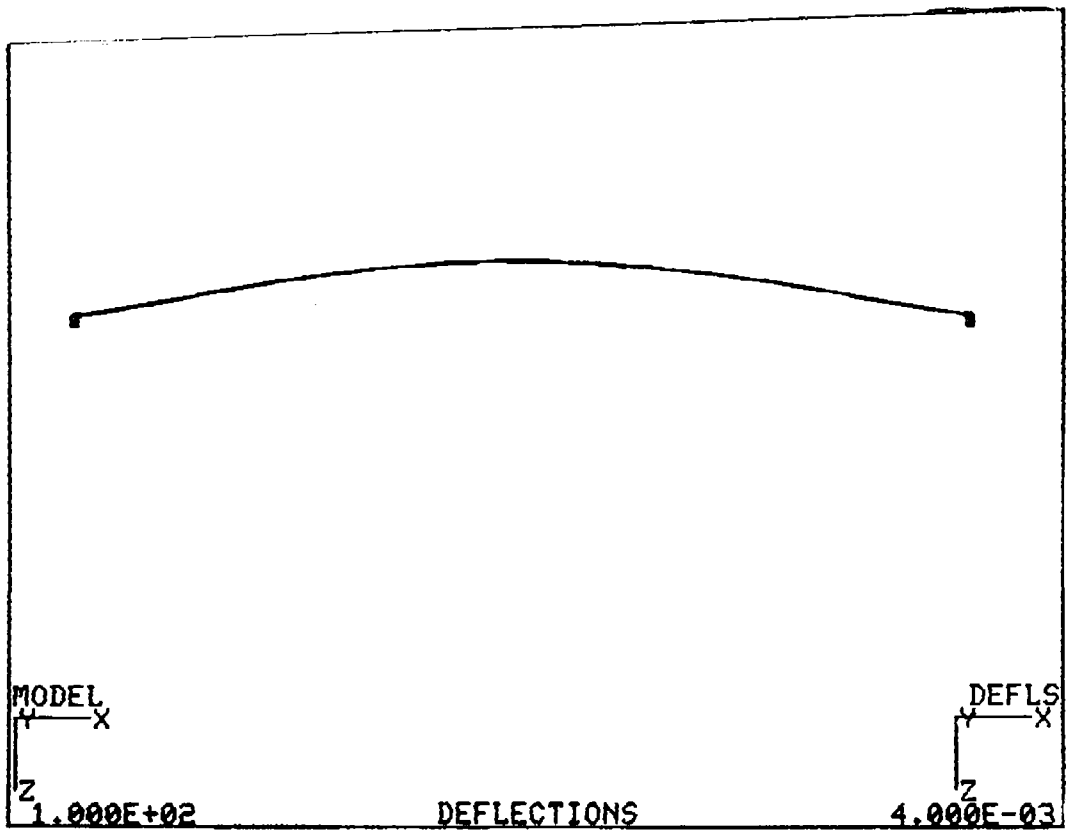

Figure 21. Second Natural 3D Mode Shape for Phoenix Monotube Structure (Plan View of Deflected Structure)

Phoenix structure. Similar to Fig. 17, the scales for the model and the deflections are given in the lower left and right corners of the figures, respectively. It should be understood that the deflected shapes shown do not indicate actual displacements, since the natural frequencies are not associated with any load. However, they do give an indication of the shapes that can be expected for a vabrating structure.

4.7 Static Load Results

Both models were analyzed for a combination of static loads. These loads included the weight of the strucutral elements, the weight of the signs, and the drag on the signs. The drag forces for various wind speeds are shown in Table 3a for the Tucson (60 ft) structure and in Table 3b for the Phoenix (100 ft) structure. These forces were applied at the attachment points of the signs.

For the wind speeds considered, the gravity loads due to the weight of the structure govern in all cases. The deflected shape of the structures can be seen in Fig. 22a and 22b. The vertical deflections due to gravity loads and static wind forces at the midspan of the beam are given in Tables 6a and 6b. It can be seen that they are identical in every case. The out-of-plane deflections did vary with the wind speed as shown in Tables 6a and 6b. However, the out-of-plane deflections are considerably smaller than the in-plane deflections. This is especially noteworthy in the case of the Tucson structure which has two relatively large signs. Even with these large signs, drag was not a major factor.

The stresses at midspan are also principally due to weight of the structure. The stress distributions for shear stress and normal stress at

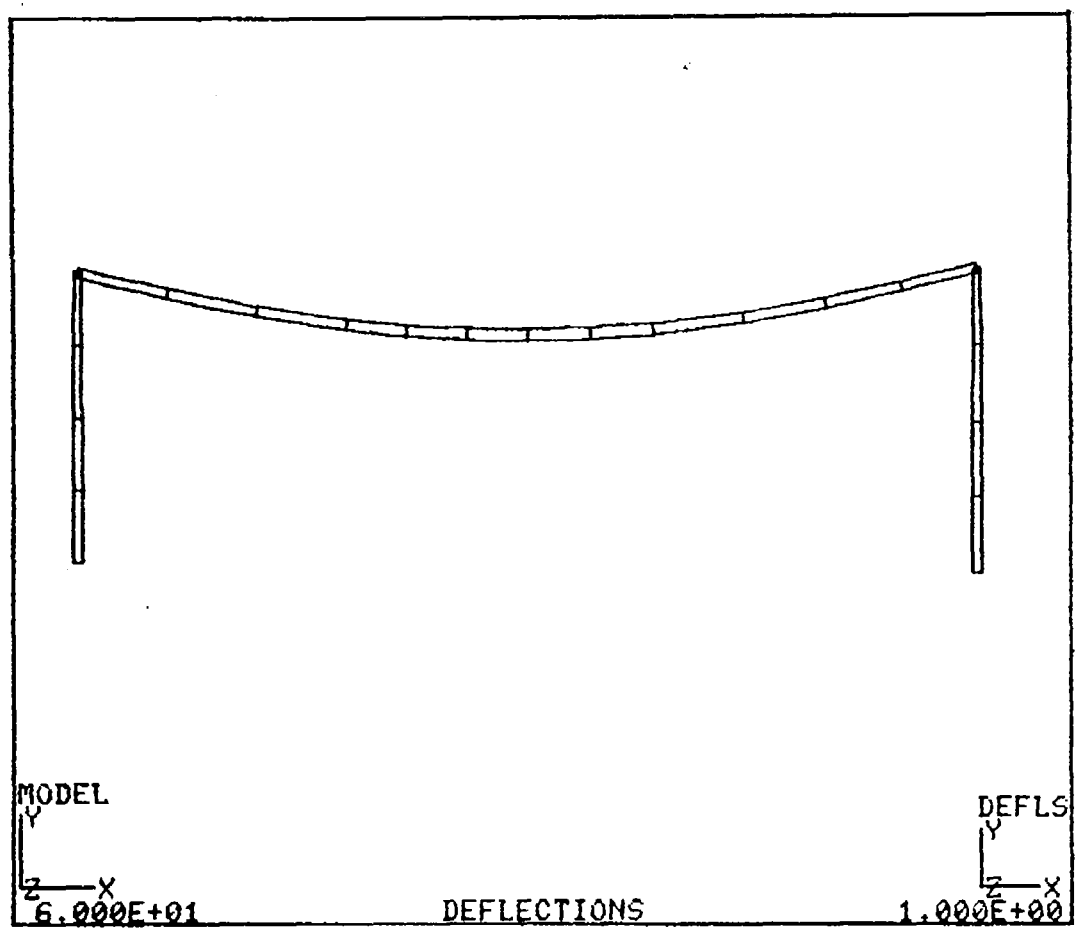

Figure 22a. Deflected Shape for Tucson Monotube Structure Subjected to Static Gravity Loads (Elevation of Deflected Structure)

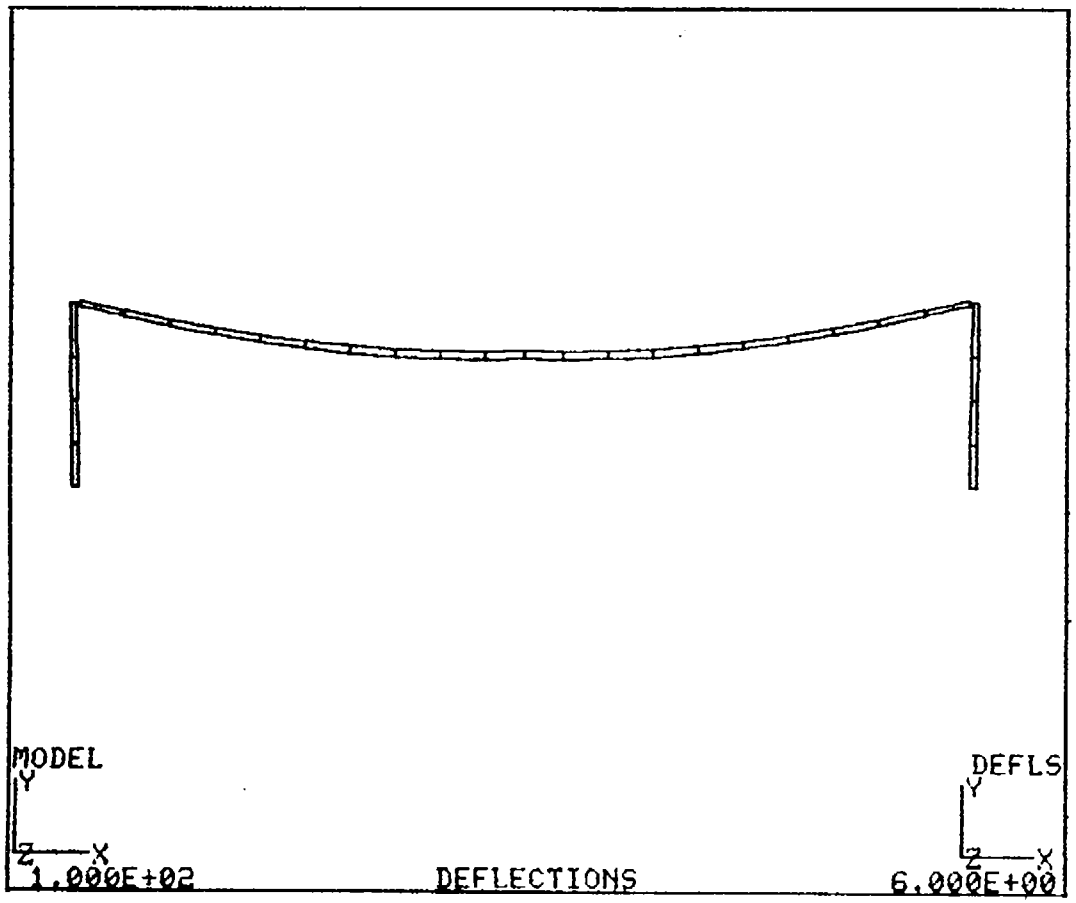

Figure 22b. Deflected Shape for Phoenix Monotube Structure Subjected to Static Gravity Loads (Elevation of Deflected Structure)

Table 6a. Midspan Deflections for Tucson Structure Due to Dead Load and Static Wind Forces (in.).

Wind Speed	Direction* x	y	z
2.5	0.002	1.123	0.008
5.0	0.001	1.123	0.019
7.5	0.001	1.123	0.038
10.0	0.001	1.123	0.065
12.5	0.001	1.123	0.099
15.0	0.001	1.123	0.141
17.5	0.001	1.123	0.190
20.0	0.000	1.123	0.247
22.5	0.000	1.123	0.312
23.2	0.000	1.123	0.331

*For labeling of x-, y- and z-axes, see Fig. 17a.

Table 6b. Midspan Deflections for Phoenix Structure Due to Dead Load and Static Wind Forces (in.).

Wind Speed	Direction* x	y	z
2.5	0.000	5.513	0.003
5.0	0.000	5.513	0.013
7.5	0.000	5.513	0.030
10.0	0.000	5.513	0.053
12.5	0.000	5.513	0.083
15.0	0.000	5.513	0.120
17.5	0.000	5.513	0.163
20.0	0.000	5.513	0.213
22.1	0.000	5.513	0.260

*For labeling of x-, y- and z-axes, see Fig. 17a.

midspan of the Tucson structure are shown in Fig. 23a. Figure 23b shows a similar plot for the Phoenix structure. The magnitudes of the stresses did not vary with the wind speed, but remained constant at the indicated values. For the Tucson structure, the maximum normal stress was ± 4.38 ksi, which is about 13% of the yield stress of 34 ksi. The magnitude of the normal stress for the Phoenix structure was 8.86 ksi, which is about 26% of the yield stress.

The stresses at the column base for the Tucson structure became larger as the wind speed increased. The stress for the Phoenix structure, however, remained close to constant. This is probably due to the larger sign area for the Tucson structure, which results in higher drag forces. The drag on the Phoenix signs appears to be negligible. The maximum normal stress at the column base for the Tucson structure is ± 1.34 ksi, and for the Phoenix structure ± 2.51 ksi. Both are well below the yield stress of the steel. The stress distributions at the column base are shown in Figs. 24a and 24b for the Tucson and Phoenix structures, respectively.

At the connection between the column and the beam, shear stress is the governing factor. For both structures, the finite element model showed some normal stress, but this is largely due to the way the joint was modeled rather than any actual stress. The shear stress at the joint was close to constant for both structures. The gravity loads appear to govern. For the Tucson structure the maximum shear stress is 2.64 ksi. For the Phoenix structure, it is 3.22 ksi. Both are well below the shear yield stress of the steel, which is 19.4 ksi. The shear stress

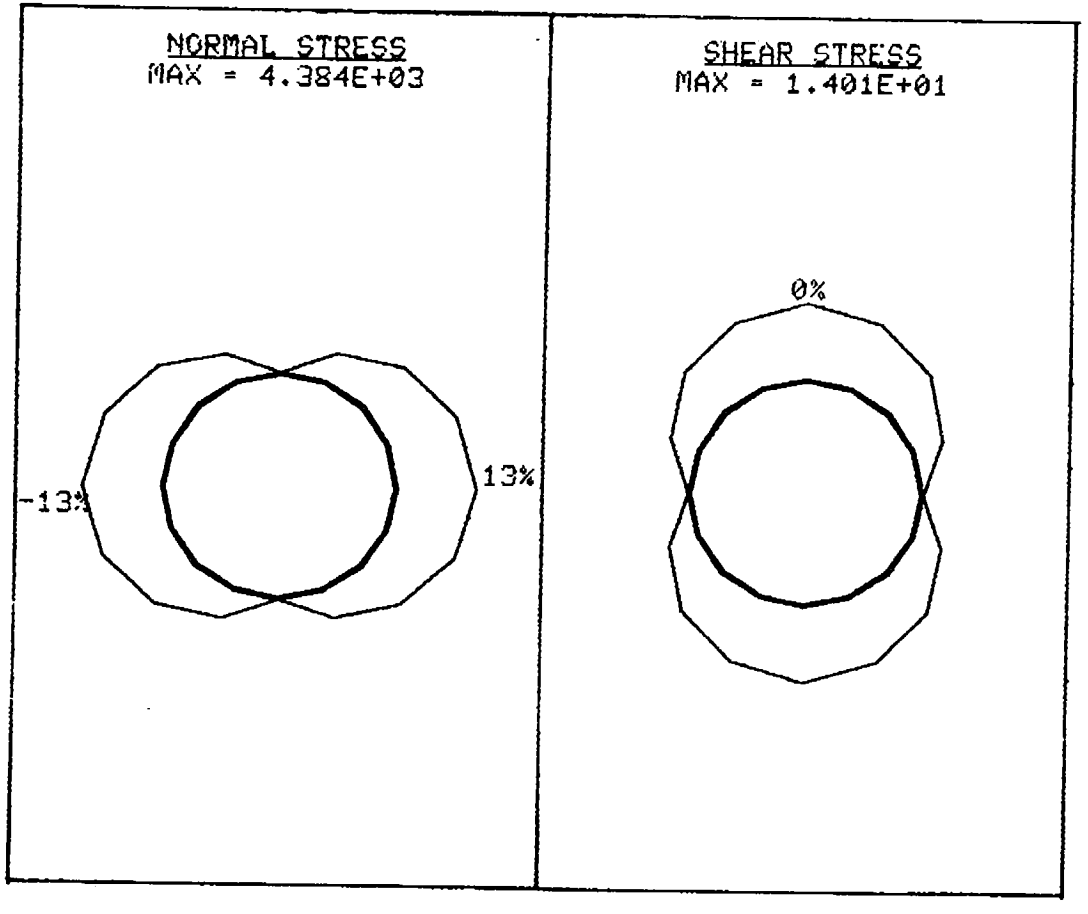

Figure 23a. Static Stresses at Midspan of Tucson Monotube Structure (psi)

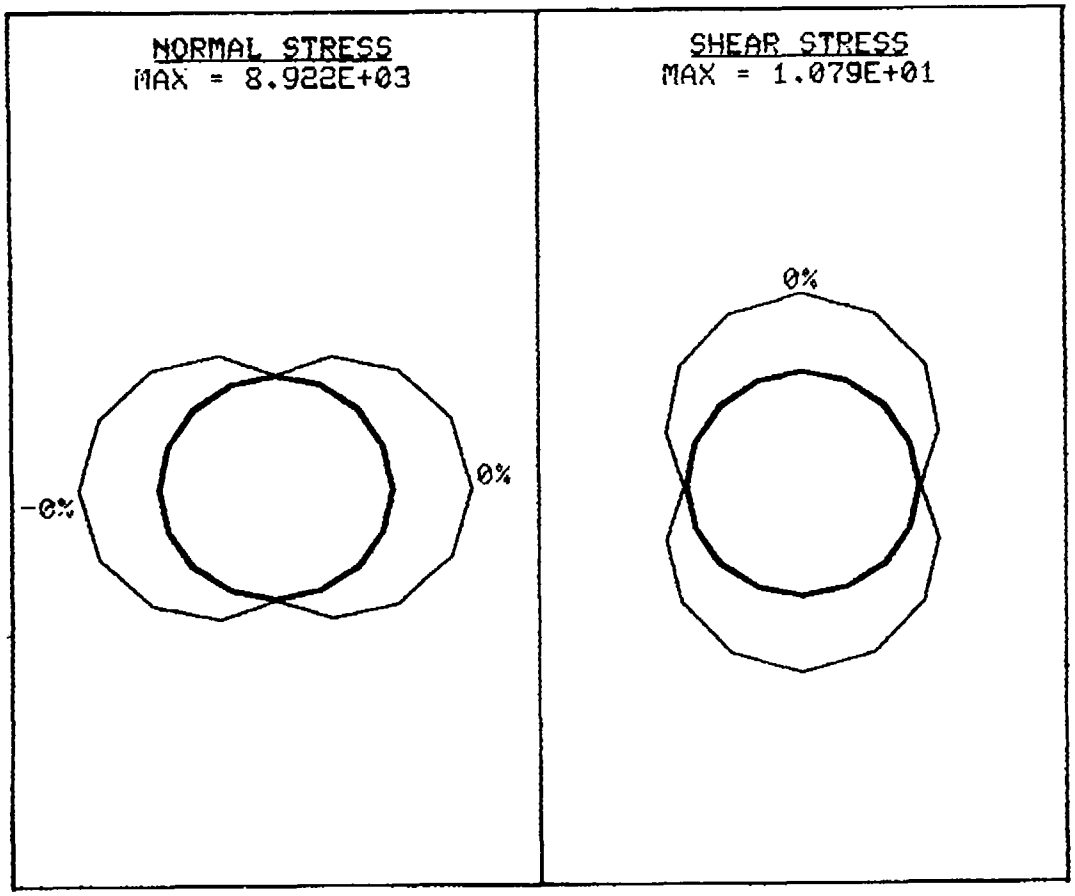

Figure 23b. Static Stresses at Midspan of Phoenix Monotube Structure (psi)

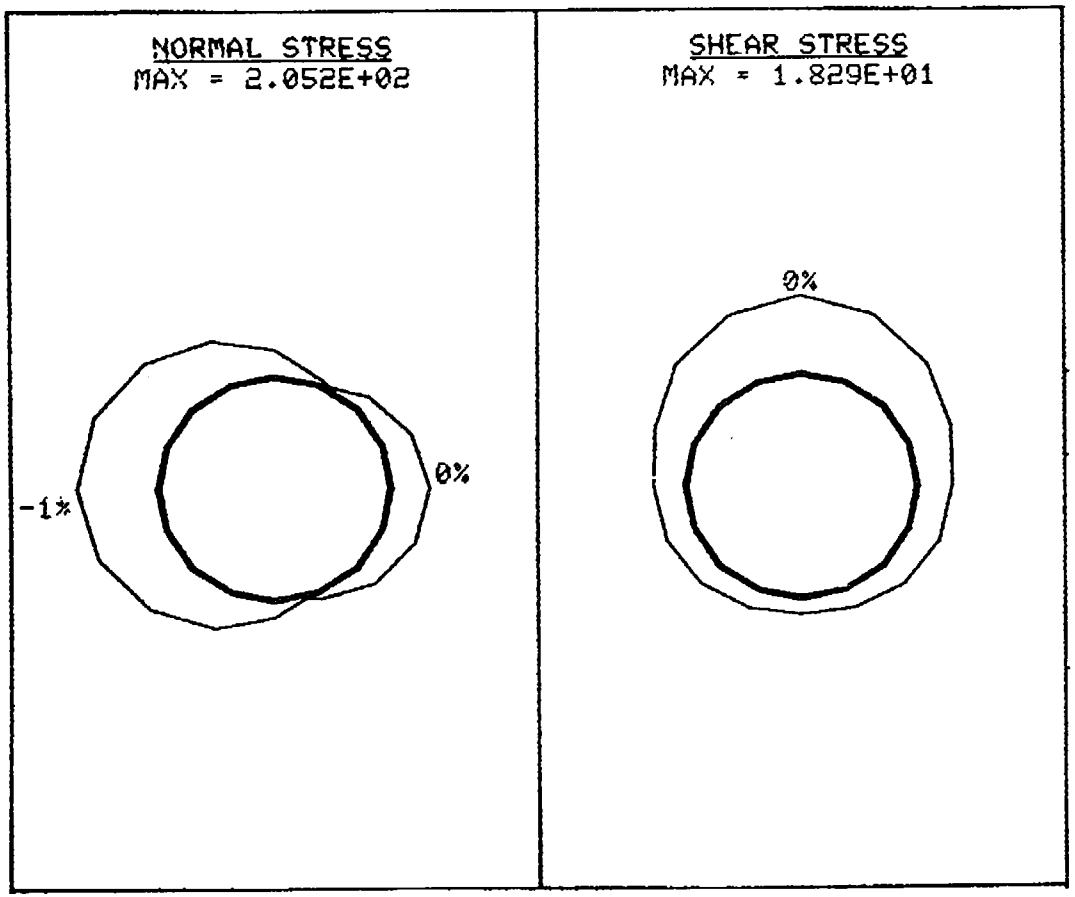

Figure 24a. Static Stresses at Column Base of Tucson Monotube Structure (psi)

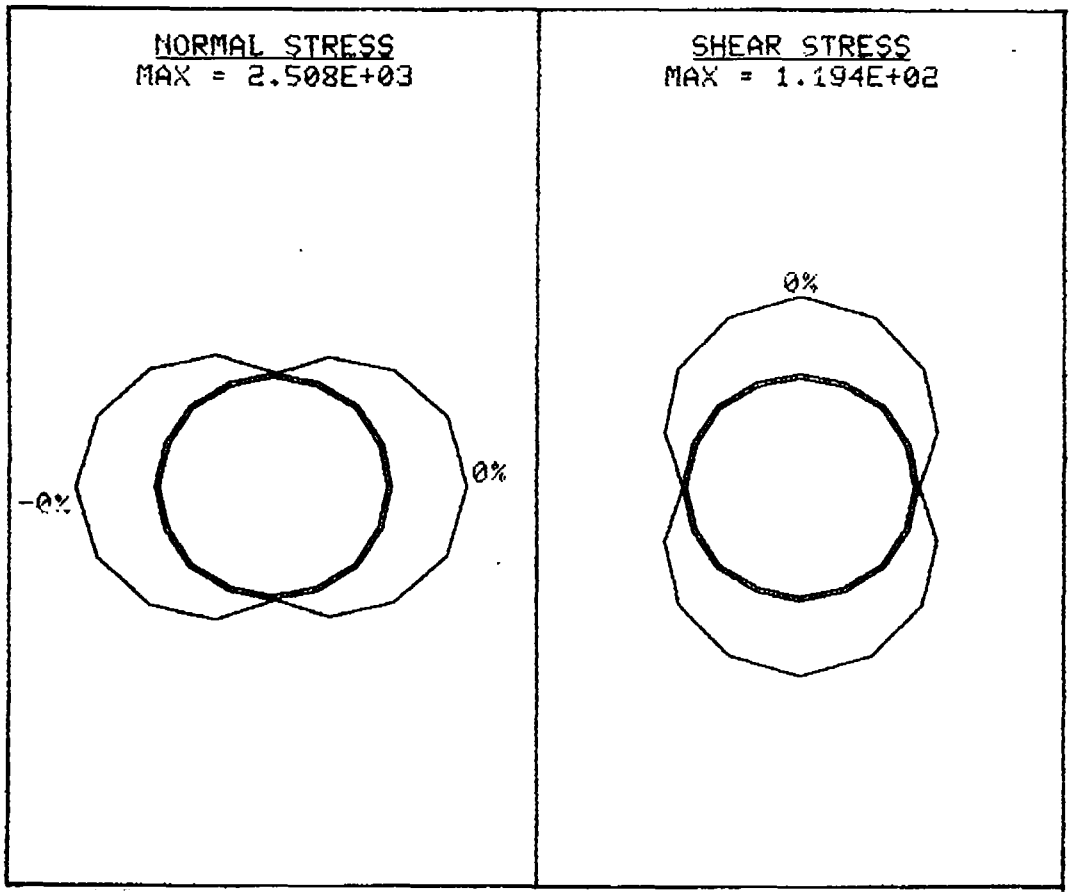

Figure 24b. Static Stresses at Column Base of Phoenix Monotube Structure (psi)

distributions are shown in Figs. 25a and 25b for the Tucson and Phoenix structures.

As has been seen, the stresses at the three critical locations on each structure are significantly below the representative yield values for the steel. For deflections, the Tucson structure has a sign depth of 7 ft., and the maximum allowable deflection according to the Specifications is:

$$\frac{d^2}{400} = \frac{7^2}{400} = 0.123 \text{ ft} = 1.48"$$

This compares to the actual value of 1.123 inches. For the Phoenix structure with 5-foot deep signs, the allowable deflection is:

$$\frac{d^2}{400} = \frac{5^2}{400} = 0.063 \text{ ft} = 0.76"$$

and the actual value is 5.513 inches. It is seen that whereas the Tucson structure satisfies the $d^2/400$ criterion, using 7-foot deep signs, the Phoenix structure with 5-foot signs exhibits a deflection very much in excess of the allowable. By the same token, however, it is also clear that if the Tucson structure were to utilize 5-foot deep signs, it, too, would violate the AASHTO deflection criterion.

4.8 Dynamic Load Results

The same models used for the static load tests were used for the dynamic load tests. The loads for these tests were determined using Eq. (4). The loads were calculated for the same wind speeds as those used in the static analysis.

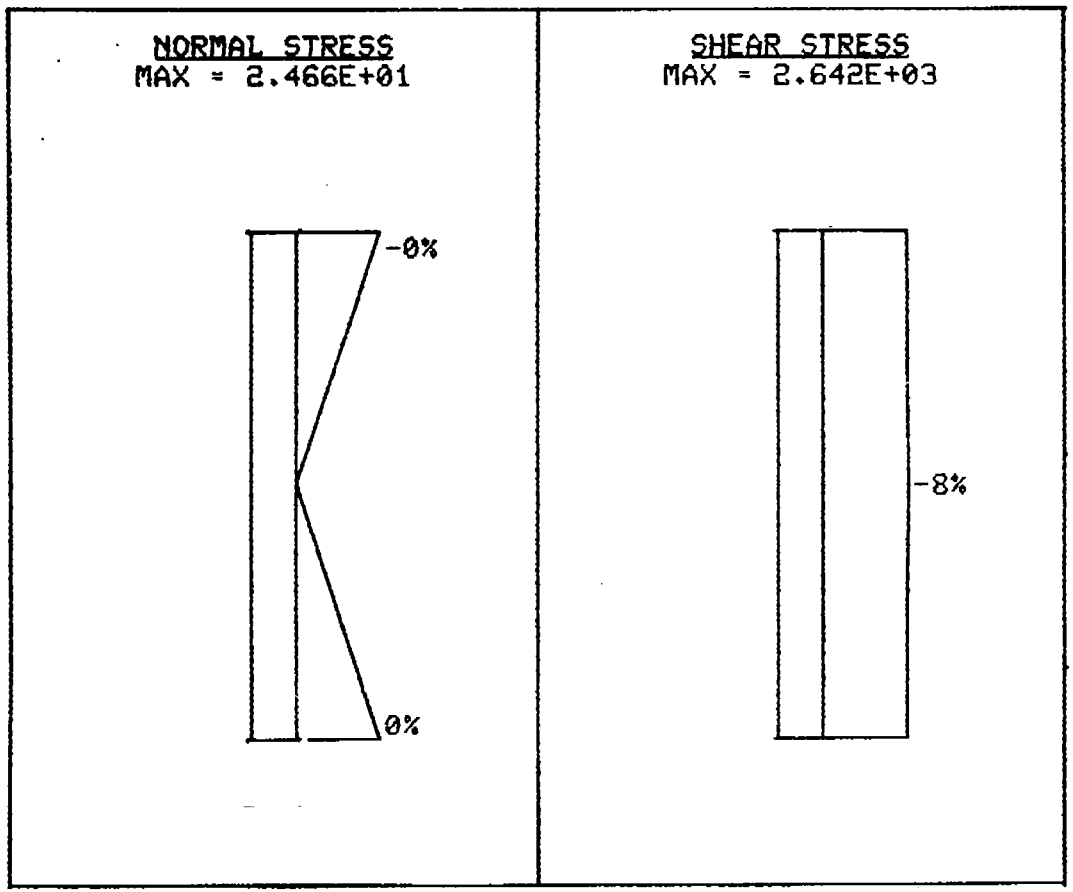

Figure 25a. Static Stresses at Joint of Tucson Monotube Structure (psi)

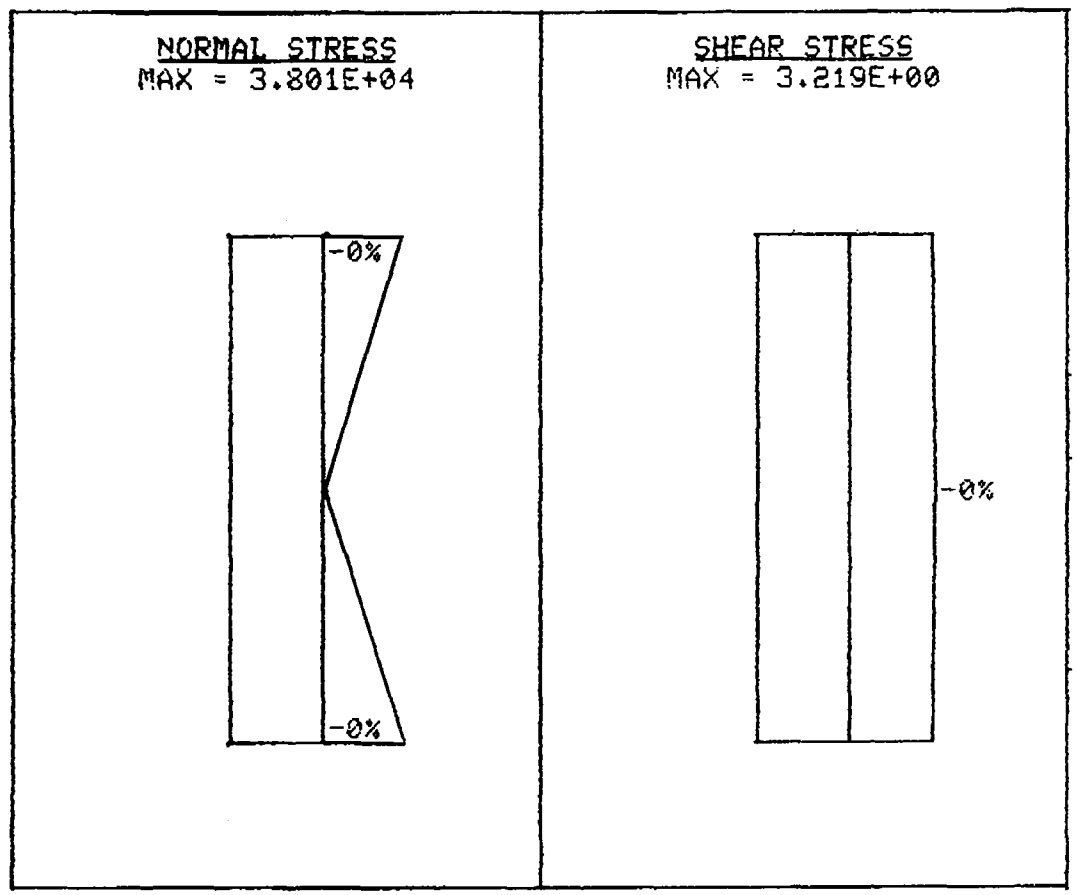

Figure 25b. Static Stresses at Joint of Phoenix Monotube Structure (psi)

Initially, the loading included only those loads calculated from Eq. (4) and the drag forces on the signs. The transient analysis was conducted over a time period of 32 seconds, with the loads from the forcing function input at 0.5 second intervals. The weight of the structure was not included in these analyses.

In order to determine the critical stress levels for each wind speed, a histogram for various points was constructed, using the GIFTS modules. Points considered included the midspan of the beam for in-plane deflections, and the top of the left column for out-of-plane deflections. A typical histogram is shown in Fig. 26.

From the histogram, the times of the maximum deflections were determined, and the corresponding stresses are shown in Tables 7a and 7b. From Table 7a, it is apparent that the column base is the most critical point for the Tucson structure. However, Table 7b indicates that the critical point on the Phoenix structure is at the midspan of the beam. This shift in the critical location is probably due to the larger relative stiffness of the beam in the Tucson structure. The average moment of inertia, I_{ave} for the beam of the Tucson structure is 206.6 in^4, while for the Phoenix structures it is 261.5 in^4. If the stiffness is defined as I_{ave}/L, then the stiffness of the Tucson sign is 206.6/(60*12) = 0.29. The corresponding values for the Phoenix structure's beam is 261.5/(100*12) = 0.22. For a simply supported beam, a larger stiffness will result in a lower stress level for a given load, thus the stresses at the midspan of the Tucson structure are relatively less critical than for the Phoenix structure.

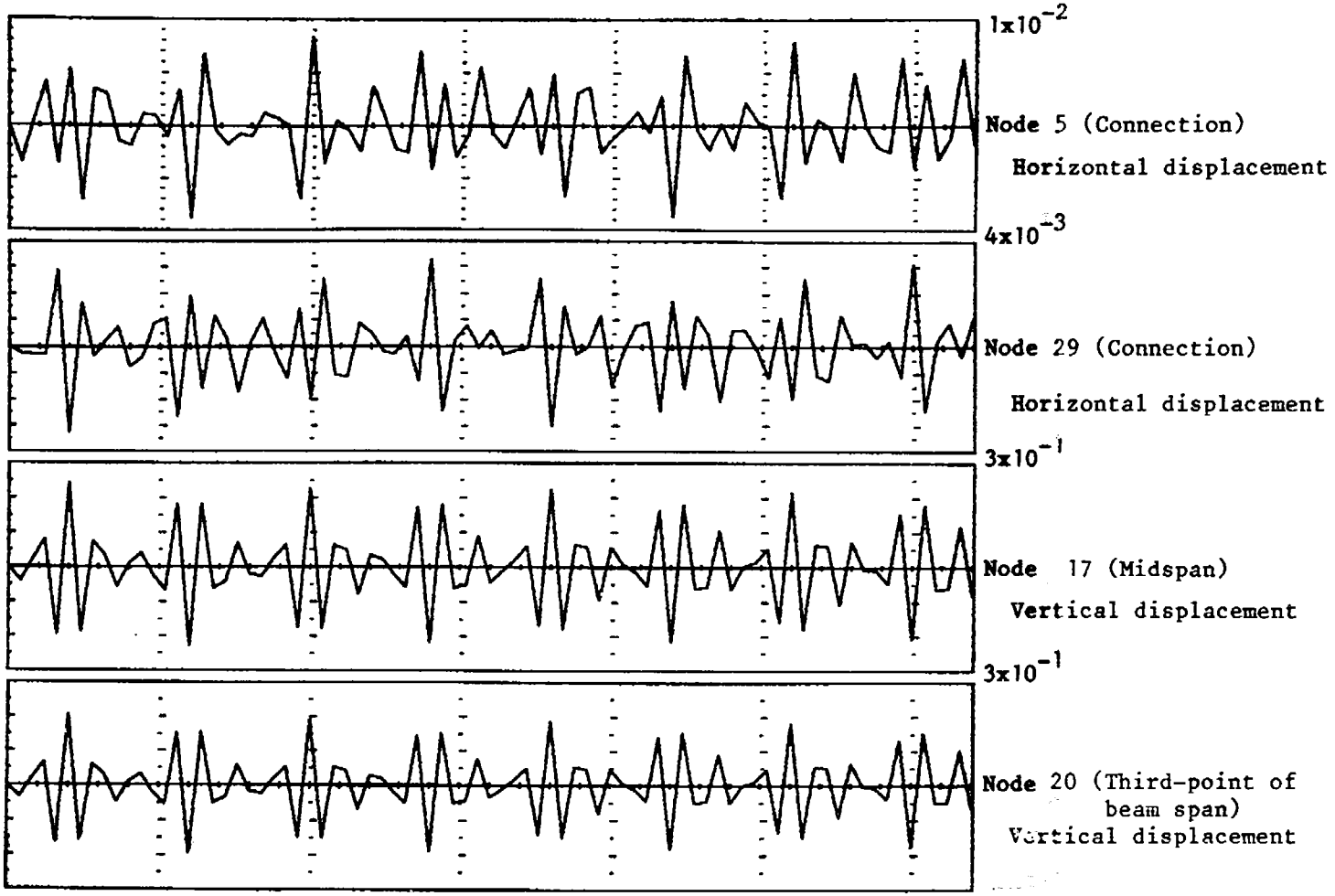

Figure 26. Typical Histogram for Dynamic Analysis of Monotube Structures
Horizontal scale is time (seconds); Vertical scale is displacement (inches)

Table 7a. Stresses at Critical Points for Dynamic Analysis of Tucson Structure (ksi).

Wind Speed	Shear at Node 5	Normal at Node 1	Normal at Node 17
2.5	0.005	0.019	0.012
5.0	0.028	0.036	0.048
7.5	0.026	0.078	0.540
10.0	0.038	0.148	0.095
12.5	0.025	0.174	0.101
15.0	0.042	0.265	0.157
17.5	0.053	0.357	0.210
20.0	0.072	0.474	0.276
22.5	0.026	0.595	0.329
23.2	0.128	1.301	0.727

Table 7b. Stresses at Critical Points for Dynamic Analysis of Phoenix Structure (ksi).

Wind Speed	Shear at Node 5	Normal at Node 1	Normal at Node 16
2.5	0.005	0.009	0.017
5.0	0.017	0.020	0.038
7.5	0.025	0.029	0.071
10.0	0.051	0.068	0.125
12.5	0.163	0.196	0.314
15.0	0.186	0.252	0.483
17.5	0.159	0.206	0.330
20.0	0.246	0.270	0.525
22.1	0.252	0.330	0.674

Another factor may be the size of the signs. The signs on the Tucson structure are significantly larger than on the Phoenix structure. The moment induced at the base by the drag on the signs will be much larger than the moment induced at midpsan. This will cause a greater stress at the column base.

An interesting development occurs between the wind speeds of 22.5 mph and 23.2 mph for the Tucson structure. The stresses more than double for the small increase in wind speed. This does not occur at any other wind speed. The deflections also show a disproportionate increase in their magnitude. This increase is due to the beam approaching one of its natural frequencies. Prior studies (2,3) indicated that a structure with this member diameter ($\approx$14") would have a natural frequency at a wind speed of approximately 23 mph.

Because the beam is simply supported, it can be considered to act by itself. For the wind speed of 23.2 mph, the beam vibrates at a frequency of 5.94 cps. The second 3D natural frequency of the beam is 6.44 cps. The deflections and stresses increase as the structural frequency approaches a natural frequency.

Another interesting phenomenon occurs for both the Tucson and Phoenix structures. For various wind speeds, the histogram for the node at the midspan of the beam shows a periodic vertical deflection. This is shown in Fig. 27. The frequency of these oscillations is very low (between 0.082 to 0.165 cps). These are well below any of the natural frequencies, nor do they cause excessive stresses or deflections, as would be expected of a natural frequency. These oscillations appear to have been caused by the

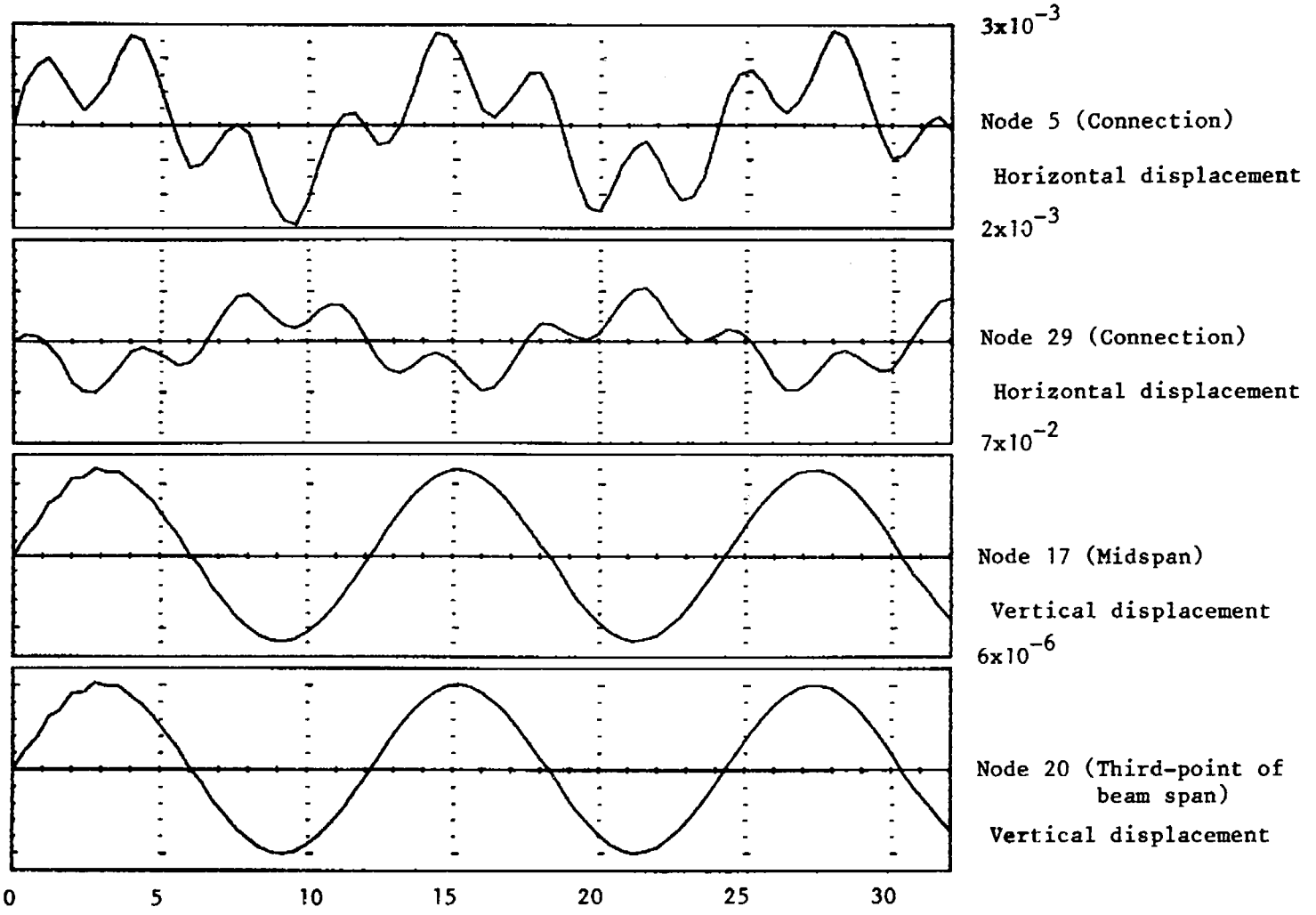

Figure 27. Periodic Histogram for Dynamic Analysis of Monotube Structures
Horizontal scale is time (seconds); Vertical scale is displacement (inches)

0.5 sec. time step chosen in the transient analysis. However, if these oscillations are real, additional studies are needed to determine their effect on the fatigue strength of the structure. The wind speeds for which these periodic oscillations occur are shown in Table 8.

The results discussed so far are somewhat misleading. For the dynamic analysis, the mass of the structure was not considered. However, the mass of the structure will increase the inertia of the vibrating structure. This may increase the deflections and stresses experienced by the structure. Therefore, additional computer analyses were run to include the mass of the structure.

The maximum stresses for each wind speed are given in Tables 9a and 9b for the three critical points on each structure. It is interesting to note that for both structures the magnitudes of the maximum stresses equal the superimposed stresses from the static analysis and the first dynamic analysis. This can render the dynamic analysis simpler by removing the structural mass from the calculations. A simple static analysis will take care of that.

The deflections can also be superimposed. The deflections caused by the self weight (= dead load) dominate. The maximum deflections for the various wind speeds are given in Tables 10a and 10b.

4.9 Conclusions for Analytical Studies

From this, it can be seen that the monotube structures as modeled are safe for the wind speeds considered. The maximum stresses were less than 40% of the yield stress in all cases. The possibility of fatigue failure warrants further study, especially where the periodic oscillations occur.

Table 8. Wind Speeds (mph) for which Periodic Oscillation Occur in the Beam.

Tucson (60')	Phoenix (100')
10.0	7.5
17.5	10.0
20.0	17.5
	20.0

Table 9a. Stresses (ksi) for Tucson Structure for Dynamic Loading with Structure Mass.

Wind Speed (mph)	Shear at Beam End	Normal at Column Base	Normal at Beam Midspan
2.5	2.64	1.34	4.38
5.0	2.64	1.34	4.38
7.5	2.64	1.35	4.39
10.0	2.65	1.48	4.39
12.5	2.66	1.65	4.49
15.0	2.70	1.61	4.54
17.5	2.78	1.70	4.59
20.0	2.82	1.81	4.66
22.5	2.87	1.93	4.71
23.2	3.12	2.64	5.11

Table 9b. Stresses (ksi) for Phoenix Structure for Dynamic Loading with Structure Mass.

Wind Speed (mph)	Shear at Beam End	Normal at Column Base	Normal at Beam Midspan
2.5	0.04	2.84	10.11
5.0	0.05	2.87	10.18
7.5	0.07	2.91	10.23
10.0	0.09	2.95	10.29
12.5	0.22	3.11	10.51
15.0	0.22	3.16	10.70
17.5	0.25	3.12	10.53
20.0	0.32	3.19	10.75
22.1	0.32	3.25	10.92

Table 10a. Vertical Downwards Deflections at Midspan for Tucson Structure with Structure Mass.

Wind Speed (mph)	Deflection (in.)
2.5	1.12
5.0	1.13
7.5	1.13
10.0	1.14
12.5	1.13
15.0	1.14
17.5	1.14
20.0	1.15
22.5	1.16
23.2	1.18

Table 10b. Vertical Downwards Deflections at Midspan for Phoenix Structure with Structure Mass.

Wind Speed (mph)	Deflection (in.)
2.5	5.52
5.0	5.53
7.5	5.55
10.0	5.55
12.5	5.63
15.0	5.75
17.5	5.65
20.0	5.74
22.1	5.86

Neither of the structures modeled meets the $d^2/400$ deflection limitation. Since the stress levels were low, even for the large deflections computed, this indicates that the $d^2/400$ limitation may be unnecessarily restrictive when applied to monotube structures.

As stated previously, these parametric studies are only as accurate as the data used to model the structures and forces. The results presented in this chapter must be compared with the results of the full-scale field testing discussed in Chapter 5.

Chapter 5

FIELD TESTING OF FULL-SCALE STRUCTURES

The second phase of the research study consisted of the testing of actual sign support structures under service conditions. This was accomplished by instrumenting two structures with electrical resistance strain gages, as well as an anemometer to determine wind velocity and direction. The data were used to determine the stresses and strains at a number of important locations in the structures, and subsequently to evaluate the correlation between theoretical and actual structural performance.

5.1 Description of Equipment and Software

The equipment used for the field testing can be categorized into two main groups: The first was the portable equipment used for the data collection, and included all sensors, electrical hardware and software used in obtaining data directly from the structures. The second group consisted of the equipment that was used for data reduction. This included all the electrical hardware and software that was utilized to manipulate and analyze the collected data. The data collection group can be further subdivided into six sections; namely, sensors, data acquisition, control, mass storage, communications, and support.

The sensors are the strain gages and the anemometer. The gages were of the bonded electrical resistance foil type, with a resistance of 120 $\pm$ 0.3 Ω, a gage length of 10 mm, and a gage factor of 2.12. A typical gage is shown in Fig. 28. The anemometer was a Weathertronics Combination Wind

Sensor, Model 2132, consisting of 3 standard anemometer cups connected to an AC generator, and a weather vane connected to a DC potentiometer. This unit can be seen in Fig. 29.

The data acquisition equipment was of crucial importance to the success of the field work. To read the strain gages as well as the anemometer, a Hewlett Packard (HP) Data Acquisition and Control Unit, Model 3421A, was used. This can measure AC and DC voltages, resistances, and amperages, and can also be used to control other devices. It also has a built-in power output that may be utilized to run peripheral devices. The unit can accept input from twenty different sources or channels. For the field measurements of this project, 16 channels were used by the strain gages, 1 by the wind speed sensor, and 1 by the wind direction sensor, for a total of 18.

The control unit of the data collection group was an HP-41CX calculator. This is a user programmable calculator whose software had been designed to control the data collection activities and a number of arithmetic functions. The calculator has a built-in clock and calendar, making it possible to record the data and time of each reading of the gages. The data were initially stored in the calculator's memory and subsequently transferred to the mass storage unit.

The software used by the HP-41CX was originally written by Geotechnical Engineering and Mining Services, Inc. of Littleton, Colorado. However, it was found necessary to modify portions of the code to better perform the required tasks. A complete listing of this software is given in Appendix A.

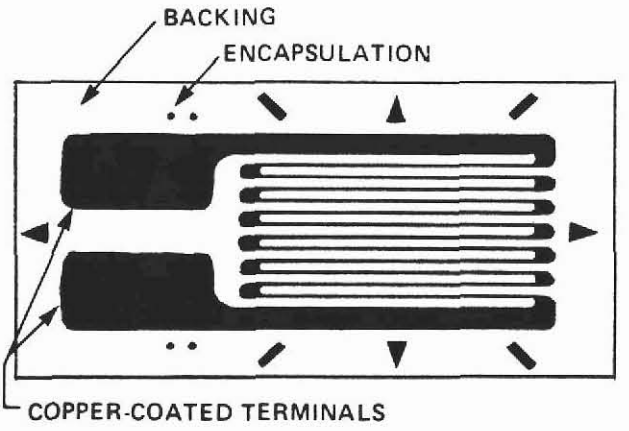

Figure 28. Typical Strain Gage

Figure 29. Anemometer Mounted on Structure

After the strain gages were read, the readings were stored in the calculator's memory. When this memory was full, the readings were transferred to the mass storage unit, an HP Model 82161A cassette drive. This tape drive uses micro-cassettes to record the data, and each cassette can store about 128 Kb of data, or slightly over 16,000 numbers.

The HP-3421A, -41CX, and tape drive were arranged to communicate by means of a HP Interface Loop (HP-IL). This is a serial loop that is controlled by the HP-IL module which is connected to the HP-41CX. Through this loop, directions and data are sent from one device to another. As this is a serial loop, any device that is shut off or disconnected will interrupt data flow in the loop.

The support equipment consisted of a multi-channel DC power supply, a Wheatstone Bridge circuit board, a 5 HP, 2000 Watt portable generator, and a radial blower. The power supply was used to provide a voltage to the gages and the wind direction potentiometer. The Wheatstone Bridge circuits were connected to the strain gages to form quarter bridges. This will be discussed in detail later in this chapter. The portable generator was needed to provide power at the remote testing sites, and the blower was necessory to keep the power supply from overheating. Figure 30 shows the 3421A, 41CX, tape drive, power supply, Wheatstone Bridge board, and blower.

The data reduction equipment group comprised of the following items: an HP Model 9836 (Series 200) desk top computer, an HP Model 82169A HP-IL/HP-IB interface, an HP 82905B dot-matrix printer, and an HP Model 7470A two-pen plotter.

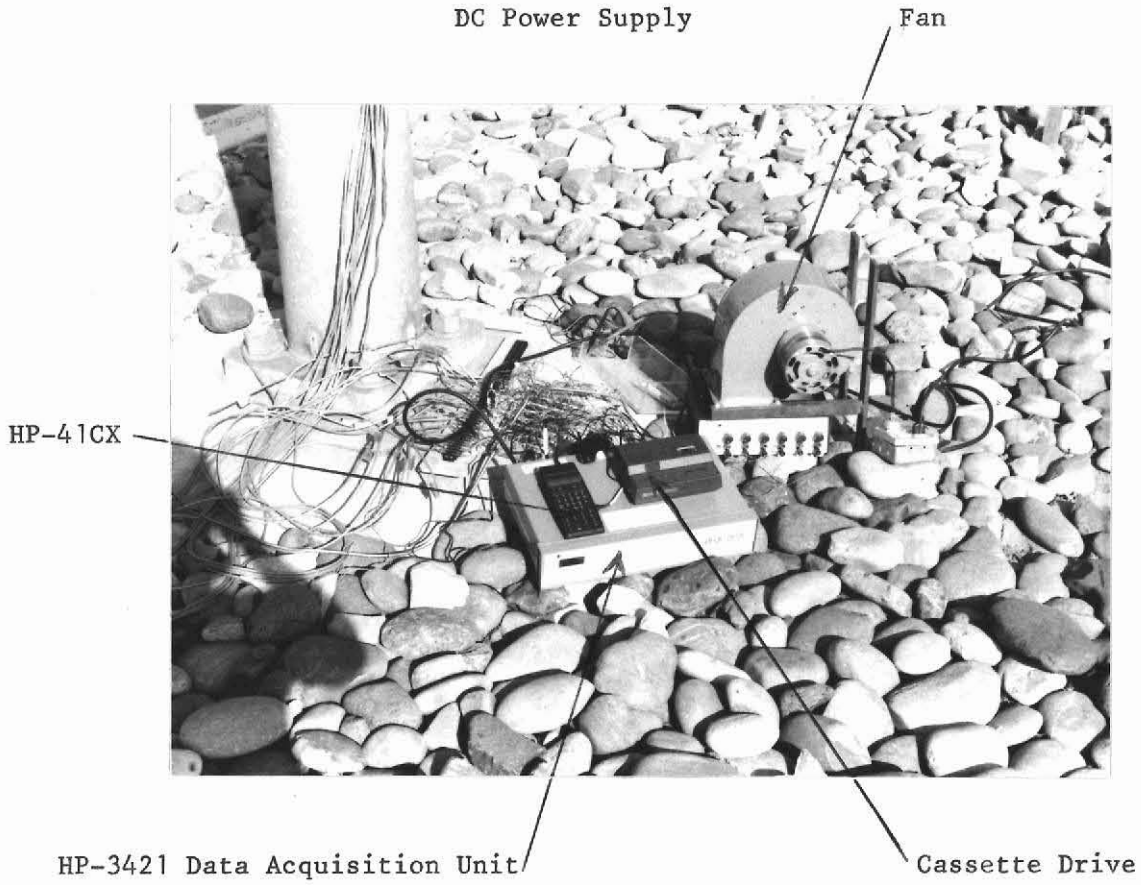

Figure 30. Data Acquisition Equipment

The HP-9836 computer was equipped with two 270 Kb double-sided disk drives, and 640 Kb of random access memory. It communicated with peripheral devices through the Hewlett-Packard Interface Bus (HP-IB). The computer was used for all the computational work of the project, with the exception of running the GIFTS program.

The dot-matrix printer and the plotter are HP-IB peripheral devices and were used to obtain hard copy output of the information generated by the HP-9836.

The HP-IL/HP-IB interface allows an HP-IL device to communicate with an HP-IB device. It can be operated with a controller on the HP-IL side, the HP-IB side, or in "mailbox" mode, where controllers exist on both sides. The latter approach was chosen for this project. Thus, the interface was used to allow data that were stored on the micro-cassette to be transferred to the HP-9836 for storage on 5-1/4" floppy disks. The controller consisted of the HP-41CX calculator on the HP-IL side and the HP 9836 on the HP-IB side. The data transfer required that programs be run simultaneously on the HP-41CX and the HP-9836. These are listed in Appendix B.

5.2 Procedure for Gage Installation

A total of 16 gages were attached to each structure. They were mounted in groups of four at the following locations: midspan of the beam, end of the beam, top of the column, and base of the column. The gages were arranged around the perimeter of the tube at 90^{o} intervals such that one

pair of gages measured in-plane strains and the other pair measured out-of-plane strains. The locations of the gages are indicated in Fig. 31.

The gages were installed in accordance with normal procedures (10), with the exception that Elmer's "Dura-Bond" contact cement was used instead of the suggested adhesive. This was done to facilitate gage installation in the field. Otherwise, the installation followed common procedures for cleaning of the steel, aligning and bonding of the gages, and so on.

Once the gages were installed, cables were soldered to the gage leads to connect them to the data acquisition unit. On the Tucson structure, a quarter bridge using two wires, as shown in Fig. 32a, was utilized. On the Phoenix structure, a quarter bridge was again used, but this time with a three-wire circuit, as shown in Fig. 32b. The three-wire arrangement helps eliminate the effect of lead wire resistance on the gage readings. After the cables had been attached, the gages were further protected by applying a covering of paraffin wax. Figure 33a shows a gage with the cables attached, and Fig. 33b shows the same gage after the wax has been applied.

5.3 Theory of Strain Gage Operation

The operational function of an electrical strain gage is based on Ohm's Law (15), which states that

$$V = IR \tag{6}$$

where V is voltage, I is current in amperes, and R is the resistance in ohms. For a constant I, a change in the resistance will cause a proportional change in the voltage. The electrical strain gage functions

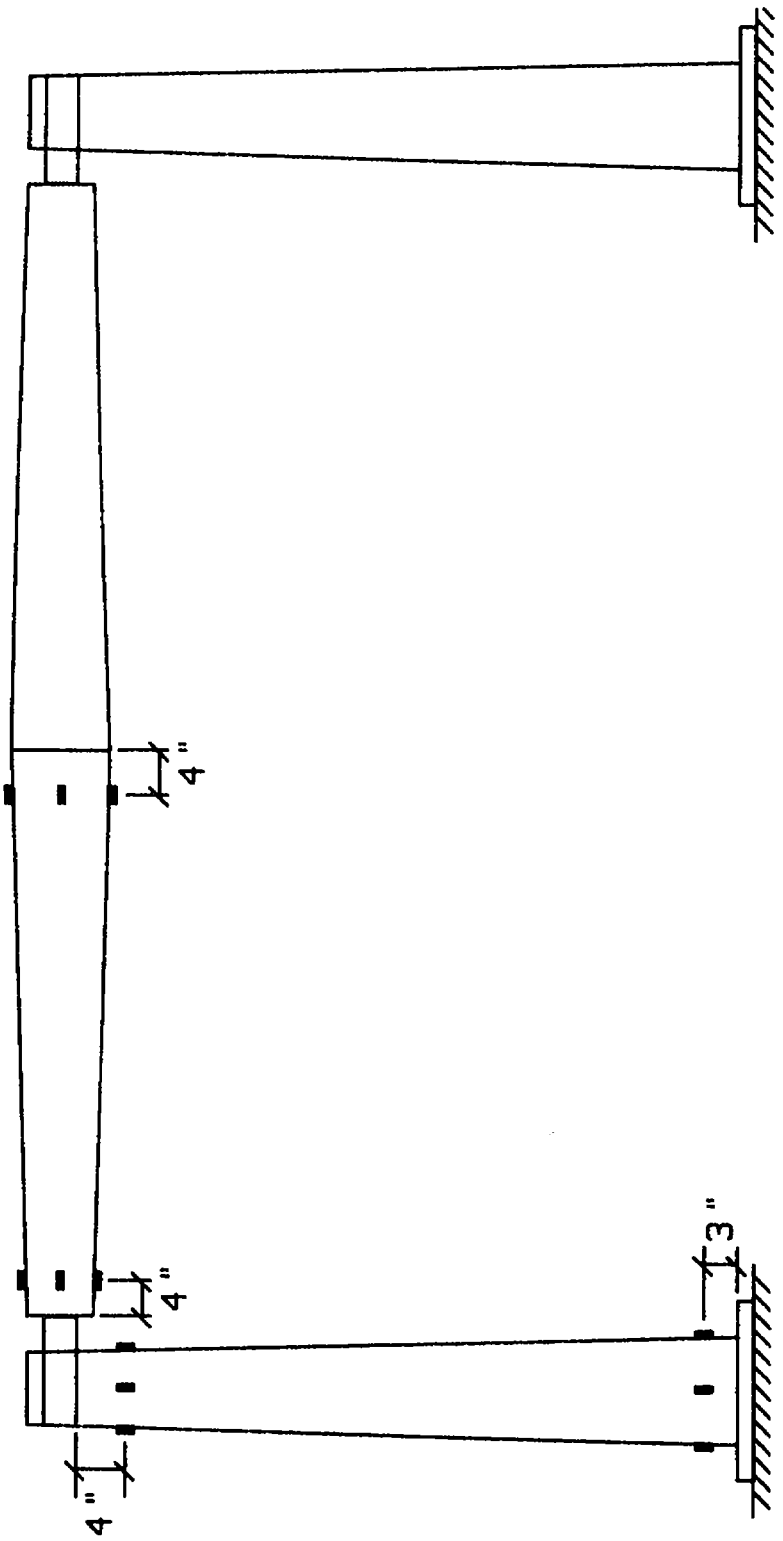

Figure 31. Locations of Strain Gages on Monotube Structure

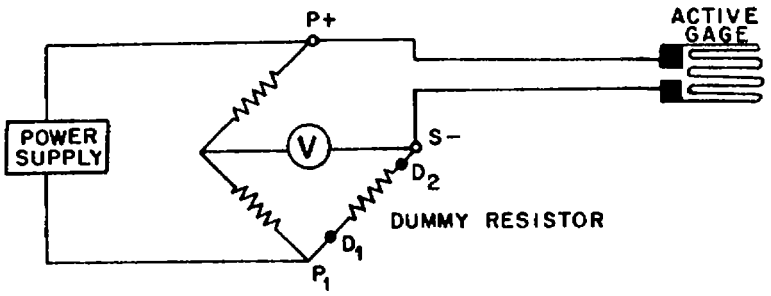

Figure 32a. Two-Wire Quarter Bridge Circuit

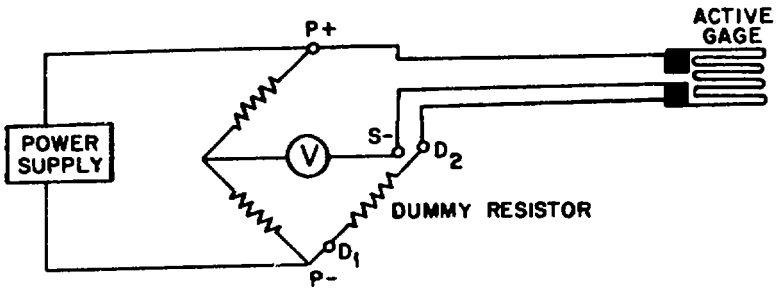

Figure 32b. Three-Wire Quarter Bridge Circuit

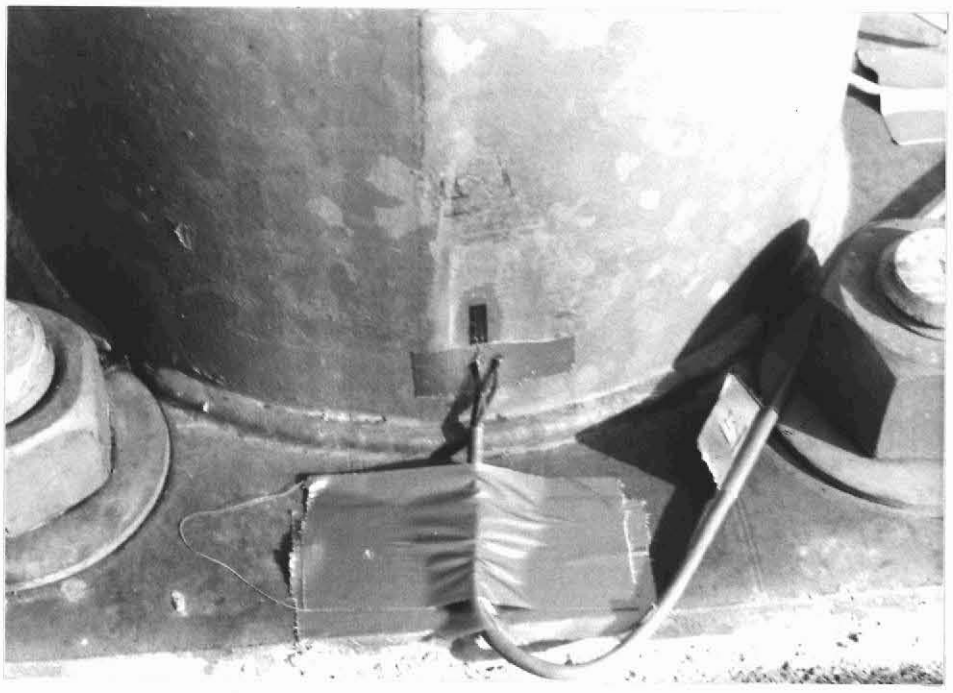

Figure 33a. Mounted Strain Gage with Cable Attached

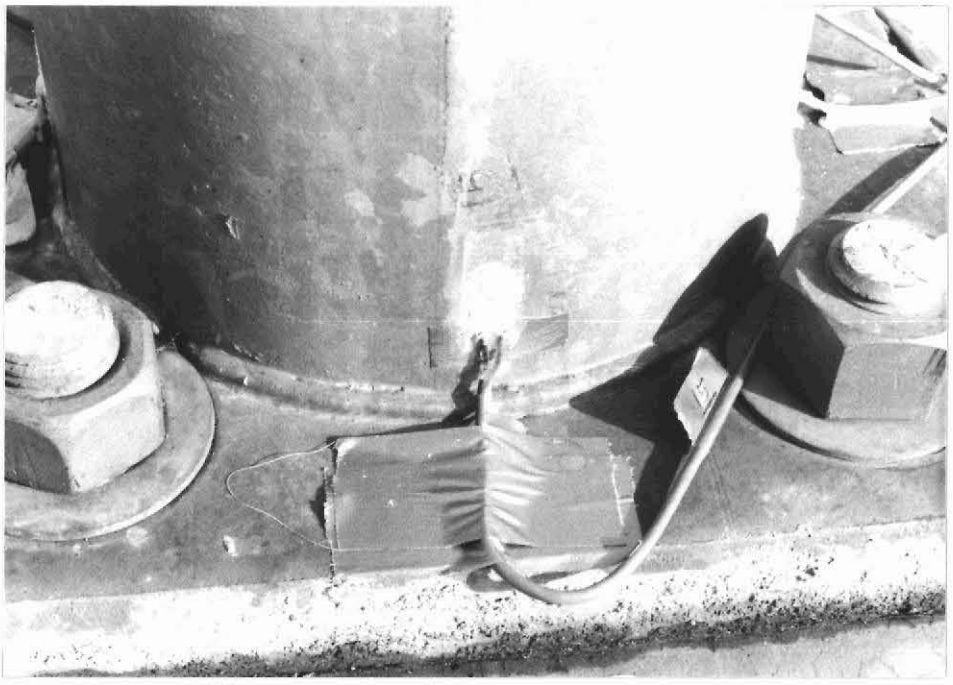

Figure 33b. Mounted Strain Gage with Protective Wax Coating

as a resistor, and as the gage is strained in tension, the resistance increases; as the gage is compressed, the resistance decreases. The corresponding change in voltage is measured to determine the strain. However, in order to keep the magnitude of the current constant, it must be supplied at a constant voltage. If the strain gage were the only element in the circuit, this would be impossible. Fortunately, by adding other elements to the gage circuit, it becomes possible to supply the current to the circuit at a constant value. One arrangement for the gage circuit is the Wheatstone Bridge, as shown in Fig. 34.

The Wheatstone Bridge consists of four resistors arranged to form a closed circuit. The voltage (and current) is supplied at a constant value across nodes A and C, and the change in voltage is measured across nodes B and D. The drop in voltage from A to B is (13):

$$V_{AB} = \frac{R_1}{R_1 + R_2} V \tag{7}$$

here R_1 and R_2 are the resistances of the resistors, and V is the applied voltage. Similarly, the voltage drop from A to D is:

$$V_{AD} = \frac{R_4}{R_3 + R_4} V \tag{8}$$

The output voltage, E, from the bridge is equivalent to: or (9)

$$E = V_{BD} - V_{AB} - V_{AD}$$

or

$$E = \frac{R_1R_3 - R_2R_4}{(R_1+R_2)\,(R_3 + R_4)} \tag{9}$$

The bridge is considered balanced when E = 0 or $R_1R_3 = R_2R_4$. When the bridge is balanced, any change in the resistance will cause a voltage differential ΔE to develop across BD. If ΔR_1, ΔR_2, ΔR_3, and ΔR_4 are the

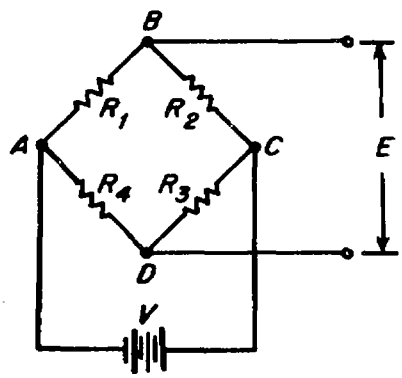

Figure 34. Typical Wheatstone Bridge

changes in resistance of R_1, R_2, R_3, and R_4, respectively, then ΔE has a value equal to:

$$\Delta E = \frac{\begin{vmatrix} (R_1 + \Delta R_1) & (R_2 + \Delta R_2) \\ (R_3 + \Delta R_3) & (R_4 + \Delta R_4) \end{vmatrix}}{\begin{vmatrix} (R_1 + \Delta R_1 + R_2 + \Delta R_2) & 0 \\ 0 & (R_3 + \Delta R_3 + R_4 + \Delta R_4) \end{vmatrix}} \qquad (10)$$

Simplifying Eq. (10) and neglecting second-order terms gives:

$$\Delta E = V \frac{R_1 R_2}{(R_1 + R_2)} \left(\frac{\Delta R_1}{R_1} - \frac{\Delta R_2}{R_2} + \frac{\Delta R_3}{R_3} - \frac{\Delta R_4}{R_4} \right) \qquad (11)$$

For quarter bridge circuits, such as those used for the sign structures, the strain gage is the only resistor that will show a change in resistance. Therefore, $\Delta R_2 = \Delta R_3 = \Delta R_4 = 0$ and Eq. (11) becomes:

$$\Delta E = V \frac{r}{(1 + r)^2} \frac{\Delta R_1}{R_1} \qquad (12)$$

where $r = R_1/R_2$.

The quantity $\Delta R/R$ represents a change in resistance and is related to the strain as

$$\Delta R/R = S_g \varepsilon \qquad (13)$$

here S_g is a proportionality constant known as the gage factor, and ε is the strain. The gage factor allows the manufacturer to calibrate his gages to give the proper values.

For this study, $R_1 = R_2$, and r becomes 1.0. Substituting into Eq. (12) gives:

$$\Delta E = \frac{V}{4} S_g \varepsilon \tag{14}$$

Rearranging and solving for the strain then yields:

$$\varepsilon = 4\Delta E/(VS_g) \tag{15}$$

This equation was used to determine the strains from the voltages recorded by the data acquisition unit.

5.4 Data Reduction Procedure

Data reduction is the process by which the strain gage voltage readings are manipulated to determine the corresponding values of stress and strain. The only unknown in Eq. (15) is ΔE. If it were possible to balance each Wheatstone Bridge before each gage reading, the gage reading (voltage) would have been ΔE, since it was recording zero before the strain occurred. However, due to the dynamic nature of the structural loading, such balancing is normally not possible. It was, therefore, necessary to determine an initial value, or offset, of the gage voltage.

After the data had been transferred to a file on a floppy disk, the HP-9836 was used to search through the data file for gage readings that were made at wind speeds of less than 0.1 mph. This value was selected as the basic "zero" wind speed, after experimentation on calm days showed that strains induced by a wind of that magnitude were negligible. An average value of all such readings was computed for each gage, and these were then defined as the gage offsets and stored on a floppy disk in a data file. The offsets were recomputed for each day of data collection. This was

necessary to do, as disconnecting the data acquisition unit from the gage cables caused the offsets to change from day to day. (It is noted that the data acquisition unit had to be disconnected from the gage cables every day, as it was not possible to monitor the unit 24 hours a day, and no provision could be made to secure the unit from weather and vandals).

Once the offsets had been determined, the strains were computed. The true value of ΔE was determined from Eq. (16):

$$\Delta E = V_i - V_o \tag{16}$$

where V_i is the voltage reading for a strain gage, and V_o is the offset for that gage. If V_i is less than V_o, a negative value of ΔE is obtained. This indicates compression. A positive value of ΔE indicates tension.

With the value of ΔE computed, the strain was determined using Eq. (14). The value of the corresponding stress was then calculated using Hooke's Law (17)

$$\sigma = E\varepsilon \tag{17}$$

where σ is the stress and E is the modulus of elasticity of steel, taken as 29×10^3 ksi. The stress and strain data were all stored, along with the corresponding normal wind component. This made them available for further data reduction and evaluations of the results, such as determining statistical characteristics of the stresses.

5.5 Statistical Analysis of Results

The data collection equipment was capable of reading the anemometer and strain gages approximately every 34 seconds. The data acquisition unit would first read and store the wind speed and direction in the calculator's

memory, which took approximately 5 seconds. Using these values, the calculator would then compute the magnitude of the wind component perpendicular to the plane of the structure and store this value in its memory. This process consumed about 2 seconds. All strain gages were now scanned, one after the other, which required about 3 seconds. The remaining 24 seconds was needed to transfer the gage readings from the data acquisition unit to the calculator's memory.

Due to the vibrating nature of the structures, the strain gage readings were not necessarily always made at the maximum, as indicated by Fig. 35. As can be seen from this figure, the deflection at time t_1 will be different from that at time t_2. The readings might have been taken at any point in the cycle, and it was therefore determined that a statistical evaluation of the data was the only way in which logical explanations of the results could be provided.

The analysis was conducted for each gage for all wind speeds, using increments of 1 mph. Each nominal wind speed covered a range of 0.5 mph on either side of the nominal value. Therefore, actual wind speed values exactly halfway between two nominal wind speed increments were rounded up to the higher value.

For the Tucson structure, a total of 1244 readings were made by each gage. For the Phoenix structure, 1133 readings were taken per gage. For each nominal wind speed, the maximum positive and negative stresses were found, and the average stress and standard deviation were computed. The average positive and negative stresses, along with their respective deviations were then determined. The standard deviations were calculated

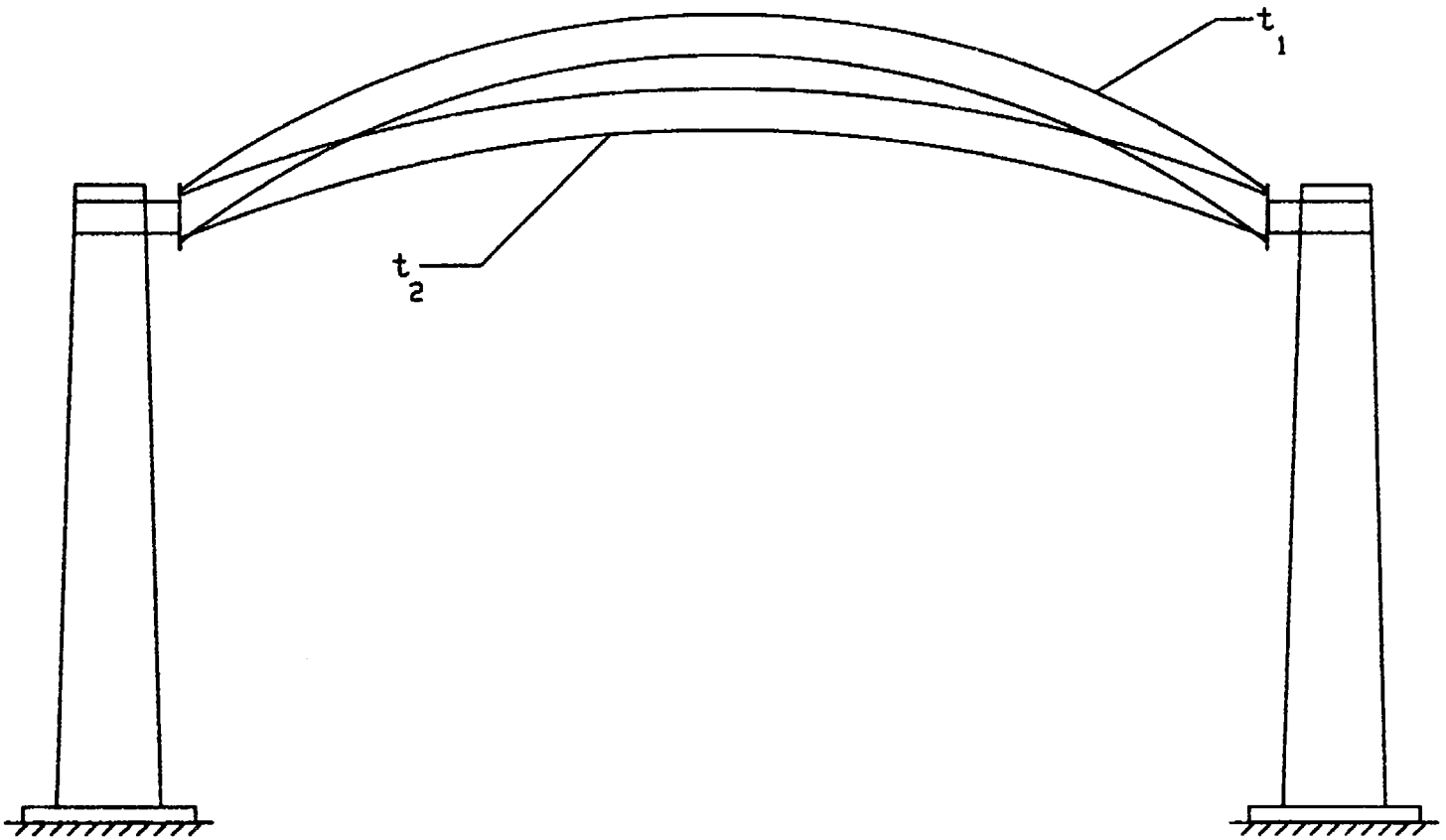

Figure 35. Dynamic Deflections in Monotube Structure at Various Times

using:

$$\sigma = \sqrt{\frac{n\Sigma x^2 - (\Sigma x)^2}{n(n-1)}} \qquad (18)$$

where σ is the standard deviation, n is the number of data points for a certain nominal wind speed, and X_1, X_2, X_3, ... X_n are the data points.

The two locations of primary interest for each structure are at the midspan of the beam and at the base of the column. A stress envelope was determined for each of these by plotting the average stresses, along with points identifying values of plus and minus 3 standard deviations to either side of the average. This envelope includes 99.5% of all possible stress levels (14), assuming that the readings are normally distributed. The envelopes for the midspan of the Tucson and Phoenix structures are shown in Figs. 36a and 36b, respectively.

It can be seen that the maximum values of the stress envelope are well within the safe range. For the Phoenix (100' span) structure, the maximum value given by the envelope is 18 ksi, which is only 53% of the yield stress of 34 ksi. For the Tucson (60' span) structure, the margin of safety is even larger. The maximum value given by the envelope is 8.2 ksi, or 24% of the yield stress. Furthermore, it is emphasized that these values tend to be extremes. The large number of tests that were made lend confidence to the statistical evaluations; further data are not likely to alter the averages nor the $\pm$ 3 standard deviations to a significant degree. It is therefore clear that the low level of service load stress that was predicted by the analytical study has been substantiated.

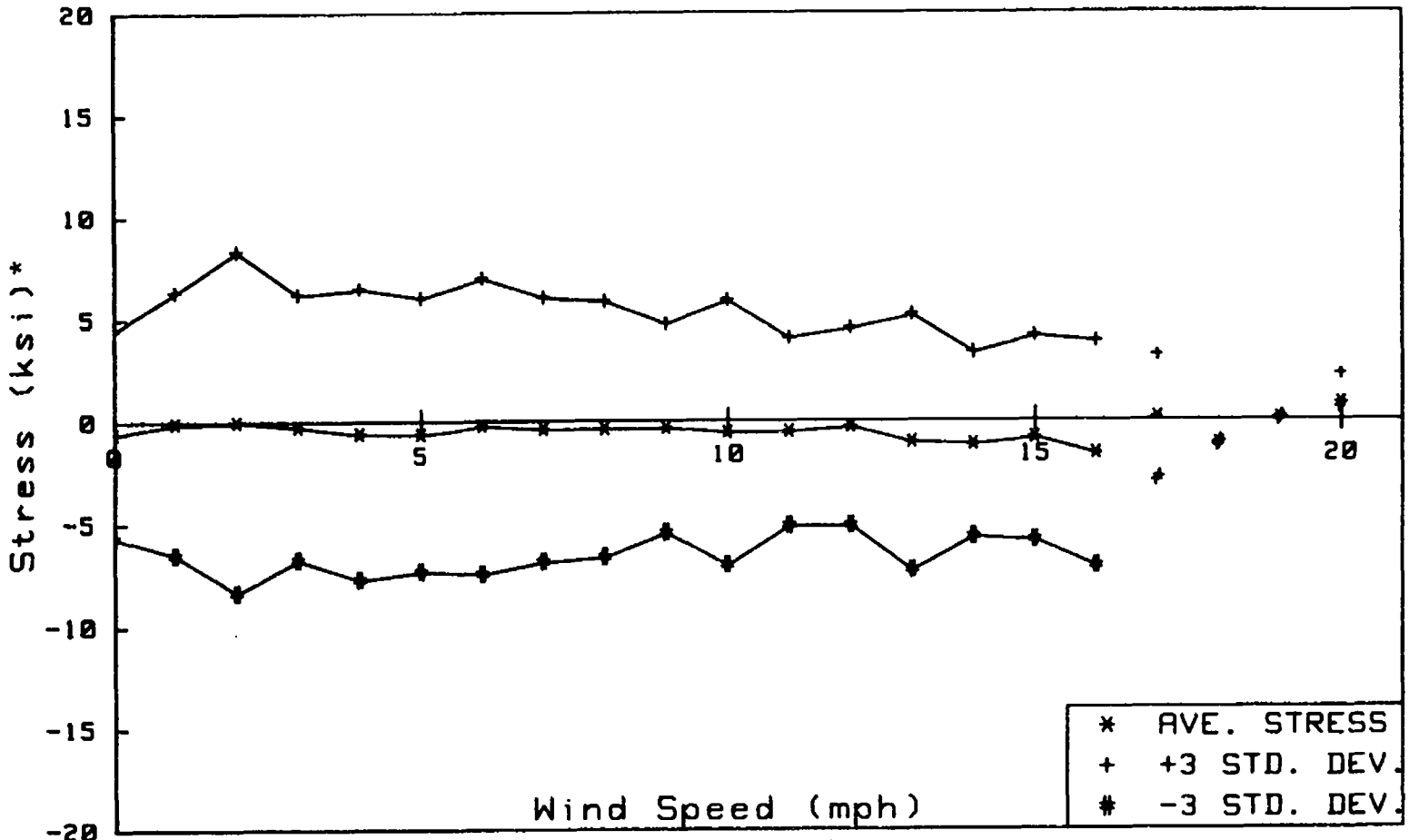

*For wind speeds greater than 16 mph, the statistical population is too small for accurate analysis

Figure 36a Stress Envelope for Midspan Stresses of Tucson Monotube Structure

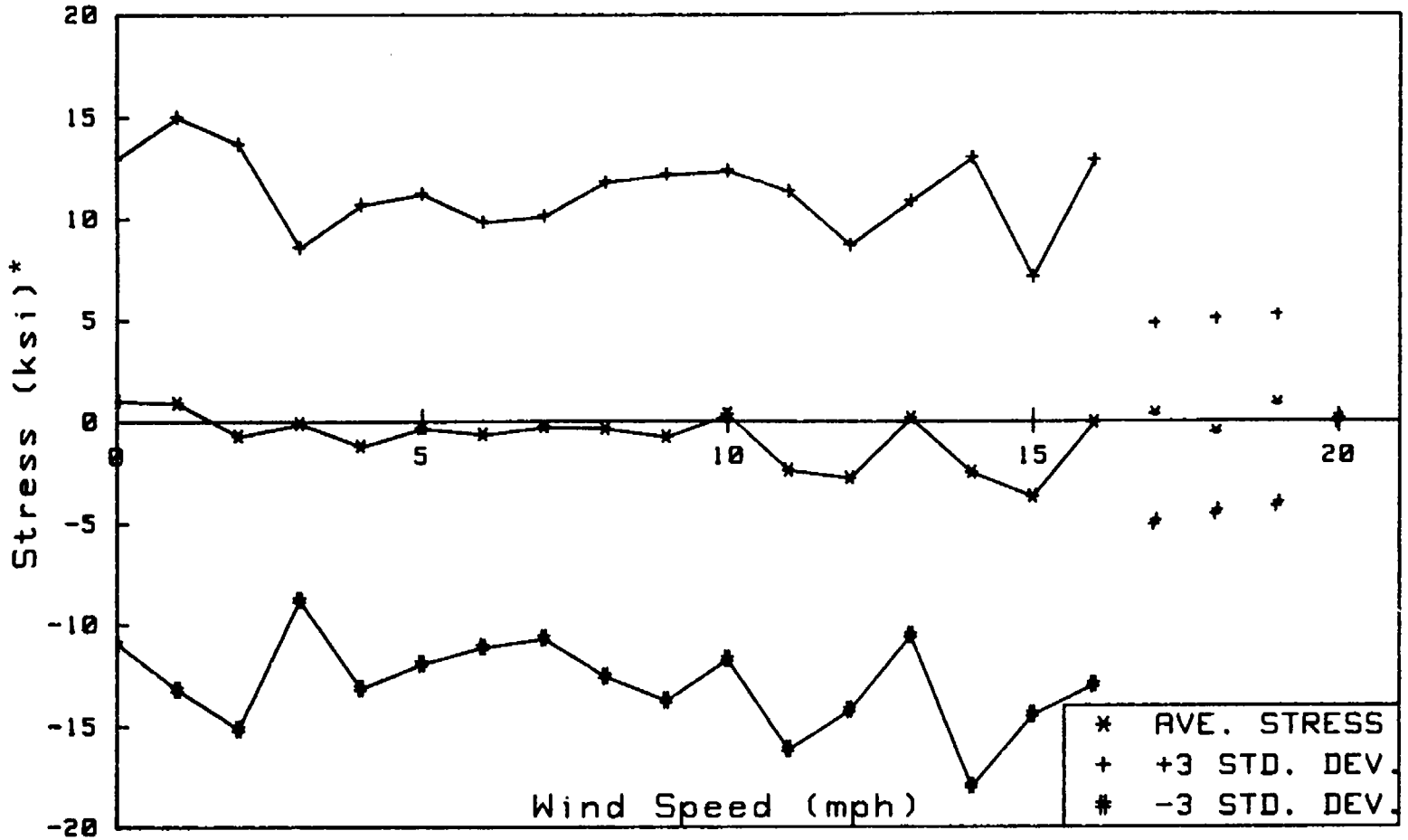

*For wind speeds greater than 16 mph, the statistical population is too small for accurate analysis

Figure 36b Stress Envelope for Midspan Stresses of Phoenix Monotube Structure

It is interesting to note that both structures exhibit local maxima in the envelopes at wind speeds of approximately 2 mph, and again at 14 to 16 mph. The frequency of oscillations at 2 mph is well below any natural frequency for both structures. However, between wind speeds of 15 and 16 mph, both structures are near a natural frequency. For the Tucson structure, the frequency corresponds to the third 3D mode of 3.26 cps. For the Phoenix structure, the mode is also the third 3D mode, at a frequency of 3.06 cps. It is believed that the maxima observed in the stress envelopes at this wind speed indicates that the structure is tending toward resonance at these points. However, due to the inherent structural damping and the gusting of the wind, the resonance condition is not achieved for the actual structure. It is noted that in the theoretical evaluations of the structures, damping was set equal to zero, and the wind was assumed to blow at constant (sustained) speeds.

The stresses at the column bases are not as large as their midspan counterparts. The envelopes for the out-of-plane stresses for both structures are shown in Figs. 37a and b. The maximum value for the Tucson structure is 7.7 ksi, and for the Phoenix structure it is 17.0 ksi. This demonstrates that the span length has a greater influence on the column base stresses than does the sign size. It is noted that the signs on the Tucson structure were about twice as large as those on the Phoenix structure, but the latter has a span that is 67% longer.

The column base stresses also exhibit local maxima at approximately the same wind speeds as was found for the beam. Here, again, the structure is vibrating at close to a natural frequency, but is prevented from

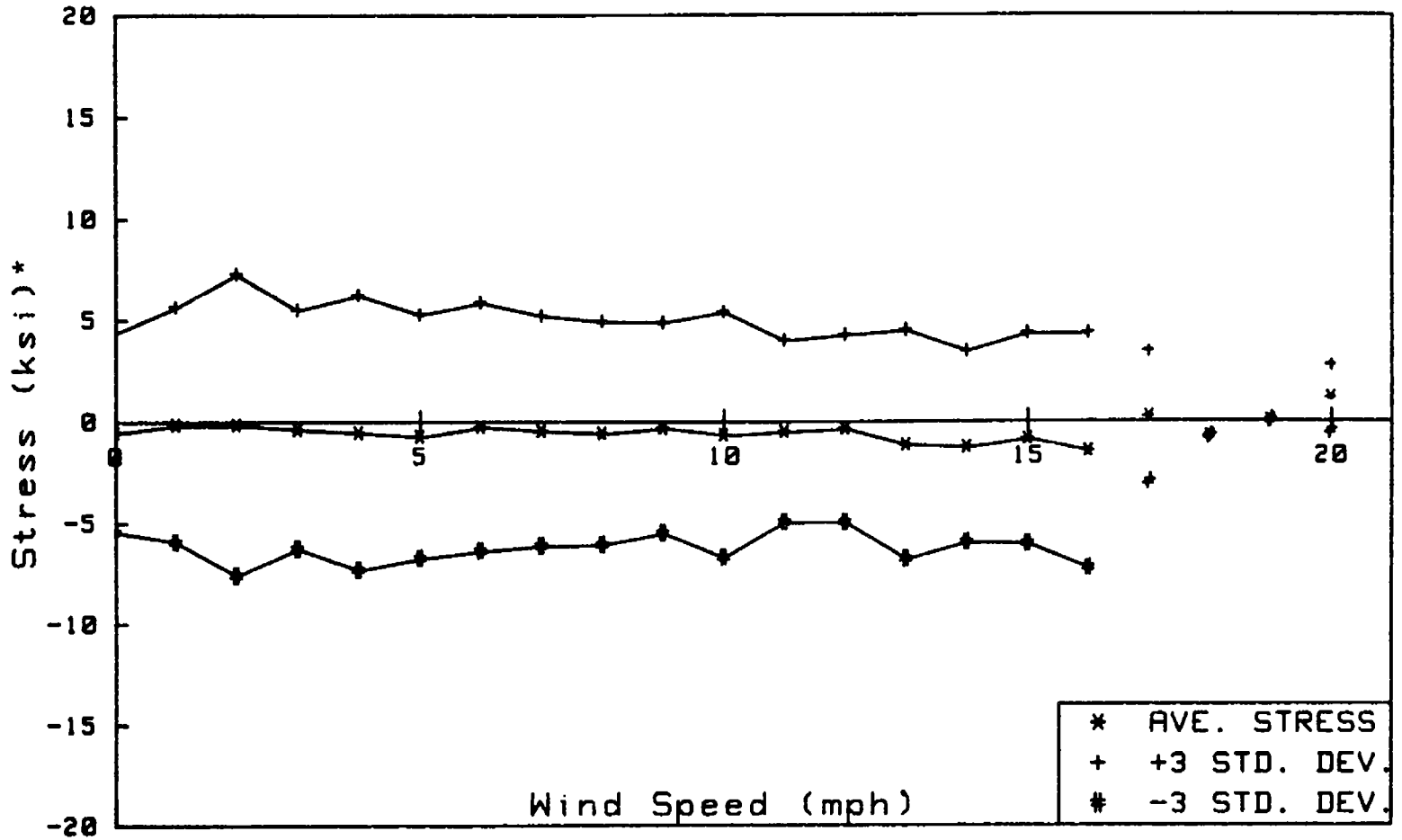

*For wind speeds greater than 16 mph, the statistical population is too small for accurate analysis

Figure 37a Stress Envelope for Column Base Stresses of Tucson Monotube Structure

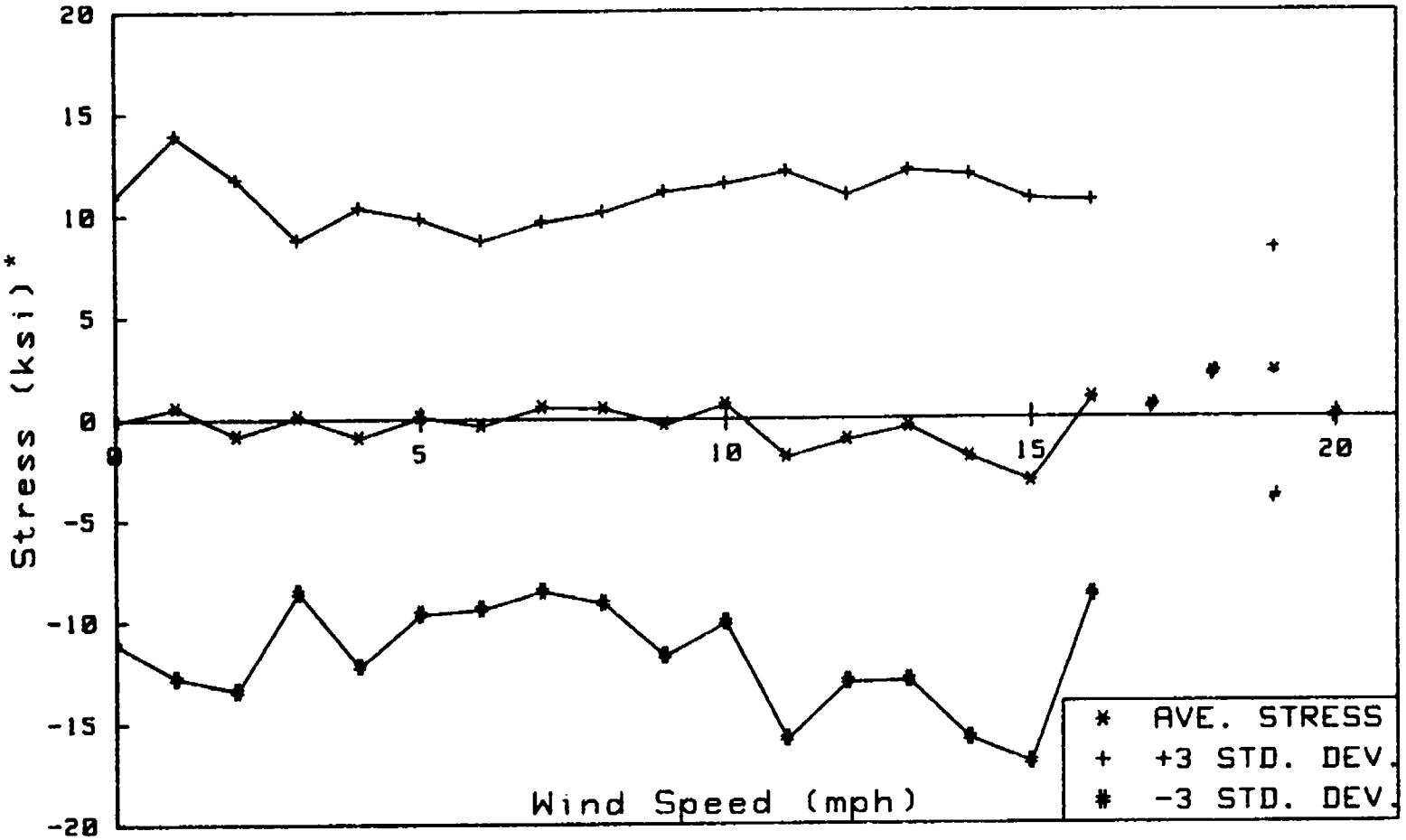

*For wind speeds greater than 16 mph, the statistical population is too small for accurate analysis

Figure 37b Stress Envelope for Column Base Stresses of Phoenix Monotube Structure

The maximum stresses discussed so far were not the actual maximum stresses recorded, but the maximum values that are likely to occur, given the statistical distribution of the data. The recorded stresses were less than those presented. For example, at 16 mph, the wind speed for which the stress envelope is the widest for the Tucson structure, the maximum recorded stress was 7.3 ksi, as compared to 12.2 ksi of the envelope. It is therefore clear that the use of a statistical approach has made it possible to include essentially all of the possible stress levels in the analysis. This also reflects the cyclic nature of the structural behavior, as well as the influence of the time lapse involved in the reading of the gages.

5.6 Calibration of Equipment

Due to the high ambient temperatures during the times when the data for the Phoenix structure were collected, it was necessary to calibrate the equipment and the gages to reflect the higher than normal operating temperatures. The data were collected during the months of June and July, with ambient temperatures ranging between 100° and 115°F. Data for the Tucson structure were also collected on one day during this period, with an ambient temperature of 102°F. It was not found necessary to apply calibration constants to the other Tucson data which were collected during the month of March when the temperature was in the mid 80's.

The first correction was made to account for the apparent and true strains caused by thermal conditions. The gages that were used had been calibrated to read zero strain at 75°F. However, much of the time these

gages were used when the ambient temperature was over 100°F, and the surface temperature of the structure was greater than 140°F. The temperature response curve of the gage that is shown in Fig. 38 indicates that this can cause an error of -50 micro strain, which corresponds to approximately 1.5 ksi compressive stress. To compensate for this, a separate gage was bonded to a piece of steel of the same thickness as the wall of the structure. The gage was covered and protected exactly as the other 16 gages were. It was then placed in the sun and read along with the other gages. When the gage readings were reduced, the voltage difference of the separate gage was subtracted from the voltage difference of the other gages, thereby canceling the elevated temperature effects.

A more significant correction was needed to compensate for the influence of higher operating temperatures on the Data Acquisition Unit. The service manual (17) states that the optimum operating temperature is in the range of 62° to 78°F. In the field, the unit would have to work in temperatures as high as 135°F, resulting in some impairment of accuracy. Since the unit had been routinely run in the sun at temperatures between 120° and 130°F, a test was conducted to see if the error was systematic, and how it could be accounted for.

The unit was set in the sun on a warm day. It was connected to a Wheatstone Bridge, across which a known voltage was applied. At intervals of approximately one hour, the bridge voltage was read by the Data Acquisition Unit, as well as by a voltmeter that was kept at its optimum temperature. The voltages and the time and temperature were recorded over a period of two days.

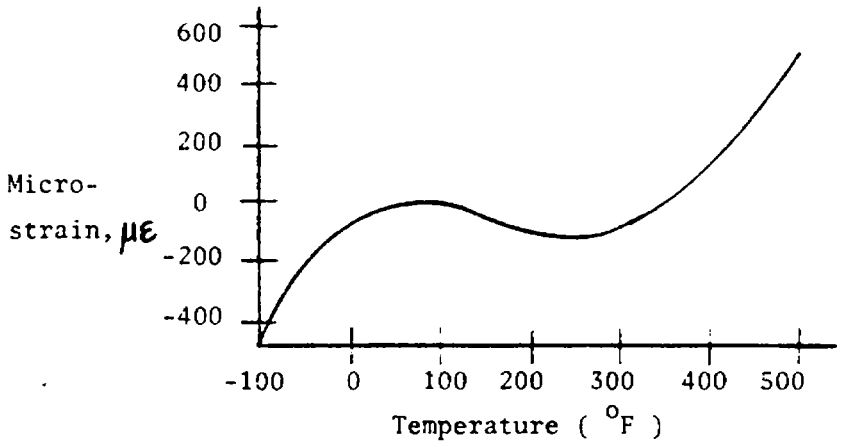

Figure 38 Apparent Strain in Strain Gage Due to Temperature

The results of the experiment are shown in Tables 11a and 11b. For temperatures above 105°F, it is seen that the voltages read by the Data Acquisition Unit were 43% greater then the actual voltages. This difference appears to be independent of the level of temperature above 105°F. During the data reduction, the voltage differences were reduced by this amount to correct for the temperature effects on the equipment.

All stress and strain values that are given in this chapter reflect these correction factors.

Table 11a. Results of Data Acquisition Unit Calibration Test - Day One

Time	Temperature (°F)	Voltage Read	Actual Voltage	% Error
9:00	100	0.8321	0.5658	32
10:00	105	0.9047	0.5130	43.3
11:00	113	0.9181	0.5242	42.9
12:00	121	0.8989	0.5142	42.8
1:00	123	0.9015	0.5121	43.2
2:00	127	0.9086	0.5106	43.8
3:00	128	0.9011	0.5190	42.4
4:00	127	0.8974	0.5151	42.6
5:00	127	0.8983	0.5075	43.5

Average % Error = 43.1%

Table 11b. Results of Data Acquisition Unit Calibration Test - Day Two

Time	Temperature (°F)	Voltage Read	Actual Voltage	% Error
9:00	102	0.8596	0.5587	35
10:00	106	0.8778	0.5030	42.7
11:00	112	0.8753	0.4998	42.9
12:00	118	0.8897	0.5053	43.2
1:00	123	0.8924	0.5149	42.3
2:00	128	0.8975	0.5044	43.8
3:00	128	0.8997	0.5101	43.3
4:00	129	0.8814	0.5033	42.9
5:00	129	0.8873	0.5066	42.9

Average % Error = 43.0%

Chapter 6

COMPARISON OF ANALYTICAL AND EXPERIMENTAL RESULTS

The full-scale test results that have been obtained in the present research project represent a new contribution to the pool of information that previously provided only theoretical data on the response of monotube sign support structures. In the following discussion, a detailed evaluation of the data will be given, affording comparisons between actual in-service behavior of the structures and the theoretical studies that have been made. In addition to giving unique comparisons between analytical and experimental research, the results will also be used to examine and verify the design recommendations that were made earlier (3).

6.1 Tucson Structure

The 60-foot Tucson structure is the lower limit of what is considered a normal span for monotube structures. The analytical and the experimental results both showed that the point of maximum in-plane stress was at the midspan of the beam; these are detailed in columns 2 and 3 of Table 12. It should be noted that the measured stresses for the 20 mph wind speed represents only two individual readings, and no readings were obtained for wind speeds greater than 20 mph. The stresses that are given for the full-scale tests are the absolute values of the maximum stresses that were recorded. In most cases, the absolute values of the positive and negative stresses were almost identical, as would be expected for the type of cross section that is used in the structures. It is also noted

Table 12. Computed and Measured Stresses for 60-Foot Structure

Wind Speed, mph	In-plane at midspan, ksi		Out-of-plane at column base, ksi	
	Computed	Measured	Computed	Measured
2.5	4.38	5.52	1.34	1.74
5.0	4.38	5.69	1.34	2.08
7.5	4.39	4.33	1.35	1.08
10.0	4.39	4.86	1.48	2.03
12.5	4.49	4.36	1.65	1.73
15.0	4.54	4.10	1.61	2.43
17.5	4.59	4.01	1.70	2.58
20.0	4.66	1.30+	1.81	1.65
22.5	4.71	*	1.93	*
23.2	5.11	*	2.64	*

---

* No data collected for this wind speed.

\+ Only two readings obtained at this wind speed.

that the stress levels do not vary a great deal over the range of wind speeds that were measured.

The data in Table 12 illustrate the good correlation that was obtained between the analytical and the experimental results. This is further emphasized when the complexities of full-scale testing, modeling of actual structures, and so on, are considered. Thus, the three-dimensional, non-prismatic nature of the structure makes it particularly difficult to model, especially when dynamic wind loads must be accounted for. The strain gages were not installed under ideal laboratory conditions, and the field measurements had to be made in a very demanding climate. In spite of these obstacles, the results of the analytical and experimental investigations are in good agreement.

The largest deviation between the measured and computed stresses occurs at a wind speed of 5 mph, although it is noted that the numerical value of the difference is still small. Also, the magnitudes of the stresses are well below the yield stress. The reasons for the differences and their magnitudes can be explained in part by examining the statistical characteristics of the measurement results.

As shown in Chapter 5, the maximum stress that is likely to appear at a wind speed of 5 mph is 7.32 ksi, which equals the mean stress of 0.63 ksi plus 3 standard deviations. The maximum recorded stress of 5.69 ksi is greater than 95% (mean plus 2 standard deviations) of the stresses that can be expected to develop at this wind speed.

It is also interesting to note that at the higher wind speeds, the analytical model consistently predicts a higher level of stress than was

measured. This may be partly due to the lower number of readings that were taken at the higher wind speeds, as compared to at the lower wind speeds. However, it is clear that the major influence is provided by the modeling of the structure. For example, the use of prismatic elements results in a smaller section at midspan of the analytical model, as compared to the real structure. This by itself will lead to somewhat higher stresses at the midspan location. The modeling of the beam-to-column connection also is important in the sense that a low restraint of same will lead to higher stresses in the beam. This difference between the results is not as consistent at the lower wind speeds, because random electrical disturbances that may have occurred during the data collection process would tend to cancel the modeling effects. The sensitivity of the equipment is also a factor in this case.

The experimental and theoretical results agree that the point of maximum out-of-plane stress is at the column base. These stresses are given in columns 4 and 5 of Table 12. The correlation between the computed and measured stresses is good, although maybe not as satisfactory as for the midspan location. However, it is emphasized that the column base stresses are very low. At these levels, a 0.5 ksi difference appears large.

It is observed that the full-scale test results are consistently higher than those of the analytical study. This is most likely due to the element chosen to model the beam-to-column connection. The in-plane bending stiffness underestimates that of the actual connection and,

therefore, less of the moment in the beam is transferred to the column. As a consequence, the stresses at the column base in the model are lower.

Perhaps the best way to comprehend how well the two studies correlate is to view the data graphically. Figure 39 displays the results for the measured and computed column base and beam midspan stresses. When drawn to scale, it is readily apparent how well the findings support each other.

The figure shows the stresses due to the dynamic effects of the wind, which is the primary live load the monotube structures will experience. However, the structural designer must know the total stress from both live and dead loads. Therefore, the computed dead load stressses (no measurements could be taken for dead loads) were added to those due to the wind load, and the sums for the in-plane and the out-of-plane directions are shown in Fig. 40. It is clear that the stress levels are still well below the yield stress of the steel. In fact, the margin of safety indicates that the Tucson structure appears to have been designed quite conservatively.

6.2 Phoenix Structure

The 100-foot Phoenix structure is close to the upper limit of the normal spans for monotube structures. Longer spans may prove to be uneconomical. As for the Tucson structure, the computations and the testing both determined that the point of maximum in-plane stress was at the midspan of the beam. Columns 2 and 3 of Table 13 give the maximum stress at each wind speed as determined by computations and measurements. It should be noted that for the wind speed of 17.5 mph only one reading

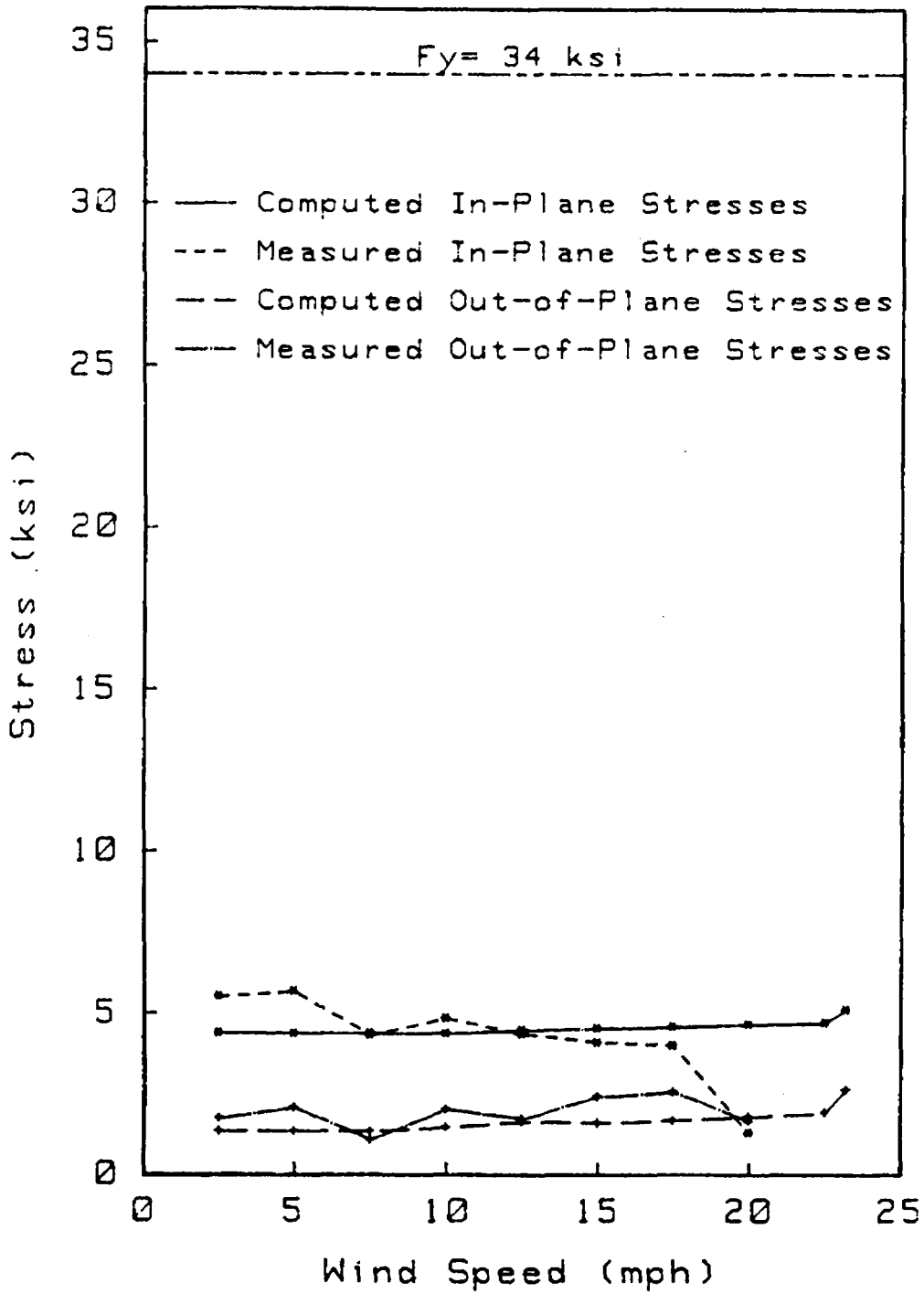

Figure 39 Correlation of Stresses for Tucson Monotube Structure

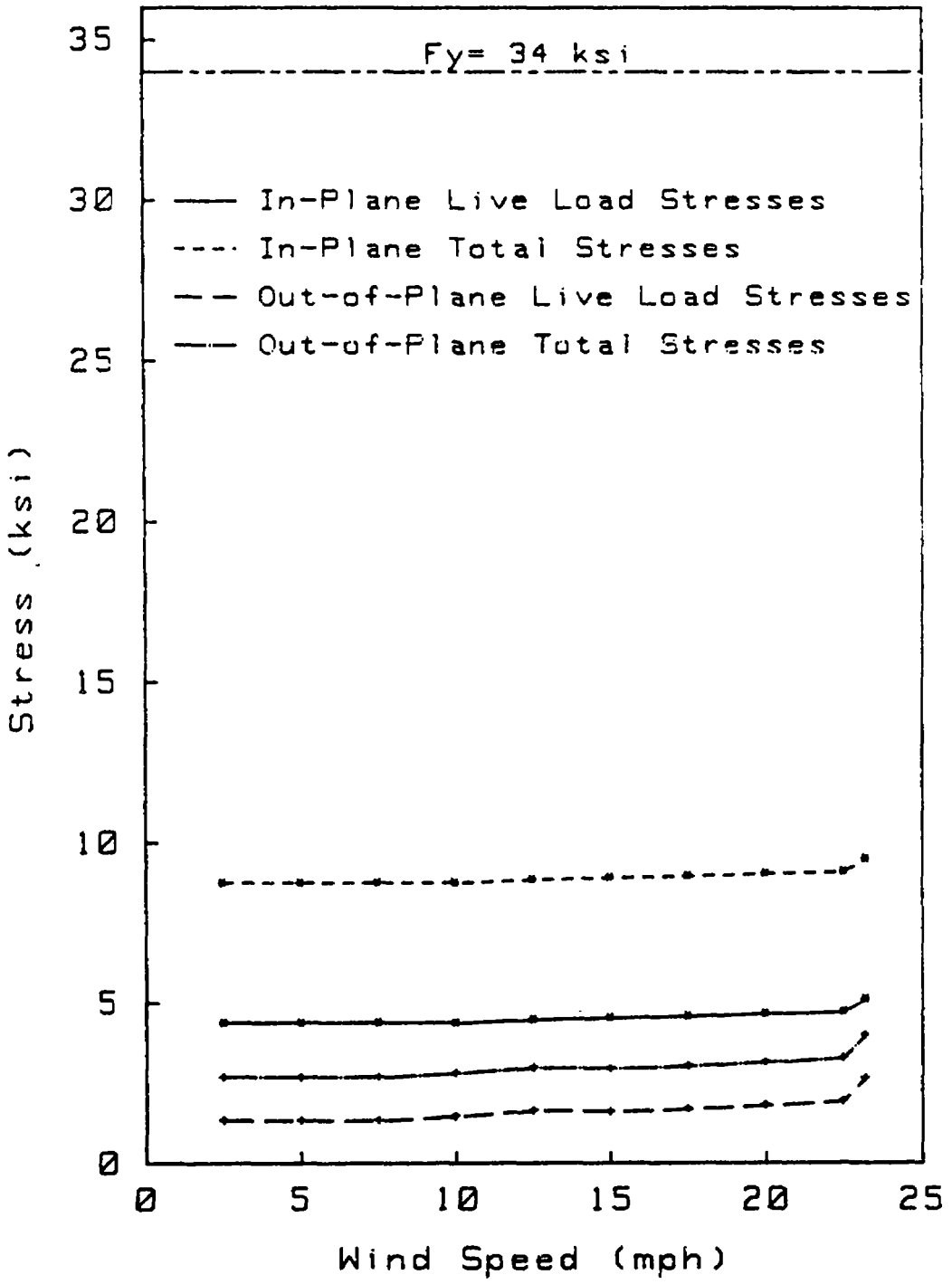

Figure 40 Total Stresses for Tucson Monotube Structure

was obtained, and none could be had for wind speeds of 20.0 mph or greater.

It is seen that the correlation between the theoretical and actual stresses is good. The stresses are greater than at the corresponding point in the Tucson structure, as would be expected due to the longer span. The analytical study also predicts stresses that are consistently higher than the measured ones. The reasons for this were detailed in the description of the Tucson test results.

In the out-of-plane direction, both studies agree that the point of maximum stress is at the base of the column, and these data are given in columns 4 and 5 of Table 13. The stresses are low, and hence the numerical values of the differences between the measured and the computed data appear more significant than they are. Similar to the Tucson results, the column base stresses predicted by the analytical study are consistently lower than those that were measured. This is attributable to the modeling of the beam-to-column connection element, as discussed earlier.

The stresses are presented graphically in Fig. 41. As in Fig. 39, this demonstrates how well the two studies correlate. Figure 42 gives the total live plus dead load stresses (computed values), providing a comparison with the level of the yield stress. It is apparent that the 100-foot monotube structure represents a more realistic design than the 60-foot one, since the margin of safety is closer to the values that are considered desirable in practice. The average total stress for all wind

Table 13. Computed and Measured Stress for 100-Foot Structure

Wind Speed, mph	In-plane at midspan, ksi		Out-of-plane at column base, ksi	
	Computed	Measured	Computed	Measured
2.5	10.11	9.74	2.84	3.25
5.0	10.18	9.96	2.87	5.39
7.5	10.23	9.96	2.91	4.98
10.0	10.29	9.91	2.95	4.13
12.5	10.51	9.60	3.11	4.04
15.0	10.70	9.13	3.16	5.36
17.5	10.53	4.33[+]	3.12	1.47
20.0	10.75	*	3.19	*
22.1	10.92	*	3.25	*

[+] Only one reading taken at this wind speed.

* No data collected for this wind speed.

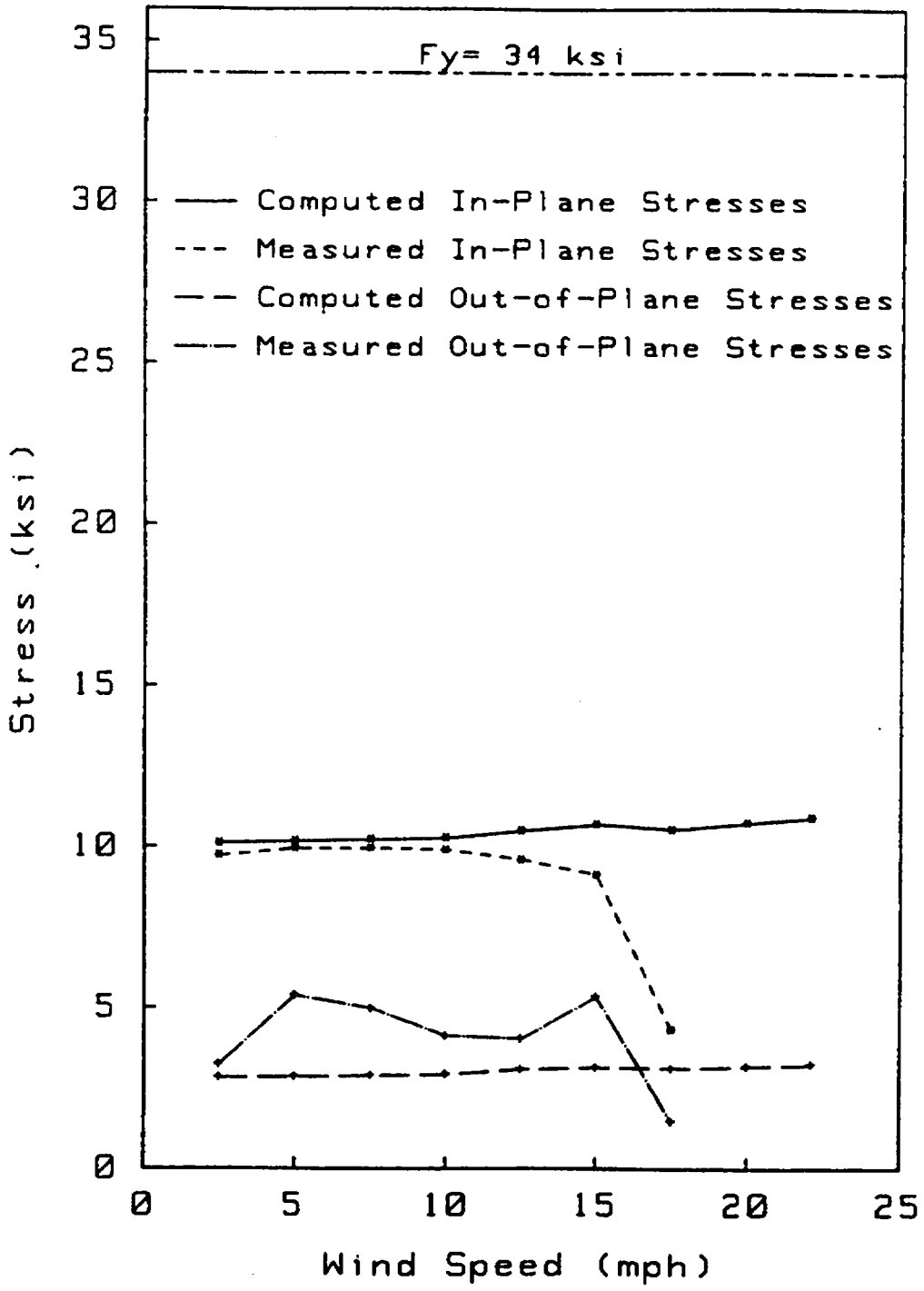

Figure 41 Correlation of Stresses for Phoenix Monotube Structure

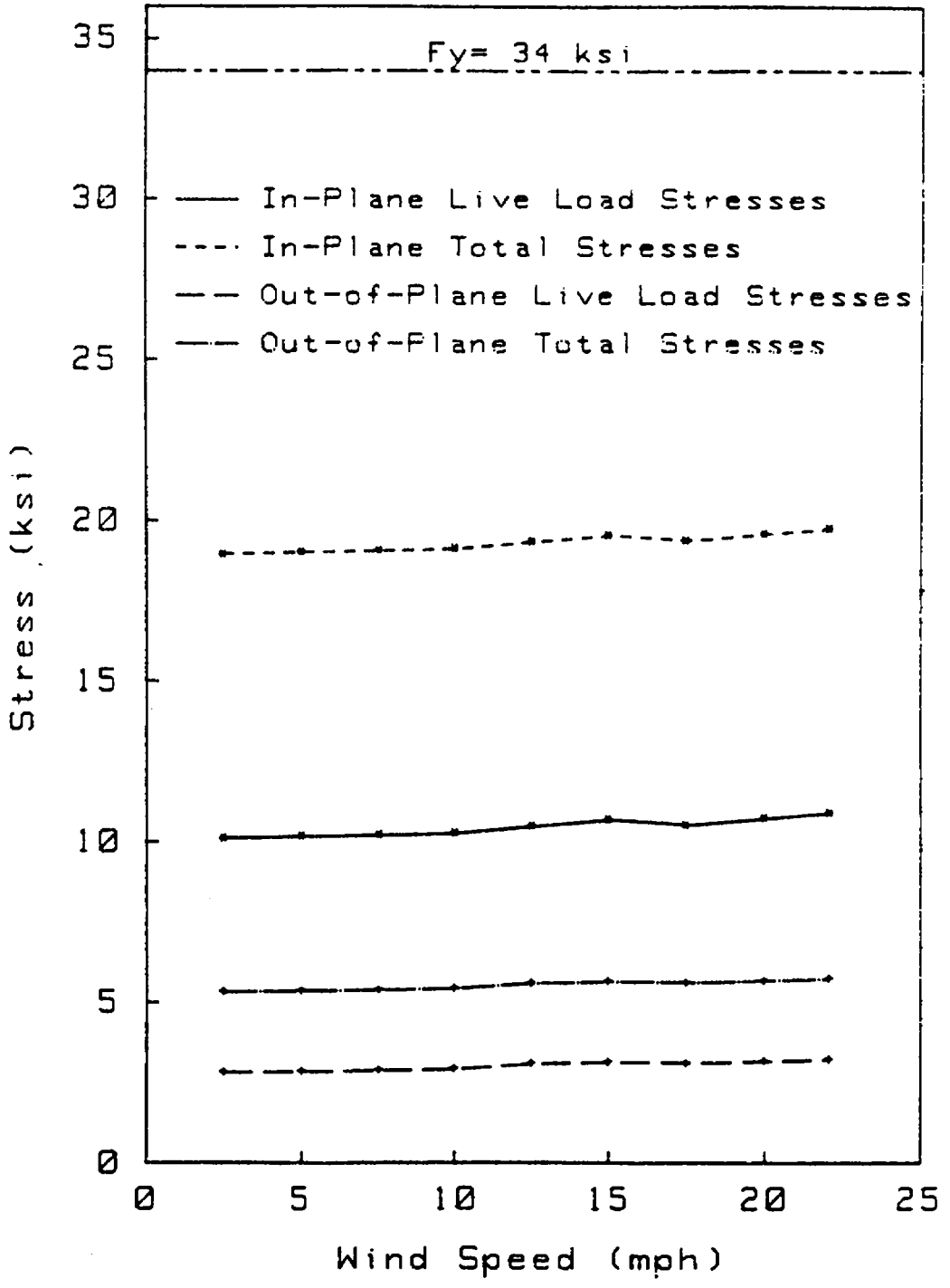

Figure 42 Total Stresses for Phoenix Monotube Structure

speeds is approximately 19 ksi; this gives a factor of safety against first yield of 1.8.

Chapter 7

SUMMARY, CONCLUSIONS AND RECOMMENDATIONS

The purposes of this study were to gather data on the performance of monotube sign support structures under service conditions, and to evaluate possible methods of structural analysis. Through the use of field testing and computer modeling, such data were collected, reduced and analyzed to determine the service load response characteristics of the monotube structures.

7.1 Summary and Conclusions

On the basis of the two full-scale structures that have been tested and analyzed, the following conclusions can be made:

1. The service load stresses can be accurately predicted by the use of finite element modeling. The computer models in this study correlate very well with the field measurements, as well as with the similar models studied by Ehsani and Bjorhovde (3).
2. Due to the correlation between past and present results, the recommendations that were made by Ehsani and Bjorhovde are well-founded and should be considered for adoption. These recommendations include suggested methods of analysis, new performance criteria, and topics in need of further study.
3. The two full-scale structures did not meet the $d^2/400$ dead load deflection requirement of the AASHTO Specifications.

4. The stress levels associated with the actual deflections are well below the magnitudes of the allowable stresses, even though the structures do not meet the $d^2/400$ deflection criterion.
5. As was found in the earlier study (3), the stress level at any point can be found by superimposing the stresses due to static loads and those due to dynamic loads.
6. The maximum in-plane stresses occur at midspan of the beam.
7. The maximum out-of-plane stresses occur at the column base.
8. Resonance did not occur in the field testing, even when vortex shedding took place at frequencies equal to the natural frequencies of the structures. It is believed that this can be attributed to the inherent damping of the structure, as well as to the gusting nature of the wind.
9. A monotube structure of moderate or greater span (> 60') cannot meet the $d^2/400$ dead load deflection requirement of AASHTO. In most cases, it would prove to be very uneconomical to design such a structure to meet this requirement. A new deflection criterion was proposed in the original monotube study (3), thus:

$$\frac{\Delta}{\ell} \leq \frac{1}{150}$$

where Δ is the dead load deflection, and ℓ is the span length. This criterion is based on stiffness requirements, as the strength (i.e., stress level) is not likely to govern.

In the original study on monotube structures (3), a number of other recommendations also were made in regard to the analysis and design of

these structures. Two of the recommendations are of particular interest in relation to the findings of the current project.

The first recommendation is to consider the analysis of the monotube structure for out-of-plane behavior independent of the in-plane behavior. The current project has shown that this is a rational approach. It makes the analysis much simpler, and does not introduce any appreciable error.

The second recommendation was to camber the beam of the monotube structure to help eliminate the undesirable visual effects of larger deflections. This is especially worthwhile if a maximum deflection-to-span ratio of 1/150 is adopted. The 100' span of the Phoenix structure that was tested in the current study had such a cambered beam. Although the dead load deflections were large, the camber kept the midpsan above the end points. Thus, the visual effect was that of a low-pitched arch, which is much more appealing than if the beam was deflected downward. Therefore, cambering the beam is a viable option in the design of monotube structures.

7.2 Recommendations for Further Studies

This study has significantly increased the pool of existing knowledge on the behavior of monotube structures. It has been shown that the design guidelines for truss-type structures cannot be rationally applied to monotube structures. New design guidelines have been recommended; however, certain additional studies of the monotube structure under high wind conditions are needed, as well as a better understanding of other characteristics. Therefore, the following subjects are in need of examination:

1. Wind Tunnel Testing - The performance of monotube structures at wind speeds up to at least 80 mph needs to be determined. This is best accomplished by using scale models in a wind tunnel. The effects of sign placement and size should also be studied.

2. Beam-to-Column Connection Behavior and Strength - The current study has indicated that the connection can play a major role in determining the stresses in the structure. More precise methods are needed to model the actual behavior of typical connections.

3. Evaluations of Fatigue Characteristics - Due to time constraints, this study did not investigate fatigue phenomena in the members or the connections of the structures. However, due to the dynamic nature of the wind load, cyclic stress variations are common. Although the stress levels are low as compared to the yield stress, the stress ranges and the fastening details of the beam-to-column connections may make them susceptible to fatigue cracking. It is recommended that connection and base details should be tested statically and dynamically in the laboratory to determine strength and fatigue life characteristics.

4. Behavior of Cantilever Structures - The current study only addressed the behavior of span-type structures. Cantilever sign structures are also in widespread use. It is expected that the deflections will be greater than for the span-type structures, as will be the stresses at the column base. Further, the dynamic response of cantilever structures is likely to be considerably more complicated, since the torsional mode of behavior may play a major role. Fatigue also would appear to be more serious.

REFERENCES

1. American Association of State Highway and Transportation Officials (AASHTO), "Standard Specifications for Structural Supports for Highway Signs, Luminaires and Traffic Signals," AASHTO, Washington, D.C., 1975 (revised 1978 and 1979).

2. Ehsani, Mohammad R. and Reidar Bjorhovde, "Deflection Criteria for Sign Support Structures," paper submitted to the Journal of Structural Division, ASCE, February 1985.

3. Ehsani, Mohammad R., S. K. Chakrabarti, and Reidar Bjorhovde, "Static and Dynamic Behavior of Monotube Span-Type Sign Structures," Report No. FHWA/AZ/194, Vols. I and II, Arizona Department of Transportation, Phoenix, Arizona, June 1985.

4. Rouse, Hunter, "Elementary Mechanics of Fluids", Dover Publications, New York, NY, 1978.

5. Hoerner, Sighard F., "Fluid Dynamic Drag", Published by Author, 1965.

6. Fung, Y. C., "An Introduction to Aeroelasticity", John Wiley and Sons, Inc., New York, NY, 1955.

7. Lamb, H. "Hydrodynamics", 6th Edition, Cambridge, London, 1932.

8. Weaver, W., "Wind-Induced Vibrations in Antenna Members," "Journal of the Engineering Mechanics Division", ASCE, Vol. 87, No. EM1, 1961, pp. 141-165.

9. American Institute of Steel Construction (AISC), "Specification for the Design, Fabrication and Erection of Structural Steel for Buildings", AISC, Chicago, Illinois, November 1978.

10. American Concrete Institute (ACI), "Building Code Requirements for Reinforced Concrete (ACI 318-83)," ACI, Detroit, Michigan, 1971.

11. Kamel, H. A. and R. R. Nagulpally, "GIFTS Primer: A First Introduction to the GIFTS-5 System," AME Department, University of Arizona, Tucson, Arizona, Rev. December 1985.

12. Micro Measurements, "Student Manual for Strain Gage Technology," Bulletin 309, Measurements Group Inc., Raleigh, North Carolina, 1983.

13. Dally, J. W. and W. F. Riley, "Experimental Stress Analysis", 2nd Edition, McGraw-Hill, New York, 1978.

14. Hoel, P. G. and R. J. Jessen, "Basic Statistics for Business and Economics", John Wiley & Sons, Inc., New York, NY, 1983.

15. Corcoran, G. F. and E. B. Kurtz, "Electrical Engineering Fundamentals", John Wiley and Sons, Inc., New York, NY, 1976.

16. Popov, E. P., "Mechanics of Materials", 2nd Edition, Prentice-Hall, Englewood Cliffs, New Jersey, 1976.

17. Hewlett-Packard, "Model 3421A Data Acquisition/Control Unit: Operating, Programming and Configuration Manual," Hewlett-Packard Company, Loveland, Colorado, 1982.

APPENDIX A

DATA COLLECTION SOFTWARE FOR HP-41CX CALCULATOR

REGISTER INPUT DATA:

The following registers must contain specific data, as given in the tabulation below, in order for the programs to execute properly.

Register No.	Value
03	Wind conversion factor = 9.2593 mph/VAC
05	Current storage pointer; must be 20 at the beginning of the data collection
06	Wind direction conversion factor; equal to 41.7633 °/VDC
12	Number of values to store before writing to tape

```
01LBL "GO"
02 FIX 9
03 "REG.=?"
04 PROMPT
05 "FILE=?"
06 PROMPT
07 XEQ "SEEKR"
08 XEQ "LOG"
09 RTN
10 END
```

Starts program. Prompts for tape file and beginning register.

```
01LBL "SET3"
02 "OPN"
03 OUTA
04 "LS3-17"
05 OUTA
06 "F1RA0ZON5R-1:T3"
07 OUTA
08 1
09 STO 01
10LBL 01
11 16
12 RCL 01
13 X=Y?
14 GTO 02
15 IND
16 XEQ "PUT5"
17 1
18 ST+ 01
19 GTO 01
20LBL 02
21 "OPN"
22 OUTA
23 RTN
24 END
```

Reads strain gages and stores values in calculator.

```
01LBL "LOG"
02 XEQ "INI3421"
03LBL 10
04 DATE
05 XEQ "PUT5"
06 TIME
07 XEQ "PUT5"
08 "OPN"
09 OUTA
10 XEQ "WNDSPD"
11 XEQ "PUT5"
12 RCL 00
13 RCL 04
14 X<=Y?
15 GTO 20
16 3
17 ST- 05
18 GTO 10
19LBL 20
20 CF 01
21 XEQ "WNDIR"
22 XEQ "PUT5"
23 XEQ "HDCLC"
24 XEQ "PUT5"
25 RCL 02
26 RCL 08
27 X<=Y?
28 GTO 30
29 5
30 ST- 05
31 GTO 10
32LBL 30
33 XEQ "SET3"
34 RCL 05
35 RCL 12
36 X<=Y?
37 XEQ "WCASS"
38 GTO 10
39 RTN
40 END
```

Main program. Directs program flow.

```
01LBL "INI3421"
02 AUTOIO
03 CF 17
04 "HP3421A"
05 FINDID
06 SELECT
07 RTN
08 END
```

Selects Data Acquisition Unit as the primary device in the IL loop.

```
01LBL "WNDSPD"
02 "RA0Z0"
03 OUTA
04 "OPN"
05 OUTA
06 "CLS00"
07 OUTA
08 "F2N4R1:T2"
09 OUTA
10 IND
11 "OPN"
12 OUTA
13 RCL 03
14 *
15 STO 00
16 RTN
17 END
```

Reads wind speed.

```
01LBL "WNDIR"
02 "RA0Z0"
03 OUTA
04 "OPN"
05 OUTA
06 "CLS01"
07 OUTA
08 "F1RA0N3R1:T2"
09 OUTA
10 IND
11 "OPN"
12 OUTA
13 RCL 06
14 *
15 STO 01
16 RTN
17 END
```

Reads wind direction.

```
01LBL "HDCLC"
02 RCL 01
03 COS
04 ABS
05 RCL 00
06 *
07 STO 02
08 RTN
09 END
```

Computes the wind velocity perpendicular to the sign.

```
01LBL "PUT5"
02 STO IND 05
03 1
04 ST+ 05
05 RTN
06 END
```

Stores values in calculator's memory in sequential order.

```
01LBL "WCASS"
02 020.119
03 WRTRX
04 20
05 STO 05
06 RCL 12
07 19
08 -
09 ST+ 13
10 RTN
11 END
```

Writes data to cassette tape.

APPENDIX B

DATA REDUCTION SOFTWARE
FOR HP SERIES 200 COMPUTER

```
10   !PROGRAM REDUCE
20   !THIS PROGRAM REDUCES THE DATA COLLECTED BY KIPP MARTIN FOR HIS
30   !THESIS PROJECT.  IT COMPUTES THE STRESSES AND STRAINS FOR THE
40   !VARIOUS WIND SPEEDS.  THIS PROGRAM HAS BEEN WRITTEN TO BE USEFUL
50   !FOR BOTH SIGNS TESTED WITHOUT MODIFICATION OTHER THAN RESIZING THE
60   !DIMENSION STATEMENTS AT THE BEGINNING
70   !
80   !DIMENSION EACH ARRAY ALONG THE FOLLOWING LINES:
90   !
100  !     1. Os(NUMBER OF GAGES)
110  !     2. D(SIZE OF DATA FILE)
120  !     3. Ep(SIZE OF DATA FILE/(NUMBER OF GAGES+5)*NUMBER OF GAGES)
130  !     4. Sig(SIZE OF DATA FILE/(NUMBER OF GAGES+5)*NUMBER OF GAGES)
140  !     5. Delv(SIZE OF DATA FILE/(NUMBER OF GAges+5)*NUMBER OF GAGES)
150  !     6. Ws(SIZE OF DATA FILE/NUMBER OF GAGES)
151  !     7. F(((2*NUM. GAGES)+1)*(SIZE OF DATA FILE/(NUM. GAGES+5)))
160  !
170  OPTION BASE 1
180  DIM Os(15),D(4500),Ep(4500),Sig(4500),Delv(4500),Ws(250),F(6975)
181  RANDOMIZE 37480660
190  OUTPUT 2;"K";                          !CLEAR SCREEN
200  CALL Offset(Ng,Os(*))                  !INPUT GAGE OFFSETS
210  CALL Check1(Ng,Os(*))                  !CHECK FOR CORRECT OFFSETS
220  CALL Gages(Bv,Gf)                      !INPUT BRIDGE VOLTAGE AND GAGE FACTOR
230  CALL Datain(Nm$,Fs,D(*))               !READ DATA FILE INTO ARRAY D
240  CALL Wind(Fs,D(*),Ws(*),Ng)            !READ WIND SPEEDS INTO ARRAY WS
250  CALL Dele(Ng,Fs,L,Os(*),D(*),Delv(*))!COMPUTE DELTA E(VOLTAGE)
260  CALL Strain(Ng,Bv,Gf,L,Fs,Delv(*),Ep(*))!COMPUTE STRAINS
270  CALL Stress(L,Ep(*),Sig(*))            !COMPUTE STRESSES
280  !
290  OUTPUT 2;"K";
300  INPUT "DO YOU WANT STRESSES AND STRAINS SAVED TO A FILE(Y/N)",An$
310  IF An$="Y" THEN
320  CALL Saveit(L,Fs,Ng,Ws(*),Ep(*),Sig(*),F(*))!STORE STRESSES AND STRAINS IN
 FILE
330  ELSE
340  END IF
350  !
360  CALL Out(Fs,Ng,Ws(*),Ep(*),Sig(*))   !PRINT STRESSES AND STRAINS
370  PRINTER IS 1                          !RETURN PRINTER TO SCREEN
380  END
390  !
```

```
400   !
410   !!!!!!!!!!!!!!!!!!!!!!!!!!!!!!!!!!!!!!!!!!!!
420   !!                                          !
430   !!              SUBROUTINES                 !
440   !!                                          !
450   !!!!!!!!!!!!!!!!!!!!!!!!!!!!!!!!!!!!!!!!!!!!
460   !
470   !
480   !!!!!!!!!!!!!!!!!!!!!!!!!!!!!!!!!!!!!!!!!!!!
490   !!                  OFFSET                  !
500   !!!!!!!!!!!!!!!!!!!!!!!!!!!!!!!!!!!!!!!!!!!!
510   !
520   SUB Offset(Ng,Os(*))
530   !
540 First:  INPUT "ENTER NUMBER OF STRAIN GAGES",Ng
550   !
560   !CHECK FOR PROPER NUMBER OF STRAIN GAGES
570   !
580   OUTPUT 2;"K";                    !CLEAR SCREEN
590   PRINT USING "15/,20X,""NUMBER OF STRAIN GAGES: "",2D";Ng
600   INPUT "ARE CORRECTIONS NEEDED IN NUMBER OF GAGES(Y/<Return>)",An$
610   IF An$="Y" THEN GOTO First
620   !
630   DISP "INSERT OFF SET DATA DISK INTO RT. DRIVE AND PRESS Continue"
640   PAUSE
650   CAT
660   INPUT "NAME OF DATA OFF SET DATA FILE",Nm$
670   ASSIGN @Path2 TO Nm$
680   FOR I=1 TO Ng
690   OUTPUT 2;"K";
700   ENTER @Path2,I;Os(I)
710   NEXT I
720   ASSIGN @Path2 TO *
730   SUBEND
740   !
750   !
760   !!!!!!!!!!!!!!!!!!!!!!!!!!!!!!!!!!!!!!!!!!!!
770   !!                  CHECK1                  !
780   !!!!!!!!!!!!!!!!!!!!!!!!!!!!!!!!!!!!!!!!!!!!
790   !
800   SUB Check1(Ng,Os(*))
810   !
```

```
820   CALL Printos(Ng,Os(*))                  !PRINT OFFSETS
 TO SCREEN
830   !
840   !CHECK FOR CORRECT OFFSET ENTRY
850   !
860   INPUT "ARE CORRECTIONS NEEDED FOR ANY OFFSET?(Y/<Return>)",An$
870   IF An$="Y" THEN CALL Correct(Ng,Os(*))
880   !
890   SUBEND
900   !
910   !
920   !*****************************************
930   !*              PRINTOS                  *
940   !*****************************************
950   !
960   SUB Printos(Ng,Os(*))
970   !
980   OUTPUT 2;"K";                           !CLEAR SCREEN
990   !
1000  !PRINT OFFSETS TO SCREEN IN MENUE FORM
1010  !
1020  PRINT USING "31X,""GAGE #"",5X,""OFFSETS"""
1030  FOR I=1 TO Ng
1040  PRINT USING "33X,2D,7X,D.5D";I,Os(I)
1050  NEXT I
1060  !
1070  SUBEND
1080  !
1090  !
1100  !*****************************************
1110  !*              CORRECT                  *
1120  !*****************************************
1130  !
1140  SUB Correct(Ng,Os(*))
1150  !
1160 Corr: CALL Correct2(Ng,Os(*))
1170  !
1180  !CHECK FOR MORE CORRECTIONS
1190  !
1200  CALL Printos(Ng,Os(*))
1210  !
1220  INPUT "ANY MORE CORRECTIONS(Y/<Return>)",An$
1230  IF An$="Y" THEN GOTO Corr
```

```
1240 !
1250 SUBEND
1260 !
1270 !
1280 !!!!!!!!!!!!!!!!!!!!!!!!!!!!!!!!!!!!!!!!!!!!
1290 !!                GAGES                !
1300 !!!!!!!!!!!!!!!!!!!!!!!!!!!!!!!!!!!!!!!!!!!!
1310 !
1320 SUB Gages(Bv,Gf)
1330 !
1340 OUTPUT 2;"K";
1350 !
1360 Bridges: CALL Bridge(Bv,Gf)
1370 !
1380 !CHECK FOR CORRECT DATA ENTRY
1390 !
1400 OUTPUT 2;"K";
1410 !
1420 PRINT USING "15/,30X,""1. BRIDGE VOLTAGE: "",D.DD,//,30X,""2. GAGE FACTOR:
 "",D.4D";Bv,Gf
1430 !
1440 INPUT "ARE CORRECTIONS NEEDED?(Y/<Return>)",An$
1450 IF An$="Y" THEN GOTO Bridges
1460 !
1470 SUBEND
1480 !
1490 !
1500 !!!!!!!!!!!!!!!!!!!!!!!!!!!!!!!!!!!!!!!!!!!!
1510 !!                DATAIN               !
1520 !!!!!!!!!!!!!!!!!!!!!!!!!!!!!!!!!!!!!!!!!!!!
1530 !
1540 SUB Datain(Na$,Fs,D(*))
1550 !
1560 OUTPUT 2;"K";                          !CLEAR SCREEN
1570 !
1580 DISP "PLACE DISK WITH DATA FILE IN RIGHT DRIVE AND PRESS CONTINUE"
1590 PAUSE
1600 !
1610 Corr3:CALL Correct3(Na$,Fs)
1620 !
1630 OUTPUT 2;"K";                          !CLEAR SCREEN
1640 !
```

```
1650 PRINT USING " 15/,30X,""FILE: "",10A,/,30X,""SIZE: "",5
D";Nm$,Fs
1660 !
1670 !CHECK FOR CORRECT DATA ENTRY
1680 !
1690 INPUT "ARE CORRECTIONS NEEDED?(Y/<Return>)",An$
1700 IF An$="Y" THEN GOTO Corr3
1710 !
1720 !OPEN I/O PATH TO FILE
1730 !
1740 ASSIGN @Path1 TO Nm$
1750 !
1760 !READ DATA FROM FILE INTO ARRAY D
1770 !
1780 FOR I=1 TO Fs
1790 ENTER @Path1,1;D(I)
1800 NEXT I
1810 !
1820 !CLOSE I/O PATH TO FILE
1830 !
1840 ASSIGN @Path1 TO *
1850 !
1860 SUBEND
1870 !
1880 !
1890 !*****************************************
1900 !*                 WIND                  *
1910 !*****************************************
1920 !
1930 SUB Wind(Fs,D(*),Ws(*),Ng)
1940 !
1950 !READ WIND SPEEDS FROM ARRAY D INTO ARRAY WS
1960 !
1970 K=5                    !FIFTH RECORD IS  FIRST WIND SPEED
1980 N=1
1990 L=Ng+5                 !TOTAL READINGS PER SCAN
2000 FOR I=1 TO Fs STEP L
2010 Ws(N)=D(K)
2020 N=N+1
2030 K=K+L
2040 NEXT I
2050 !
2060 SUBEND
```

```
2070 !
2080 !
2090 !*****************************************
2100 !*                 DELE                  *
2110 !*****************************************
2120 !
2130 SUB Dele(Ng,Fs,L,Os(*),D(*),Delv(*))
2140 !
2150 !COMPUTE VOLTAGE CHANGE
2160 !
2170 M=Ng+5                          !TOTAL READINGS PER SPAN
2180 L=1                             !NUMBER OF GAGE READINGS
2190 K=1
2200 !
2210 FOR J=1 TO Fs STEP M
2220 K=K+5
2230 FOR I=1 TO Ng
2240 Delv(L)=D(K)-Os(I)              !DELTA V=READING - OFFSET
2250 K=K+1
2260 L=L+1
2270 NEXT I
2280 NEXT J
2290 L=L-1                           !CORRECT FOR LAST TIME THROUGH LOOP
2300 !
2310 SUBEND
2320 !
2330 !
2340 !*****************************************
2350 !*                 STRAIN                *
2360 !*****************************************
2370 !
2380 SUB Strain(Ng,Bv,Gf,L,Fs,Delv(*),Ep(*))
2390 !
2400 !STRAIN=(DELTA V)/(GAGE FACTOR*BRIDGE VOLTAGE)
2410 !
2420 L=Fs/(Ng+5)*Ng
2430 FOR I=1 TO L
2440 Ep(I)=Delv(I)/(Bv*Gf)
2441 IF ABS(Ep(I))>.000689655 THEN
2442 IF Ep(I)<0 THEN Ep(I)=-1*(RND*10)/29000.0
2443 IF Ep(I)>0 THEN Ep(I)=(RND*10)/29000.0
2444 ELSE
```

```
2445 END IF
2450 NEXT I
2460 !
2470 SUBEND
2480 !
2490 !
2500 !*****************************************
2510 !*                STRESS                 *
2520 !*****************************************
2530 !
2540 SUB Stress(L,Ep(*),Sig(*))
2550 !
2560 !STRESS = STRAIN*E
2570 !
2580 FOR I=1 TO L
2590 Sig(I)=Ep(I)*29000
2600 NEXT I
2610 !
2620 SUBEND
2630 !
2640 !
2650 !*****************************************
2660 !*                SAVEIT                 *
2670 !*****************************************
2680 !
2690 SUB Saveit(L,Fs,Ng,Ws(*),Ep(*),Sig(*),F(*))
2700 !
2710 !SAVE WIND SPEED ,STRAINS, AND STRESSES
2720 !
2730 INPUT "NAME OF NEW DATA FILE?",Nm$
2740 !
2750 M1=Fs/(Ng+5)
2760 Size=2*Ng*M1+M1              !SIZE OF NEW FILE
2770 !
2780 CREATE BDAT Nm$,Size,8       !CREAT FILE WITH SIZE RECORDS AT 8 BITS/RECORD
2790 !
2800 !OPEN I/O PATH TO NEW FILE
2810 !
2820 ASSIGN @Path2 TO Nm$
2830 !
2840 OUTPUT 2;"K";
2850!PRINT USING "10/,10X,""STORING DATA IN FILE "",10A";Nm$
```

```
2860 !
2870 !STORE DATA IN FILE
2880 !
2890 M=Fs/(Ng+5)
2900 K=1
2910 N=1
2920 FOR J=1 TO M
2930 F(N)=Ws(J)
2940 N=N+1
2950 FOR I=1 TO Ng
2960 F(N)=Ep(K)
2970 F(N+1)=Sig(K)
2980 N=N+2
2990 K=K+1
3000 NEXT I
3010 NEXT J
3020 !
3030 !CLOSE I/O PATH TO FILE
3040 !
3041 OUTPUT @Path2;F(*)
3050 ASSIGN @Path2 TO *
3060 !
3070 SUBEND
3080 !
3090 !
3100 !!!!!!!!!!!!!!!!!!!!!!!!!!!!!!!!!!!!!!!!!!!!
3110 !!                 OUT                    !
3120 !!!!!!!!!!!!!!!!!!!!!!!!!!!!!!!!!!!!!!!!!!!!
3130 !
3140 SUB Out(Fs,Ng,Ws(*),Ep(*),Sig(*))
3150 !
3160 INPUT "DO YOU WANT RESULTS PRINTED ON PRINTER?(Y/<Return>)",An$
3170 IF An$="Y" THEN PRINTER IS 701
3180 !
3190 Nr=Fs/(Ng+5)              !TOTAL NUMBER OF SCANS
3200 !
3210 FOR J=1 TO Nr-1 STEP 2
3220 !
3230 C=(J-1)/6
3240 D=INT(C)
3250 IF D=C THEN PRINT CHR$(12)        !ONLY PRINT 6 DATA SETS PER PAGE
3260 !
```

```
3270 L=J*Ng-(Ng-1)
3280 K=L+Ng-1
3290 PRINT USING "//,12X,""WIND SPEED: "",2D.2D,23X,""WIND SPEED: "",2D.2D";Ws(J
),Ws(J+1)
3300 PRINT USING "/,2(2X,""GAGE NO."",2X,""STRAIN(in/in)"",2X,""STRESS(KSI)"",2X
)"
3310 N=1
3320 FOR I=L TO K
3330 PRINT USING "5X,2D,8X,D.5D,7X,5D.2D,9X,2D,8X,D.5D,7X,5D.2D";N,Ep(I),Sig(I),
N,Ep(I+Ng),Sig(I+Ng)
3340 N=N+1
3350 NEXT I
3360 NEXT J
3370 !
3380 SUBEND
3390 !
3400 !
3410 !*****************************************
3420 !*              CORRECT2                 *
3430 !*****************************************
3440 !
3450 SUB Correct2(Ng,Os(*))
3460 !
3470 CALL Printos(Ng,Os(*))
3480 !
3490 INPUT "NUMBER OF GAGE TO CORRECT",N
3500 INPUT "NEW OFFSET",Os(N)
3510 !
3520 SUBEND
3530 !
3540 !
3550 !*****************************************
3560 !*               BRIDGE                  *
3570 !*****************************************
3580 !
3590 SUB Bridge(Bv,Gf)
3600 !
3610 INPUT "WHAT IS THE BRIDGE VOLTAGE?",Bv
3620 INPUT "WHAT IS THE STRAIN GAGE FACTOR?",Gf
3630 !
3640 SUBEND
3650 !
```

```
3660 !
3670 !*****************************************
3680 !*              CORRECT3                 *
3690 !*****************************************
3700 !
3710 SUB Correct3(Na$,Fs)
3720 !
3730 OUTPUT 2;"K";                  !CLEAR SCREEN
3740 !
3750 CAT                             !DISK DIRECTORY
3760 !
3770 INPUT "NAME OF DATA FILE TO USE?",Na$
3780 INPUT "SIZE OF DATA FILE USED(NUMBER OF RECORDS)?",Fs
3790 !
3800 SUBEND
```

APPENDIX C

SET UP AND OPERATION OF FIELD TESTING EQUIPMENT

These procedures should be followed when using the HP3421 Data Acquisition Unit to collect strain gage data.

List of needed equipment:

A. HP3421A - Data Acquisition Unit
B. HP-41CX - Calculator
C. HP-IL - Module
D. HP83161A - Cassette Drive
E. DC Power Supply
F. Wheatstone Bridge

Steps 1-5 must be completed in the laboratory.

1. Make sure that all battery packs in all devices are fully charged.

2. It is necessary to initialize and create a file on a tape before data can be stored on it. It is recommended to make the file big enough to fill the entire tape. Detailed instructions can be found in the HP-IL module's owner's manual.

3. For strain gage measurements, it is necessary to use a Wheatstone Bridge. The Wheatstone Bridge requires an external DC power supply. There are many different ways to configure the Wheatstone Bridge. The user should refer to the strain gage manual for these variations. Figure A1 shows a two-wire circuit.

4. Once a Wheatstone Bridge configuration has been selected, connect the appropriate wires from the bridge to the terminal block. Make sure to connect the wires to the correct channel slots. Each slot has a high terminal and a low terminal. These are clearly marked on the terminal block. Take care not to connect any wires in the unnumbered slots between slots 1 and 2, or the unit will not function properly. It does not matter which wire goes in the "hi" slot or the "low" slot as long as they remain the same for the entire study.

5. If it will be necessary to disconnect and reconnect the gage cables to the bridge, it is recommended to use some sort of quick disconnect device, such as the spade connectors shown in Figure A2.

Steps 6-20 are to be completed in the field.

6. Make sure all devices are turned OFF.

7. Connect the terminal blocks to the option slots on the back of the HP3421A. The block for channels 0-9 goes in slot 0, the block for channels 10-19 goes in slot 1.

8. Connect the strain gage cables to the Wheatstone Bridge, following the manner of the bridge configuration selected. Use the quick disconnect devices, if available.

9. Plug the HP-IL module into an expansion port on the calculator. If the calculator has memory modules installed, the IL module must be in a higher-numbered port than a memory module.

10. Plug the lead from the IL module with the male end into the HP-IL receptacle marked "IN" on the back of the HP3421A. Only one of the leads will fit, so there is no possibility of a mixup.

11. Using the short IL cable supplied with the cassette drive, plug the female end into the receptacle marked "OUT" on the rear panel of the HP3421A. Plug the other end of the cable into the receptacle marked "IN" on the rear of the cassette drive.

12. Plug the other lead from the IL module into the receptacle marked "OUT" on the cassette drive. The HP3421A calculator and cassette drive should form a continuous, uninterrupted loop. If they do not, repeat Steps 6-12.

13. Connect the power supply to the Wheatstone Bridges.

14. Turn on all devices and check for proper operation.

15. Adjust the voltage across the Wheatstone Bridge to the desired value.

16. Place prepared data cassette in drive. It will only fit in one way.

17. Set tape to proper file and data register. Refer to IL module owner's manual for details.

18. Set any parameters required by calculator software and begin data collection.

19. Check equipment frequently to insure proper operation.

20. When disconnecting devices, make sure all devices are turned "OFF" before beginning to disconnect.

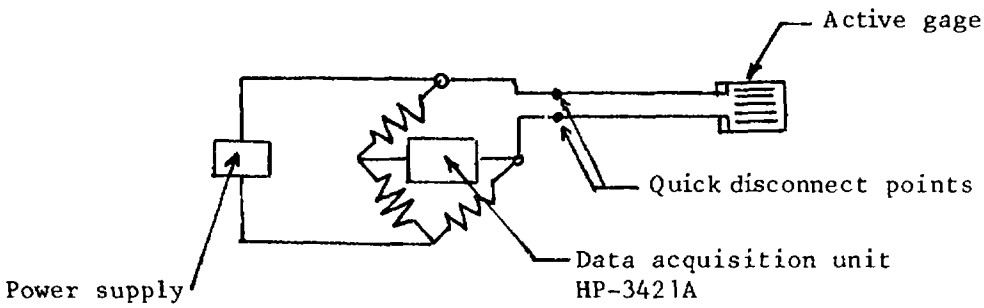

Figure A1. Two-wire Wheatstone Bridge

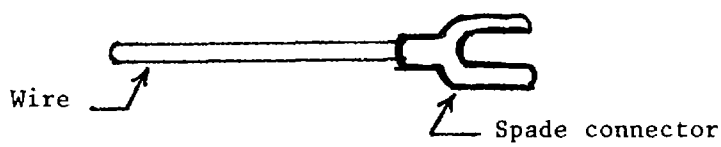

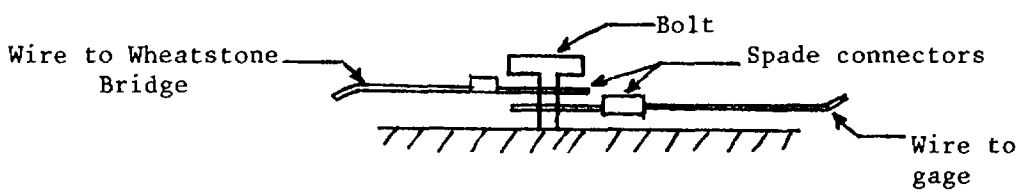

Figure A2. Spade Connector and How to Use

APPENDIX D:

DATA TRANSFER
FROM CASSETTE DRIVE TO SERIES 200 COMPUTER

These procedures should be followed to transfer data from a tape in the cassette drive to the Series 200 computer for storage on a floppy disk.

List of needed equipment:

A. HP Series 200 Computer
B. HP-41CX Calculator
C. HP-IL Module
D. HP82161A Cassette Drive
E. HP82169A HP-IL/HP-IB Interface
F. Floppy Disk for Storage

1. Floppy disk must be initialized before it may be used. Refer to computer manual for details.

2. To facilitate data transfer, two programs have been written. TRANS runs on the HP-41CX and TRANSFER runs on the Series 200 computer. Listings of these programs are given in Appendices E and F.

TRANS first prompts the user to enter the beginning and ending registers of the desired data, as well as the data file where the data are located. It then reads a portion of the data into the calculator's memory. One register at a time, it recalls the data into the alpha register of the calculator, selects the IL/IB interface as the primary device and outputs the alpha register to the interface.

TRANSFER also prompts the user for the beginning and ending tape registers plus the name of file where the data are to be stored. It creates this file, reads the data from the interface, and stores it.

3. TRANS and TRANSFER continue until all the data have been transferred and stored.

4. To use these programs, follow Steps 5-29. The user may wish to write his own program(s).

5. Make sure all devices are turned OFF.

6. Plug the HP-IL module into an expansion port on the calculator. Make sure that no memory modules are plugged into a higher numbered port than the IL module.

7. Plug the lead of the IL module with the male end into the receptacle marked "IN" on the IL/IB interface.

8. Using the short IL cable supplied with the cassette drive, plug the female end into the receptacle marked "OUT" on the IL/IB interface and the other end into the receptacle marked "IN" on the cassette drive.

9. Plug the remaining lead from the IL module into the receptacle marked "OUT" on the IL/IB interface and the other end into the receptacle marked "IN" on the cassette drive.

10. The calculator, cassette drive, and IL/IB interface should form a continuous loop. If they do not, repeat steps 5-9.

11. Plug an HP-IB cable from the computer into the IL/IB interface. It will only fit on one way.

12. Plug the power cord into the IL/IB interface. Turn on all devices.

13. Boot operating system on computer.

14. Make sure IL/IB interface is set to "Mailbox" mode. See IL/IB Owner's Manual for details.

15. Place proper cassette in drive.

16. Execute "TRANS" on the calculator.

17. To "START REG?" prompt, enter the starting register of the tape and press R/S.

18. To "END REG?" prompt, enter the ending register of the tape and press R/S.

19. To "FILE?" prompt, enter the tape data file name and press R/S.

20. When "WRT DATA" appears in calculator display, load program "TRANSFER" into Series 200 computer. <u>DO NOT touch the calculator</u>.

21. Re-dimension the arrays used in "TRANSFER", using the guidelines found at the beginning of the program.

22. Place the floppy disk to contain the data in the logged-in drive.

23. RUN program "TRANSFER".

24. The program will prompt the user to enter the data file name and the beginning and ending tape registers. Press the ENTER Key after each item.

25. After a short pause, the Series 200 will display "Ready to read data, press CONTINUE". When this happens, press the R/S Key on the calculator and watch the red "BUSY" light on the tape drive.

26. VERY IMPORTANT: When the "BUSY" light on the tape drive goes off (after approximately 6 seconds) IMMEDIATELY press the "CONTINUE" Key on the Series 200 computer.

27. Check the first number on the Series 200 screen to see if it is correct.

28. Wait until finished. Calculator will display "END OF DATA".

29. Turn all devices OFF before disconnecting.

APPENDIX E

DATA TRANSFER SOFTWARE TO HP-41CX CALCULATOR

HP-41CX program to transfer data from cassette tape to an HP Series 200 computer via the HP-IL/HP-IB interface.

```
01LBL "TRANS"
02 XEQ "AUTOIO"
03 FIX 9
04 "START REG?"
05 PROMPT
06 STO 00
07 "END. REG?"
08 PROMPT
09 STO 01
10 RCL 00
11 "FILE?"
12 PROMPT
13 SEEKR
14 RCL 00
15 1
16 -
17 STO 02
18 STO 04
19 MANIO
20 "WRT DATA"
21 AVIEW
22 STOP
23LBL 01
24 2
25 SELECT
26 10.219
27 READRX
28 10
29 STO 03
30 XEQ 02
31 210
32 ST+ 02
33 RCL 02
34 RCL 01
35 X<=Y?
36 GTO 03
37 GTO 01
38LBL 02
39 1
40 SELECT
41 LISTEN
42LBL 04
43 CLA
44 ARCL IND 03
45 OUTA
46 1
47 ST+ 03
48 ST+ 04
49 RCL 04
50 RCL 01
51 X=Y?
52 GTO 03
53 RCL 03
54 220
55 X=Y?
56 RTN
57 GTO 04
58LBL 03
59 "END OF DATA"
60 AVIEW
61 AUTOIO
62 .END.
```

APPENDIX F

DATA TRANSFER SOFTWARE FOR HP SERIES 200 COMPUTER

```
10    DIM D(21),A(20,10)
20 Start:   OUTPUT 2;"K";     !CLEAR SCREEN
30    !
40    ! INPUT STARTING REGISTER, ENDING REGISTER, AND DATA FILE NAME
50    !
60    CALL Data_in(Br,Er,Nm$)
70    !
80    Size=Er-Br+1.0    !COMPUTE SIZE OF DATA FILE
90    !
100   !CREATE DATA FILE
110   !
120   CREATE BDAT Nm$,Size,8
130   !
140   !RECEIVE DATA FROM HPIL/HPIB INTERFACE
150   !
160   CALL Mail(Size,Nm$,D(*))
170   !
180   !PRINT DATA
190   !
200   !CALL Data_out(Nm$,D(*))
210   END
220   !
230   !
240   SUB Data_in(Br,Er,Nm$)
250   OUTPUT 2;"K";
260   Nm$=""
270   !
280   !INPUT DATA FILE NAME
290   !
291   CAT
300   INPUT "NAME OF DATA FILE TO CREATE?",Nm$
310   !
320   !INPUT STARTING AND ENDING REGISTERS
330   !
340   INPUT "STARTING REGISTER OF TAPE?",Br
350   INPUT "ENDING REGISTER OF TAPE?",Er
360   SUBEND
370   !
380   !
390   SUB Mail(Size,Nm$,D(*))
400   !
410   !ASSIGN I/O PATHS TO DATA FILE AND INTERFACE
```

```
420   !
430   ASSIGN @Path1 TO Nm$
440   ASSIGN @Ibi1 TO 703
450   !
460   OUTPUT 2;"K";
470   DISP "Ready to read data. Press CONTINUE to procede."
480   PAUSE
490   !
500   DISP "READING DATA AND WRITING DATA TO DISK FILE"
510   !
520   !READ IN DATA FROM INTERFACE
530   !
531   N=1
540   FOR I=1 TO Size STEP 21
550   FOR J=1 TO 21
560   ENTER @Ibi1;D(J)
570   !
580   !USE ONLY ABLOLUTE VALUES
590   D(J)=ABS(D(J))
600   !
610   !PRINT VALUES TO SCREEN
620   PRINT USING "5X,4D,4D.10D";N,D(J)
630   !STORE DATA IN FILE
640   !
650   K=I+J-1
660   OUTPUT @Path1,K;D(J)
670   !
680   !CONTINUE LOOP
690   !
691   N=N+1
700   NEXT J
710   NEXT I
720   SUBEND
730   !
740   !
750   SUB Data_out(Nm$,A(*))
760   !PRINTER IS 701
770   PRINT CHR$(12)
780   SUBEND
```